



Nikolai P. Ponomarev

**A SALT AND ALKALI SYNERGY FOR SYNTHESISING ACTIVE
CARBONS FROM LIGNIN: POROSITY DEVELOPMENT AND
TECHNO-ECONOMIC ASSESSMENT**



Nikolai P. Ponomarev

A SALT AND ALKALI SYNERGY FOR SYNTHESISING ACTIVE CARBONS FROM LIGNIN: POROSITY DEVELOPMENT AND TECHNO-ECONOMIC ASSESSMENT

Dissertation for the degree of Doctor of Science (Technology) to be presented with due permission for public examination and criticism in Hall D at South-Eastern Finland University of Applied Sciences, Mikkeli, Finland on the 22nd of August, 2023, at noon.

Acta Universitatis
Lappeenrantaensis 1083

Supervisors Professor Mari Kallioinen-Mänttari
LUT School of Engineering Sciences
Lappeenranta-Lahti University of Technology LUT
Finland

Professor Amit Bhatnagar
LUT School of Engineering Sciences
Lappeenranta-Lahti University of Technology LUT
Finland

Reviewers Professor Fred Cannon
Department of Civil and Environmental Engineering
The Pennsylvania State University
USA

Professor Éder Cláudio Lima
Institute of Chemistry
The Federal University of Rio Grande do Sul (UFRGS)
Brazil

Opponent Professor Ulla Lassi
Department of Sustainable Chemistry
University of Oulu
Finland

ISBN 978-952-335-955-0
ISBN 978-952-335-956-7 (PDF)
ISSN 1456-4491 (Print)
ISSN 2814-5518 (Online)

Lappeenranta-Lahti University of Technology LUT
LUT University Press 2023

Abstract

Nikolai P. Ponomarev

A salt and alkali synergy for synthesising active carbons from lignin: porosity development and techno-economic assessment

Lappeenranta 2023

71 pages

Acta Universitatis Lappeenrantaensis 1083

Diss. Lappeenranta-Lahti University of Technology LUT

ISBN 978-952-335-955-0, ISBN 978-952-335-956-7 (PDF), ISSN 1456-4491 (Print),

ISSN 2814-5518 (Online)

Active carbons (AC) are the most common and efficient adsorbents. Alkali activation (using NaOH or KOH) was found to be a promising method for AC production since it allows gaining large surface area, high yield and controlled pore size. However, the method is not widely used due to high alkali consumption in the production process. To obtain active carbon with a developed porosity at a high yield and a reduced alkali amount, a new method was developed utilizing lignin. A salt (NaCl or KCl) and an alkali (NaOH or KOH) were used simultaneously to facilitate a decrease alkali consumption. To understand the activation mechanism, the roles of salt and alkali were methodically disclosed. The parameters that facilitate the highest surface area, the largest yield and controlled porosity at the minimized alkali amount were defined by the response surface method (RSM). To demonstrate the benefits of the method, a techno-economic assessment (TEA) was accomplished. The produced active carbon with a high surface area was compared to commercial carbon to show the benefit of natural organic matter (NOM) removal in the water treatment process.

This method using a lignin-KOH-KCl mixture allows producing superactive carbon (SAC) with a high surface area of $>2900 \text{ m}^2/\text{g}$ at a yield of $>28\%$. Furthermore, the consumption of KOH was significantly reduced to 1 g/g compared to $3\text{--}4 \text{ g/g}$ in the previous methods. In addition, KOH as well as KCl were recovered after use. The template mechanism shows that macropores are the same size as salt crystals and alkali grains. Microporosity originated from the elemental potassium formation with its subsequent intercalation between graphene layers. Moreover, the simultaneous use of salt and alkali promotes the synergy between them, which further facilitates the reduced amount of alkali. By altering the alkali amount, temperature and time, the size of pores can be altered. The higher the values of the parameters, the more developed the porosity. Based on TEA, the minimum selling price of the SAC produced by this method is $2.93\text{--}4.36 \text{ kEUR/t}$. Also, there are appreciable process savings of $23\text{--}55\%$ for NOM removal by SAC in the water treatment process compared to commercial AC.

Keywords: active carbon, alkali, salt, lignin, NaOH, KOH, NaCl, KCl, template carbon, high surface area

Acknowledgements

This work was carried out at the LUT School of Engineering Science at the Lappeenranta-Lahti University of Technology LUT, Department of Separation Sciences, Mikkeli, Finland, between 2018 and 2022.

I appreciate LUT University for giving me the opportunity to perform this study. I am also thankful to Business Finland for financing the projects related to this research.

Nikolai P. Ponomarev
June 2022
Mikkeli, Finland

Contents

Abstract

Acknowledgements

Contents

List of publications	11
Nomenclature	13
1 Introduction	15
1.1 General information about active carbon	15
1.2 Porosity of active carbon	15
1.2.1 Pores of active carbon	15
1.2.2 Surface area.....	16
1.3 Methods for producing active carbons	17
1.3.1 Physical activation	17
1.3.2 Chemical activation.....	19
1.4 Methods for producing active carbons having a high surface area	20
1.4.1 Using elemental alkali metals	20
1.4.2 Using alkali hydroxides	21
1.4.3 Template method.....	23
1.5 Precursors of active carbon	24
1.6 Techno-economical aspects of active carbon production.....	25
1.7 Use of active carbon for water treatment	26
2 The objectives of the thesis	29
3 Materials and methods	31
3.1 Materials.....	31
3.2 Methods	31
3.2.1 Synthesis of active carbon.....	31
3.2.2 Regeneration of chemicals	31
3.2.3 Characterization of obtained active carbons and the intermediate products.....	32
3.2.4 Studies of the process factors on active carbon properties using RSM	33
3.2.5 Techno-economic assessment	34
3.2.6 Estimation of the benefit of the use of active carbon with a high surface area for NOM adsorption	35
4 Results and discussion	37
4.1 Synthesis of the active carbon with a diverse porous structure applying simultaneous use of salt and alkali	37

4.2	Study of the pore formation mechanism disclosing the role of salt, alkali and the synergy between them	39
4.2.1	The role of alkali	40
4.2.2	The role of salt	48
4.2.3	A synergy between salt and alkali.....	48
4.3	Influence of chemical ratio, temperature and time on the porosity origin and yield of the prepared active carbons	49
4.3.1	Parameters which promote the most developed porosity and yield at the minimized consumption of alkali.....	49
4.3.2	Pore size control by varied process parameters	52
4.4	Techno-economic assessment of the production of the superactive carbon and its benefit for the water treatment process	54
4.4.1	Techno-economic assessment	54
4.4.2	Benefit for the water treatment process	56

5 Conclusion and future perspectives 59

References 61

Publications

List of publications

This thesis is based on the following papers. The rights have been granted by publishers to include the papers in dissertation. The papers are published under creative common licenses CC BY-NC-ND 4.0 and CC BY 4.0 (open access).

- I. Ponomarev, N.P. and Sillanpää, M. (2019) ‘Combined chemical-templated activation of hydrolytic lignin for producing porous carbon’, *Industrial Crops and Products*, 135, pp. 30–38. doi: 10.1016/j.indcrop.2019.03.050
- II. Ponomarev, N.P and Kallioinen, M. (2021) ‘Synergy between alkali activation and a salt template in superactive carbon production from lignin’, *Nanotechnology*. doi: 10.1088/1361-6528/abc9eb.
- III. Ponomarev, N.P., O’Shea, G., Nuortila-Jokinen, J., Kiljunen, S. and Kallioinen-Mänttari, M. (2022), ‘Techno-Economic assessment for superactive carbon production from side stream lignin.’ *Biofuels, Bioprod. Bioref.*. doi:10.1002/bbb.2445

Author's contribution

Nikolai P. Ponomarev is the principal author and investigator in papers I–III. The design of experiments, their implementation and the drafting of the manuscripts were performed by the principal author.

Nomenclature

Abbreviations

AC	active carbon
BET	Brunauer, Emmett and Teller
CAC	commercial active carbon
CAPEX	capital expenditures
DTA	differential thermal analysis
DSC	differential scanning calorimetry
DR	Dubinina and Radushkevich
FTIR	Fourier transform infrared
ICP-OES	inductive coupled plasma – optical emission spectroscopy
IRR	internal rate of return
IUPAC	International Union of Pure and Applied Chemistry
MSP	minimum selling price
NLDFT	non-local density functional theory
NPV	net present value
NOM	natural organic matter
OPEX	operational expenditures
PSD	pore size distribution
QMS	quadrupole mass spectrometry
RQ	research question
RSM	response surface method
SSA	specific surface area
SAC	superactive carbon
SEM	scanning electron microscopy
TEM	transmission electron microscopy
TEA	techno-economic assessment
TGA	thermo gravimetric analysis
TOC	total organic carbon
XRD	X-ray diffraction

1 Introduction

1.1 General information about active carbon

Active carbon (AC) is a time-honoured adsorbent that can be produced using carbonaceous materials usually through physical (water steam or CO₂) or chemical activation (H₃PO₄, ZnCl₂, KOH, etc.) (Sing, 2013). The feature of active carbon is a versatile porous structure that develops an appreciable specific surface area (SSA) of 500–1500 m²/g for most conventional samples. Active carbon is mainly used for water treatment and gas purification followed by pharmaceuticals, food and automotive applications (Figure 1.1) (Grand View Research, 2022). The global active carbon market in 2021 was about 1.6 million tons, and it is exponentially growing (Mordor Intelligence, 2022). Among the applications for the purification of fluids, studies related to the application of AC for electrical charge storage (supercapacitors) and gas storage (adsorbed natural gas) have attracted considerable attention (Boos, 1970), (Matranga et al., 1992). Therefore, active carbon has a diversity of applications, and its global demand is substantial (Marsh & Rodríguez-Reinoso, 2006a).

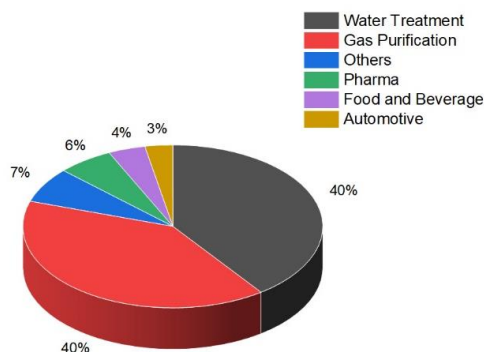


Figure 1.1 Application fields of active carbon.

1.2 Porosity of active carbon

1.2.1 Pores of active carbon

The distinguishing feature of active carbons is the diverse porosity that makes this material an efficient adsorbent. The porous structure is represented by the versatility of pores of different sizes. The first classification of pores of active carbon was proposed by Dubinin M. M., which is established on various widths of pores: micropores, transitional pores (named mesopores nowadays) and macropores (Dubinin, 1960; F. Rouquerol et al., 2014). The IUPAC now adopts this classification with the following widths: macropores (> 50 nm), mesopores (2–50 nm) and micropores (< 2 nm) (F. Rouquerol et al., 2014;

Thommes et al., 2015). A simplistic picture of pores of active carbon is presented in Figure 1.2. Pores larger than 100 nm are also called nanopores. Micropores, in turn, are subclassified into ultramicropores (< 0.7 nm) and supermicropores (0.7–2 nm).

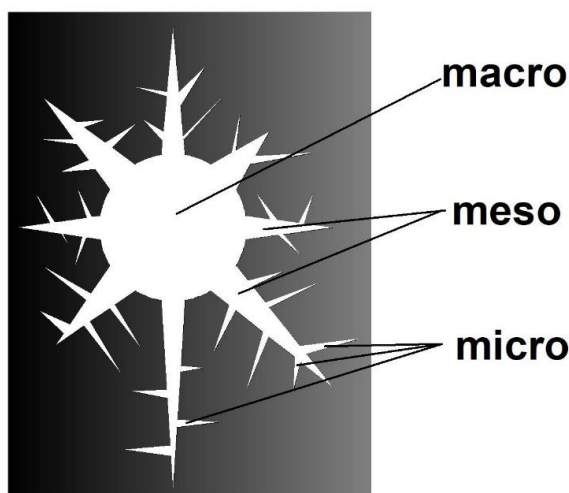


Figure 1.2. Pores of active carbon.

Small molecules (e.g. gases) are adsorbed in micropores, while larger molecules (e.g. organic molecules of high molar mass) can be adsorbed in mesopores (Ando et al., 2010; Perrich, 1981). Moreover, mesopores and macropores are the pathways to the micropores, which also facilitate the faster rate of adsorption. Therefore, the diverse porosity of active carbon is beneficial for various applications in which molecules of different sizes are needed to be adsorbed.

1.2.2 Surface area

Active carbons with a developed porosity possess a large surface area. A large surface area means a large number of pores which are adsorption sites for molecules being adsorbed. For instance, active carbon with a dominant microporosity having a surface area of about 1000 m²/g has approximately 10²⁰ adsorption places (Marsh & Rodríguez-Reinoso, 2006b). The larger the surface area, the more 'active' the carbon. Therefore, the active carbons with high values of surface area are preferable. However, the large surface area does not surely imply a high adsorptive capacity since the latter depends on many factors such as size of pores versus molecule size to be adsorbed; the hydrophobic or hydrophilic nature of the adsorbent and adsorptive; pH of the solution, ionic strength, temperature, etc. (Perrich, 1981). The value of a surface area cannot be used alone but can be used as an indication of adsorbent porosity (J. Rouquerol et al., 2007). In other words, the surface area can be considered a standard property of active carbon. In the literature, the values of the surface area are usually given to the unit of mass of the adsorbent, i.e. as a specific surface area (SSA).

The problem related to the surface area is how this value is estimated for microporous solids. The most common method is the BET equation, which is not relevant to microporous solids that are active carbons. There is no multilayer formation in micropores like the BET theory postulates for macropores and mesopores smaller than 4 nm (Brunauer et al., 1938; Thommes et al., 2012). The micropores are filled by pore-volume-filling according to the Dubinin theory (Dubinin, 1960; Dubinin, M.M., Radushkevich, L.V., 1947). However, values of the surface area estimated by the BET equation are commonly used in scientific literature and patents. Therefore, to make a comparison of the research results easier, the BET equation can be applied for the estimation of surface area as an empirical equation according to the standard procedure (J. Rouquerol et al., 2007; Sing, 2013; Thommes et al., 2015). The value of the BET surface area does not show the real surface area of microporous solids but rather could be used as an indication of the adsorbent ‘activity’ (J. Rouquerol et al., 2007). In this thesis, surface area values are determined according to the mentioned standard procedure and used as a ‘fingerprint’ of the obtained active carbons.

1.3 Methods for producing active carbons

1.3.1 Physical activation

Most of the commercial active carbons are produced by physical activation, usually by water steam or carbon dioxide at 500–1200 °C. The water steam activation process is schematically presented in Figure 1.3a. At first, the precursor is carbonized to produce char, which is secondly activated by steam. The activation of carbon by water steam or carbon monoxide occurs through the redox reaction between carbon and water or CO₂, which can be simply written as (Alcañiz-Monge & Illán-Gómez, 2008; Wigmans et al., 1983):



The reactions (1.1) and (1.2) are gasification reactions of carbon because carbon is converted to gaseous products: carbon monoxide and hydrogen (Marsh & Rodríguez-Reinoso, 2006a). The formed carbon oxide of the reaction (1.1) can also interact with water steam through a gas-shift reaction at high temperatures:



Thus, there is a contribution of the reaction (1.2) to the water steam activation process even if carbon dioxide is not intended to be used. Since reactions (1.1) and (1.2) are

endothermic and can be easily controlled, activation through the water or CO₂ gasification is used, unlike oxygen gasification which is exothermic and occurs at high rates that make control difficult. Thus, activation using water or carbon dioxide can be considered a selective gasification of carbon. The porosity development via physical activation depends on (Yue & Economy, 2017):

- the form of the precursor (powder, granules, fibres, etc.)
- the original texture of the starting material
- composition and the amount of the ash
- gas for activation
- temperature and time of activation
- flow of gas and pressure
- contact between gas and solid.

Gasification reactions are also catalyzed by inorganic substances, for example, salts, oxides or alkalis. Even a small amount of a catalyst (about 100 ppm) can rise the reaction rate by orders of magnitude (Marsh & Rodríguez-Reinoso, 2006c). Because raw materials for active carbons always contain ash, the gasification by reactions (1.1) and (1.2) is catalyzed by the inorganic species of the ash. The carbon matter is consumed due to its gasification, which promotes the formation of pores, while the yield is also reduced due

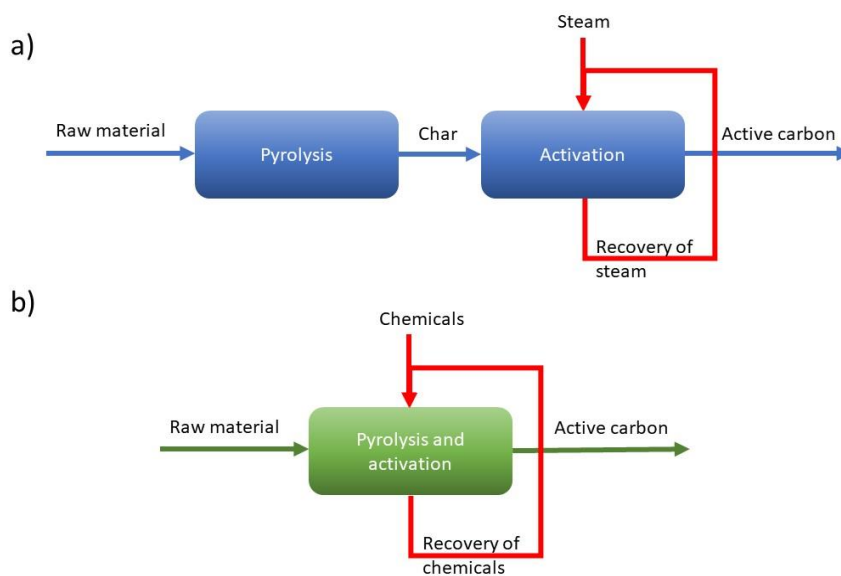


Figure 1.3. Simplified process scheme of active carbon production using (a) steam activation and (b) chemical activation.

to this chemical reaction as well. Consequently, the low product yield coupled with the two-stage process are drawbacks of this process (Maciá-Agulló et al., 2004).

1.3.2 Chemical activation

Different raw materials (coconut shells, wood, coals, etc.) can be activated using chemicals, usually H_3PO_4 , ZnCl_2 and KOH . The activation agents are mixed with precursors by impregnation with a chemical solution or by direct mixing with a solid chemical of an activation agent. The temperature of the chemical activation is typically 300–900 °C. Chemical activation is generally accomplished in a single step, where carbonization and activation occur simultaneously unlike physical activation (Figure 1.3b) (Yue & Economy, 2017). However, an additional leaching step is necessary for the removing of the residual chemicals from the obtained carbon. Chemically activated carbons are produced at lower temperatures and a shorter process time having a higher yield, larger surface area and a controlled porosity compared to steam activation (Maciá-Agulló et al., 2004). The porosity of the obtained carbons by chemical activation is influenced by (Yue & Economy, 2017):

- the original structure of the starting material
- the type of chemicals used for the activation
- how chemicals are mixed with a precursor (impregnation or direct mixing)
- the amount of the activation agent
- temperature and time
- leaching conditions.

Chemicals such as phosphoric acid and zinc chloride are dehydrating agents. The porous structure is simultaneously formed with dehydration reactions, cross-linking reactions and carbon aromatization (Yue & Economy, 2017). The formed ZnO (from ZnCl_2) also acts as a template for a porous structure after the washing stage. The activation mechanism using the KOH activation agent is discussed in more detail in the following chapter. The advantages and drawbacks of chemical activation compared to steam activation are also summarized in Table 1.1.

Table 1.1. Advantages versus drawbacks of chemical activation compared to physical activation (Maciá-Agulló et al., 2004; Rodríguez-Reinoso & Molina-Sabio, 1992; Romanos et al., 2011; Yahya et al., 2015).

Advantages	Drawbacks
1) Higher surface area	1) Washing is needed after carbonization
2) Higher yield	2) Recovery of chemicals
3) Pore size distribution can be easily controlled	3) Corrosiveness
	4) High chemical amount (to achieve high surface area)
4) One step process	
5) Reduced ash content	

1.4 Methods for producing active carbons having a high surface area

High surface area active carbon having SSA higher than 2500 m²/g is the so-called superactive carbon (SAC) (Sing, 2013). As mentioned above, typical active carbons have a specific surface area from 500 to 1500 m²/g, but it is more technologically challenging to manufacture carbons with a surface area larger than these values. The reason for the interest to enable the production of active carbons with a large surface area originates from their extraordinary performance compared to the typical active carbons. More specifically, supercapacitors based on carbons with a high surface area demonstrated higher capacitance (Qiao et al., 2006). The application of high surface area carbon for natural gas storage is promising since more adsorbed gas can be stored on its surface compared to conventional active carbon (T. Zhang et al., 2010). In addition to that, active carbons that possess a high surface area demonstrated superior adsorptive capacity of organic matter from wastewaters compared to commercial steam-activated carbons (O'Grady & Wennerberg, 1986; Wennerberg & O'Grady, 1978). Increased adsorptive capacity means that a lower amount of active carbon with a high surface area is needed to treat a similar amount of water compared to typical active carbon. For cost reduction, this is an appreciable advantage. This promotes less frequent carbon makeup and regeneration. Moreover, transportation costs are lower. Thus, the use of high surface area active carbon could be more efficient than conventional active carbon. The methods to produce carbons with a high surface area could be attributed to the chemical activation methods. Only some of them are described here.

1.4.1 Using elemental alkali metals

The trailblazing work on the synthesis of active carbons with an SSA ranging from 2500–4000 m²/g was conducted in Czechoslovakia in 1975 using elemental lithium amalgam through the electrochemical reduction of polytetrafluoroethylene (PTFE) at low temperature (< 100 °C) (Dousek et al., 1975; Dousek & Jansta, 1975; Jansta et al., 1975). However, this method did not go beyond the lab scale because of environmental concerns and a sophisticated implementation despite low-temperature synthesis.

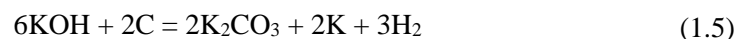
Based on this approach, the mesoporous carbons were then prepared by defluorination of PTFE using elemental lithium, sodium, potassium and rubidium (Liang et al., 2001; Tanaike et al., 2002b, 2002a). The obtained carbons are mesoporous and possessed a lower surface area ($< 2000 \text{ m}^2/\text{g}$). The methods are also challenging for industrial-scale applications.

1.4.2 Using alkali hydroxides

Alkali hydroxides, KOH and NaOH, are commonly used as activation agents. Potassium hydroxide is used more often since it favours a higher surface area and higher yield compared to NaOH (Fierro et al., 2007; Okada et al., 2003). However, sodium hydroxide is cheaper since sodium is a more common element on the earth compared to potassium.

A patent application for a method to produce high surface area carbon from petroleum coke using an excess amount of KOH was filed in 1976 (Wennerberg & O'Grady, 1978). This method was also piloted, and commercial active carbon is produced nowadays by this method, but not in bulk amounts (O'Grady & Wennerberg, 1986; Otowa et al., 1993). The drawback of this method is the significant chemical consumption of KOH: four parts of potassium hydroxide per one part of raw material is needed. This disadvantage leads to a substantial price increase. Therefore, the market size of superactive carbon is negligible compared to active carbon.

The caustic properties of KOH facilitate porosity formation due to erosion and etching of the carbon precursor. Furthermore, micropores (whose contribution to the surface area is the highest) are formed through the elemental potassium intercalation between graphitic layers with their subsequent expansion (Marsh et al., 1982; Marsh & Rodríguez-Reinoso, 2006d; McEnaney, 2002; Sing, 2013). Metallic potassium is reduced from the corresponding hydroxide through the redox reactions with carbon. The possible reactions are (Hüttinger & Mingos, 1986; Lillo-Ródenas et al., 2003):



Reaction (1.4) is a gasification reaction since the carbon is converted to the gaseous product – carbon dioxide. Pores might also be formed due to the carbon matter consumption by reactions (1.4) and (1.5) in a similar fashion to gasification reactions (1.1) and (1.2). Elemental potassium could also be reduced from the intermediate potassium oxide and potassium carbonate (Hüttinger & Mingos, 1986; Otowa et al., 1997):



The carbon dioxide and hydrogen of the above-mentioned chemical reactions could be products of precursor decomposition (e.g. biomass pyrolysis) or a carbon gasification reaction (1.4) that includes a gas-shift reaction (1.3). In addition, porosity can be induced through the carbon gasification reactions (1.1) and (1.2) since a considerable amount of CO_2 and H_2O is formed.

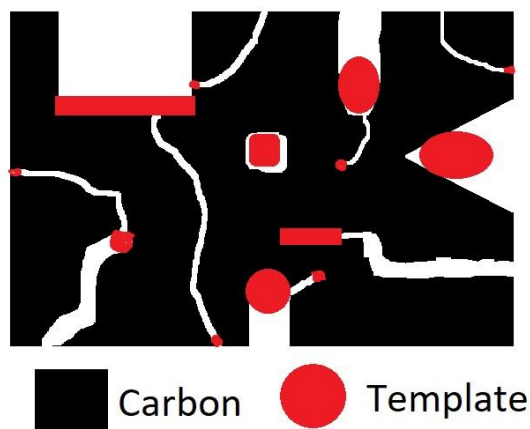


Figure 1.4. Schematic representation of the template mechanism of the pore formation.

An additional possible mechanism is self-templating. Particles of the alkali hydroxides could be a self-template of the pore formation like inorganic particles of the catalyst in the carbon gasification reaction (Marsh & Rodríguez-Reinoso, 2006c). Moving particles can produce channel-like, slit-like or pit-like pores whose dimension is corresponding to the dimension of the inorganic particle (Figure 1.4). Furthermore, macropores of KOH-activated carbons might originate from the KOH grains in the same way (Li et al., 2014;

W. Zhang et al., 2015). Thus, alkali particles can be considered the pores' templates. All in all, the porosity of active carbon activated by KOH originated from the metallic potassium intercalation between graphitic layers, self-templating and the caustic properties of an alkali. It is believed that the microporous structure is mainly formed by alkali metal intercalation rather than by carbon consumption (i.e. carbon gasification) since the yield of the obtained active carbon is high and the process does not obey the stoichiometry of the chemical reactions (Alcañiz-Monge & Illán-Gómez, 2008). This promotes a higher yield than steam activation. For instance, the yield of active carbon produced by the typical steam activation process is 10–15% (Johns et al., 1999), while KOH-activated carbon from the kraft lignin can be obtained at a yield over 50% (Fierro et al., 2007). In addition, alkali activation allows methodically conducting pore-size control and produces carbon with a high surface area ($> 2500 \text{ m}^2/\text{g}$) (Romanos et al., 2011). Nevertheless, the significant alkali consumption and the challenging regeneration of the alkali are the severe reasons for the limited application of alkali activation in the manufacturing of active carbon compared to physical activation. Therefore, there is a need to develop methods that enable a decrease in the used alkali amount and allow its straightforward regeneration.

1.4.3 Template method

The template method is an alternative method to obtain porous carbon materials (Nishihara & Kyotani, 2012). It allows producing carbons with a porous structure that is a replica of a template. The template mechanism is schematically presented in Figure 1.5. For instance, the polymer matrix (1) is mixed with a template (2). Next, the obtained mixture is carbonized to obtain the carbon matrix (3) from the polymer. The template remains unchanged during the carbonization process, and it is removed through leaching with a further formation of pores (4) of a similar size in its place into the carbon matrix. The polymer matrix can be carbonaceous material, for example, oil-based polymer, biomass or plant polymers (Cao et al., 2018; Morishita et al., 2010; Shao et al., 2017). There are a variety of templates. For instance, a zeolite template can be used for the

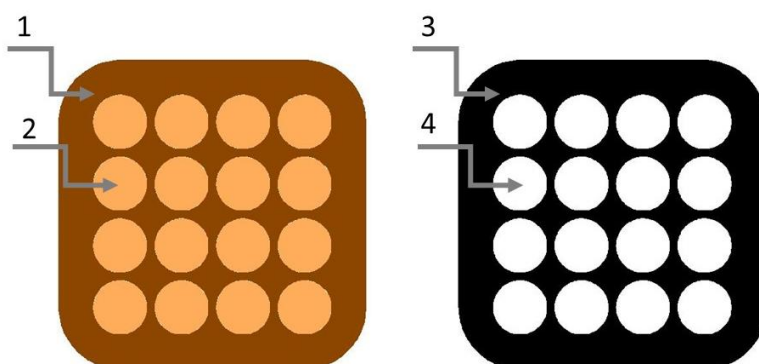


Figure 1.5. Schematic representation of pores formation through the template mechanism: polymer matrix (1), template (2), carbon matrix (3), pores (4).

production of microporous carbons with a high surface area (Matsuoka et al., 2005). In this case, the polymer solution permeates the zeolite structure, and after the polymerization, the carbonization is carried out with the following leaching of zeolite. Similarly, mesoporous silica templates can be used (Kruk et al., 2005). Magnesium oxide as a template was employed to obtain mesoporous carbon (Morishita et al., 2006). Templated carbons have a porosity like the structure of the ordered template used, which usually leads to the ordered structure: most of the pores have the same size (Morishita et al., 2010). By contrast, active carbons synthesized by physical or chemical activation demonstrate a diverse porous structure (Thommes et al., 2015). For most applications, carbons having different pore sizes are needed. In addition, if the template is not water-soluble, a special leaching agent is needed to obtain a carbon replica. For example, if zeolite or silica templates are used, strong mineral acid or alkali are needed to dissolve the templates. Therefore, to overcome these drawbacks, new template methods to produce superactive carbon are needed.

1.5 Precursors of active carbon

In general, active carbon could be produced from any kind of carbon-rich raw material that can be carbonized with a porous structure formation. However, only a few raw materials lead to the economic feasibility of active carbon manufacturing. In addition, the high content of carbon of the starting material is required since it increases the yield of the obtained active carbon, and the space of the carbonization/activation furnace is used more efficiently. The production of active carbons from carbonaceous wastes (e.g. waste paper, scrap tires, sewage sludge, etc.) has gained significant research interest (Merchant & Petrich, 1993; Ros et al., 2006; Zhihang et al., 2017). But most commercial carbons are produced from coconut shells, fossil coals, deciduous wood and fruit stones (Marsh & Rodríguez-Reinoso, 2006a).

Lignin, being the second-most abundant polymer after cellulose, could be used as a precursor for the active carbon. From 40% to 55% of carbon can be yielded from the lignin (Azarov, V.I., Burov, A.V., and Obolenskaya, 1999; Sadakata et al., 1987). Lignin has already been utilized as raw material for active carbon on an industrial scale (Chudakov, 1983). Moreover, lignin is a side stream of the enzymatic-hydrolysis treatment of wood for ethanol production (Xu et al., 2021). The use of hydrolysis lignin as precursor for active carbon brings added value compared to straightforward incineration. In addition to that, there are approximately up to 100 million tons of hydrolysis lignin wastes in Russia and post-Soviet Union territory from the discontinued acid-hydrolysis industry (Evstigneyev et al., 2016; Rabinovich, 2014; Rabinovich et al., 2016). These wastes are located in landfills and can cause fires and soil pollution and natural water because of the leaching of the residual acid from lignin (Figure 1.6). Thus, the application of lignin for the active carbon manufacturing might help in solving ecological problems.

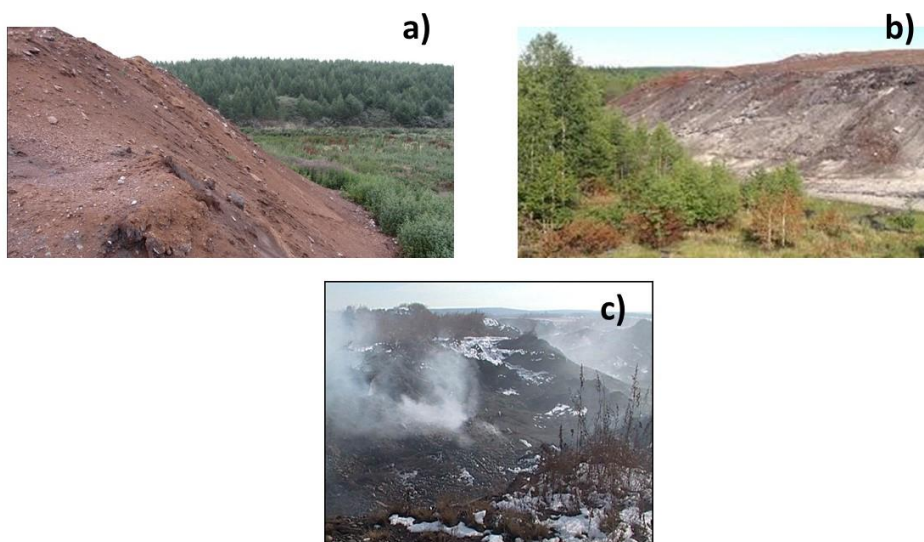


Figure 1.6. Wastes of lignin in landfills (a,b) and smouldering lignin wastes (c).

1.6 Techno-economical aspects of active carbon production

There are a number of studies related to active carbon preparation and its application. However, for the past 20 years, only a few are focused on the techno-economical aspects of its production (Choy et al., 2005; Fingolo et al., 2019; Ko et al., 2004; Lima et al., 2008; Ng et al., 2003; Vanreppelen et al., 2011). Moreover, the studies disclose the profitability of conventional active carbon manufacturing, and it is challenging to find similar studies for the active carbon manufacturing having a large surface area.

In line with the benefits of the chemical activation (Table 1.1), active carbon of high surface area can be produced by direct carbonization of the precursor and KOH without preliminary pyrolysis (Fierro et al., 2007). This could lead to reduced total capital investments (CAPEX) since fewer equipment units are needed compared to the production of active carbon activated by steam. Furthermore, the energy consumption would be lower because less heating is used. In other words, fewer process steps would also result in reduced energy consumption and therefore decrease the overall operational expenditures (OPEX). On the other hand, OPEX is increased since water is needed to wash out the activation agent from the resultant product, and chemicals should be regenerated after use. The lower the amount of chemicals used, the less water is needed for washing and the fewer chemicals are lost after the recovery. Therefore, methods that facilitate reduced chemical consumption are necessary.

1.7 Use of active carbon for water treatment

From the end-user standpoint, the benefit from the usage of the product is more important than the aspects of how the product was produced. Since the global consumption of active carbon for drinking water purification is the highest, the studies demonstrating its performance in this field are essential (FEECO International, 2022; Newcombe, 2006). As mentioned in the previous chapter, the high surface area carbon might result in higher adsorptive capacity for the pollutant compared to conventional active carbons with less developed porosity. As mentioned in the previous chapter, the high surface area carbon might result in higher adsorptive capacity for the pollutant compared to conventional active carbons with less developed porosity.

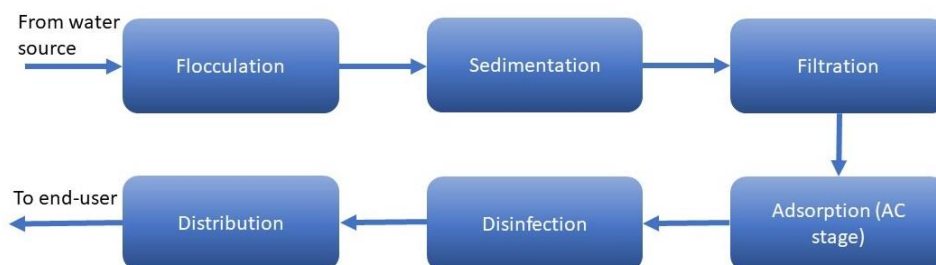


Figure 1.7. A simplified example of the water treatment process.

A water treatment plant is a plant that produces drinking water that flows from the domestic water tap. The source of water could be a local reservoir (e.g. lake, river, pond). The basic water treatment process is presented in Figure 1.7. The water from the source is pumped to the flocculation and filtration stages for the natural organic matter (NOM) removal, which causes colour and odour (Newcombe, 2006). Active carbon is used for ‘polishing’ after these steps to remove the residual NOM (Perrich, 1981). Also, an additional active carbon adsorption stage can be used after the disinfection stage, for

example, to adsorb residual chlorine or hypochlorite and the resultant products after interaction with NOM (Otowa et al., 1997). NOM can be quantitatively measured in water as total organic carbon (TOC). Consequently, the performance of active carbon can be expressed as its adsorptive capacity for TOC (Ando et al., 2010; Randtke & Snoeyink, 1983). The higher the adsorptive capacity, the lower the amount of active carbon needed to treat the water. Therefore, active carbons of high adsorptive capacity for NOM are preferable for the process of water treatment.

2 The objectives of the thesis

The thesis discloses a new method for active and superactive carbon production applying the synergy of the concurrent use of alkali activation and the salt template. The development of the new method aims to enable the production of porous carbon at reduced alkali consumption using lignin as a precursor. The mechanism of combined chemical-templated activation was studied in this work. The effect of process factors like chemical ratio, temperature and time on the properties of the obtained active carbon was also investigated using the response surface method (RSM). In addition, the techno-economic assessment (TEA) of the method was performed, and the benefit of the water treatment by superactive carbon (SAC) produced using this method was evaluated.

This thesis aims to give an answer to the listed below research questions (RQs):

RQ1: How can carbon be produced with a developed porous texture at a decreased amount of alkali?

For this purpose, a method for producing active carbon aiming to reduce alkali consumption was invented during the thesis work. The patent was granted (FI128625B). The granted patent means that the claims of the method fulfil the criteria: novelty, inventive step and industrial applicability. Therefore, this method is novel. The claimed feature of the method is a synergy between a salt template and the alkali activation that promotes a decreased amount of the latter compared to existing methods. The results are discussed in Paper I. The method is further expanded to produce superactive carbon, and results are presented in Paper II. Further development of the method allows producing carbon with a high surface area by mixing two potassium salts instead of an alkali-salt mixture (patent pending FI20205673A1).

RQ2: What is the role of alkali and salt in their simultaneous use for (super)active carbon production?

To get insight into the underlying feature of the method, the mechanism of pore formation was studied methodically. The role of salt and alkali and their simultaneous use were disclosed. The mechanism of the porosity origin was described in papers I and II. Furthermore, an attempt to explain why the alkali consumption is reduced compared to already existing methods was made under the studied mechanism.

RQ3: What process parameters facilitate the highest surface area and yield of carbons at the minimized consumption of the alkali? How can pore size be controlled using process parameters?

To obtain active carbon with the highest possible surface area and yield at the minimum alkali amount, factors such as chemical ratio, temperature and time were studied. The response surface method (RSM) was used for the mathematical description of the effect

of these factors. Pore size distribution can also be controlled by varying these parameters. The research outcomes are discussed in papers I and II.

RQ4: What would be the benefit to produce active carbon in this way, using alkali and salt simultaneously?

To demonstrate the advantage of this method, a techno-economic assessment was performed. Also shown the potential benefit for the water treatment process using superactive carbon as produced by our method. The obtained results are described in Paper III.

Consequently, the objectives of the thesis and their connection with the papers are summarized below in Table 2.1.

Table 2.1. The objectives of the thesis and their connection with papers.

Objective of the thesis	Paper
Synthesis of the active carbon with a diverse porosity applying the simultaneous use of salt and alkali, aiming to reduce the amount of alkali.	I and II
Study the pore formation mechanism disclosing the role of alkali and salt and the synergy between them.	I and II
Study the effect of chemical ratio, temperature and time on the porosity and yield of the prepared active carbons.	I and II
Techno-economic assessment of the novel method for producing active carbon with a high surface area and its potential benefit for the water treatment process.	III

3 Materials and methods

3.1 Materials

The industrial hydrolysis lignin from coniferous wood with 6.0–8.5% moisture from the waste stream of ethanol manufacturing from wood hydrolysate was used as a precursor. The reagents (Sigma-Aldrich) used for experiments were of analytical grade. NaOH and NaCl were used as received. KOH and KCl were vacuum-dried at 105 °C overnight before use. The nitrogen was of 99.999% purity. Deionized water was used for all purposes. Hydrochloric acid 0.1 M was used as a leaching agent and titrant.

3.2 Methods

3.2.1 Synthesis of active carbon

The lignin was mixed with alkali and salt in the mortar. The alkali was NaOH (Paper I) or KOH (Paper II and III). A salt was NaCl (Paper I) or KCl (papers II and III). The ratio between alkali and lignin varied between 0.1 and 3.0 g/g. The ratio between salt and lignin varied between 0.1 and 2.7 g/g. The alkali and salt were always used simultaneously. The *(alkali + salt)/lignin* ratio varied between 0.2 to 3.0 g/g. The obtained mixture containing alkali, salt and lignin was carbonized from 500 to 950 °C for 10 to 90 minutes at a 5 °C/min heating rate and 2 L/min of N₂ flow in a tube furnace. As soon as the carbonization is completed, in the case of the KOH-KCl mixture, some amount of elemental potassium is formed. To convert the metallic potassium to potassium hydroxide, the flow of N₂ was saturated by water. Next, the resultant mixture containing carbon and the side products was mixed with a leaching agent to wash out the residual salts and alkali. For NaOH and NaCl, the leaching agent was 0.1 mol/L HCl. For the mixtures containing KOH and KCl, the leaching agent was water. The carbon was separated from the leaching solution using a Buchner funnel and washed a few times until pH \approx 7. The obtained carbon using NaOH and NaCl was dried at 130 °C overnight at atmospheric pressure. The obtained carbon using KOH and KCl was dried at 105 °C overnight under vacuum.

3.2.2 Regeneration of chemicals

Within the process of activation, potassium hydroxide is transformed to atomic potassium and potassium carbonate through the redox reactions (Hayashi et al., 2002; Hüttinger & Minges, 1986). The temperature of the process (900–950 °C) is higher than the boiling point of the atomic potassium (759 °C). Consequently, the potassium is in gas form and condensed on the reactor parts (i.e. tube furnace), whose temperature is lower than the boiling point of elemental potassium. Vaporization of potassium hydroxide, potassium chloride and potassium carbonate is also probable at this temperature. Then the atomic potassium interacts with water of saturated nitrogen flow, which promotes the potassium hydroxide formation that remains on the inner parts of the reactor. Then, the chemicals

that participated in the process were quantitatively collected by water from the inner parts of the reactor. The content of hydroxide, carbonate, potassium and chloride in the water samples was analysed by potentiometric titration, ICP-OES and ion chromatography, respectively. The filtrate after leaching was analysed in the same manner. The recovery degree of KOH and KCl was estimated as the amount of the corresponding chemical used prior to the experiment and the amount estimated by the aforementioned methods. The experiments were replicated two or three times and standard deviation was calculated.

3.2.3 Characterization of obtained active carbons and the intermediate products

Structural properties of the produced carbons such as surface area, pore volume and pore size distribution were estimated from nitrogen physisorption isotherms obtained at 77 K using Tristar II® Micromeritics. Before nitrogen physisorption, samples were outgassed at 90 °C for 60 minutes and then at 350 °C for 240 minutes. Specific surface area (SSA) was estimated using the nitrogen physisorption at 77 K and calculated by the BET equation using the Rouquerol approach for the microporous materials (Brunauer et al., 1938; J. Rouquerol et al., 2007). Total volume of pores was estimated at $p/p^0=0.95-0.99$ using the corresponding amount of adsorbed nitrogen, its molar mass and density, following the Gurvich rule (Gurvich, 1915; Thommes et al., 2015). Volume of micropores was derived using the Dubinin-Radushkevich equation (Dubinin, M.M., Radushkevich, L.V., 1947). Mesopore volume was estimated as the difference between total pore volume and micropore volumes. The pore size distribution (PSD) was derived from nitrogen physisorption isotherms using non-local density functional theory (NLDFT), applying slit-like pores kernel for active carbons (Ravikovitch et al., 2000). To study the crystallinity of the materials and estimate the crystal size, X-ray powder diffraction (XRD) on a high-resolution PANalytical diffractometer applying Co K α radiation was used. The size of crystals was estimated from the diffractogram by applying the Williamson-Hall method (Williamson & Hall, 1953). To analyze surface functional groups of the samples, a Bruker Vertex 70 was used for Fourier transform infrared (FTIR) spectroscopy. The scanning electron microscopes (SEM) JEOL JSM-7900 and Hitachi S-4800 were used to get SEM images to visually study the surface texture of the materials. The transmission electron microscope (TEM) Hitachi H-7600 was employed to obtain TEM images for the same purposes. To study the thermal behaviour of the samples, a NETZSCH TG thermal analyser was used for thermogravimetric analysis (TGA) at a 5 °C/min from room temperature to 1000 °C. To study the exothermic and endothermic effects as well as calculating the heat balance of the process by estimating the enthalpy of the reactions (ΔH), the calibrated differential thermal analyser (DTA) Netzsch STA449F3 was used. Furthermore, to estimate the chemical reaction pathway using the information on the composition of the evolved gases, the quadrupole mass spectrometer (QMS) Netzsch QMS403D was used. The analytical equipment used for these studies is summarized in Table 3.1.

Table 3.1. Physico-chemical methods used in these studies.

Equipment	Purpose
Potentiometric titration	Determination of hydroxides and carbonates in the washing water samples
ICP-OES	Determination of potassium in the washing water samples
Ion chromatography	Determination of chlorides in the washing water samples
Nitrogen physisorption	Adsorption isotherms of N ₂ , SSA, PSD
X-ray powder diffraction (XRD)	Study the ordered structures of the materials
Fourier transform infrared (FTIR) spectroscopy	Chemical functional groups of the studied materials
Scanning electron microscope (SEM)	Textural properties of the materials
Transmission electron microscope (TEM)	
Thermal gravimetric analysis (TGA)	Thermal behaviour of the studied materials
Calibrated differential thermal analysis (DTA)	Exo- and endo-effects, estimation of the enthalpy of the process
Quadrupole mass spectrometry (QMS)	Composition of the evolved gases

3.2.4 Studies of the process factors on active carbon properties using RSM

The production of active carbons was mathematically described and optimized by the response surface method (RSM) (Box & Wilson, 1951). In accordance with the information in literature, the following process conditions were selected for the NaOH-NaCl-lignin mixtures (Fierro et al., 2007). The temperature was 600, 700 and 800 °C. The reaction time was 30, 60 and 90 minutes. The chemical ratio (NaOH-NaCl-to-lignin) ratio was 0.5, 1.0 and 1.5 g/g. The NaOH-to-NaCl ratio was kept constant at 4:6, according to the results in Paper I. Furthermore, samples were prepared at temperatures of 530 and 870 °C for 10 and 110 minutes and chemical ratios of 0.16 and 1.84 g/g. The KOH-KCl-to-lignin ratio was constant 3 g/g. Meanwhile, the amount of potassium hydroxide in the KOH-KCl-lignin mixture was 0.3, 0.9 and 1.5 g/g, and the amount of KCl was 2.7, 2.1 and 1.5 g/g. The high chemical ratio and the potassium-contained mixture were selected because (a) the high chemical ratio leads to a high surface area > 2500 m²/g (Marsh et al., 1982; Otowa et al., 1993; Wennerberg & O'Grady, 1978), (b) potassium is favourable compared to sodium in terms of high surface area and high yield (Fierro et al., 2007; Okada et al., 2003). As discussed above, the microporous structure originated through the elemental potassium intercalation between graphene layers. Metallic K is formed at a temperature above 700 °C (Otowa et al., 1993; Romanos et al., 2011). Therefore, the temperatures of 700, 800 and 900 °C were selected. Since the effect of time is less intensive among chemical ratio and temperature, this parameter was kept constant at 60 minutes. The specific surface area (m²/g) and yield (%) were selected as responses for

Depreciation is accepted to be 10% of the costs of the equipment (Peters et al., 2003). The MSP is determined at the corresponding selling price when NPV becomes zero and the IRR equals the discount rate (20%) (Ou et al., 2021; Vanreppelen et al., 2011). Values used for the economic assessment are presented in Table 3.1.

Table 3.1. Values used for economical assessment

Year of assessment	2021
CEPCI 2020/2008	596/575
Discount rate	20 %
Plant lifetime	10 years
Tax	20 %
CAPEX (Lima et al., 2008)	3 x Equipment Costs
OPEX (Peters et al., 2003)	
Depreciation	10 % of Equipment costs
Fixed costs	
Maintenance and repairs	10 % of Equipment costs
Operating supplies	15 % of maintenance and repairs
Labor	15 % of product costs
Supervision	15 % of labor
Administrative costs	20 % of labor
Sales and marketing	15 % of product costs

3.2.6 Estimation of the benefit of the use of active carbon with a high surface area for NOM adsorption

For this purpose, the adsorptive capacity for natural organic matter (NOM) of active carbon having a high surface area and the adsorptive capacity of commercial active carbon were determined. The water sample was gathered prior the active carbon process step at the on-site water treatment plant. The adsorptive capacity was estimated by the static method using the Freundlich isotherm (Perrich, 1981; Randtke & Snoeyink, 1983). The temperature was 23 °C, and the contact time was 17–19h (overnight). Each experiment was performed three times, and the standard deviation was calculated. In water, NOM is represented as total organic carbon (TOC). The initial concentration of TOC of water samples was 3.4–4.6 mg/L. The initial pH was 7.8. The required dose (g/m^3) of carbon to purify the water, prepared in this study and for commercial active carbon, is determined according to values of the adsorptive capacities of carbon, the TOC inlet concentration and the TOC limit. The costs to treat one cubic metre of water (EUR/m^3) are estimated based on the required dose and the price of active carbon.

4 Results and discussion

4.1 Synthesis of the active carbon with a diverse porous structure applying simultaneous use of salt and alkali

As discussed in the previous chapter, the diverse porous structure of active carbon is necessary for the desired applications. Furthermore, from the process economics standpoint, it is essential to produce the product with the lowest amount of chemicals. In the case of alkali activation, the chemical being consumed is alkali hydroxide (NaOH or KOH). Thus, the methods aiming at minimization of alkali consumption in the production of active carbon with a diverse porosity are worth developing. In this chapter, the textural properties, amount of used chemicals and yield of the samples prepared by using alkali metal chlorides and/or alkali hydroxide are discussed. Alkali metal is sodium or potassium. The results were published in Paper I and Paper II.

Based on the outcomes of present study, the application of NaOH-NaCl or KOH-KCl mixtures for the production of active carbons from lignin promotes an appreciable reduction in the amount of alkali, while the obtained carbons possess similar textural properties to NaOH- or KOH-activated carbons. Table 4.1 shows a comparison between process conditions and properties of the obtained active carbons from lignin using only NaOH or KOH and NaOH-NaCl or KOH-KCl. The data of samples prepared using only NaOH or KOH are adopted from the literature for comparison purposes (Fierro et al., 2007). Characteristics of the carbons produced by using NaOH-NaCl or KOH-KCl are taken from Paper I and Paper II of this study. The samples were prepared in accordance with the optimized process conditions discussed in Paper I. According to the literature, active carbons prepared at 1 g/g of NaOH or KOH have a surface area of 1100 m²/g and 0.5 cm³/g of the pore volume. The differences in textural properties are negligible whatever NaOH or KOH are used in the present process conditions. The yield of samples prepared using KOH is 50%, while NaOH-activated carbons have a lower yield of 40%. Carbon samples prepared by use of NaOH-NaCl mixture have a slightly lower surface area (< 1000 m²/g), pore volume (0.44 cm³/g) and yield (37%) compared to the literature data of samples prepared by NaOH activation. A larger surface area (> 1700 m²/g) and pore volume (0.6 cm³/g) can be achieved using a KOH-KCl mixture, while the yield is slightly lower (46%) compared to KOH-activated carbons. The temperature of carbonization was 870 °C for the mixtures of this study compared to 700 °C in the literature data (Fierro et al., 2007). The difference in processing time is negligible: 60 minutes and 47 minutes, respectively. While the surface area and pore volume of the active carbons prepared by the MOH-MCl (M=Na,K) mixture are similar or even higher compared to MOH-activated carbons, the amount of alkali used is substantially lower. In particular, the required amount of NaOH or KOH is 1 gram of alkali per 1 gram of lignin, while for the MOH-MCl combination, the alkali amount is only 0.24 g/g. The amount of MCl is 0.36 g/g. The total inorganic amount is 0.6 g/g, which is still lower than the amount

of alkali used. It is worth noting that the contribution of alkaline chloride to the chemical reaction with carbon is less intense or negligible compared to alkali hydroxide (Hüttinger & Minges, 1986). Thus, chloride can be easily recovered after use by evaporation, and its consumption can be neglected. In addition, the active carbons using an MOH-MCl mixture allow producing carbons with a similarly developed porous structure as alkali-activated carbons at a significantly reduced amount of alkali.

Table 4.1. Active carbons were prepared using NaOH, KOH, NaOH-NaCl and KOH-KCl from lignin.

Activation mixture	NaOH	KOH	NaOH-NaCl	KOH-KCl
Reference	(Fierro et al., 2007)	(Fierro et al., 2007)	Paper I	Paper II
Alkali metal (M)	Na	K	Na	K
MOH (g/g)	1	1	0.24	0.24
MCl (g/g)	-	-	0.36	0.36
Temperature (°C)	700	700	870	870
Time (min)	60	60	47	47
SSA (m ² /g)	1100	1100	998	1765
V _{micro} (cm ³ /g)	0.5	0.5	0.34	0.58
V _{total} (cm ³ /g)	0.5	0.5	0.44	0.61
Yield (%)	40	50	37	46

The textural properties of the carbons prepared by the use of an MOH-MCl are described with the help of nitrogen physisorption isotherms and NLDFT pore size distribution taking into account IUPAC recommendations (Figure 4.1) (Thommes et al., 2015).

Both samples, whichever mixture was used in their preparation (NaOH-NaCl or KOH-KCl) possess a microporous structure with an appreciable amount of mesopore and macropores. The microporous structure can be concluded from the shape of the physisorption isotherm, which has a distinctive plateau beginning at low relative pressure ($< 0.1 p/p^0$) due to micropore filling. This is an adsorption isotherm Type I of microporous solids (Sing, 2013; Thommes et al., 2015). NLDFT pore size distribution also exhibits the most intensive peaks attributed to the pore size of less than 2 nm. The sample prepared by the mixture of KOH-KCl demonstrated high nitrogen uptake at relative pressure below 0.1 p/p^0 promoting a higher surface area and micropore volume compared to the samples prepared by NaOH-NaCl (Table 4.1).

In addition to that, isotherms also show the adsorption hysteresis H4, which is ascribed to the mesopore and macropore filling or emptying through the capillary condensation. Thus, the active carbons have developed mesoporosity. Peaks of mesopores and macropores can also be observed from the NLDFT pore size distribution. Furthermore, materials prepared by the sodium hydroxide-chloride mixture exhibit enhanced adsorption hysteresis and more pronounced NLDFT peaks of mesopores and macropores. In other words, samples prepared by NaOH-NaCl mixture are more mesoporous and macroporous, unlike KOH-KCl-activated carbons. According to the previous studies,

NaOH-activated carbons might have fused micropores into mesopores (or even macropores) due to strong burn-off facilitated by NaOH compared to KOH (Fierro et al., 2007; Sing, 2013). Moreover, potassium atoms induce microporosity better because of the appropriate atom size among other atoms of alkali metals (Li, Na, Rb and Cs) (Jiménez et al., 2009; Okada et al., 2003).

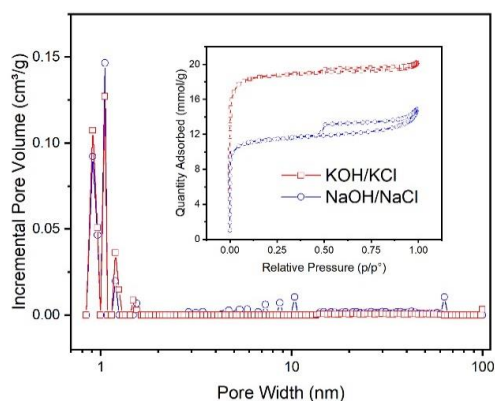


Figure 4.1. NLDFT pore size distribution and nitrogen physisorption isotherms (inset) of active carbons prepared by MOH/MCl (M=Na,K) (Paper II).

Active carbons produced applying NaOH-NaCl or KOH-KCl demonstrated a developed porous structure having dominated micropores among mesopores and macropores. Potassium-contained mixtures promote microporosity and a higher surface area, while sodium-contained mixtures also lead to a developed microporosity but with a more noticeable mesoporous and macroporous structure. In addition, using the mixture of alkali hydroxide and alkali metal chloride, the active carbons with a developed porosity can be produced with a substantially reduced amount of the alkali.

4.2 Study of the pore formation mechanism disclosing the role of salt, alkali and the synergy between them

As discussed in the introduction, pores are formed through (a) elemental alkali metal intercalation between graphene layers, (b) carbon matter consumption due to redox reactions between precursor (e.g. carbon and/or lignin) and alkali hydroxide or alkali metal chloride (gasification) and (c) self-templating. All these mechanisms are discussed below, disclosing the alkali and salt contribution to the origin of the porous structure.

4.2.1 The role of alkali

Chemical reactions between precursor and alkali

To get insight into the chemical reaction pathway, the solid products of the resulting carbon-salt mixture using mixtures of lignin and sodium chloride; lignin and sodium hydroxide; lignin and NaOH-NaCl together, after carbonization, were analysed by FTIR and XRD. In addition, TGA was performed for the non-carbonized starting mixtures. The results are presented in Paper I.

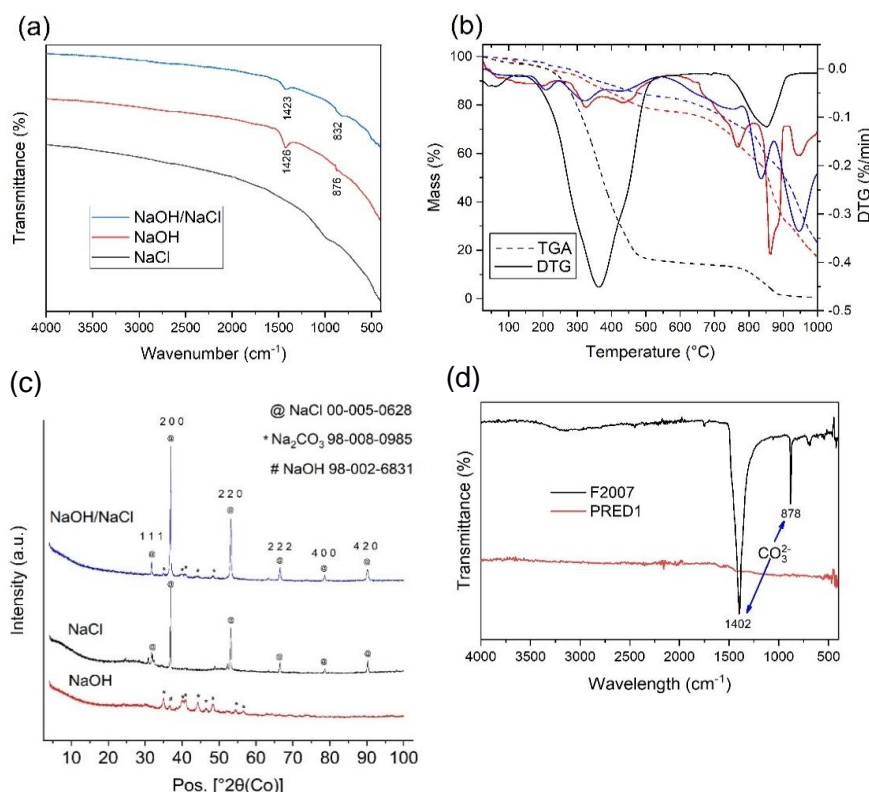


Figure 4.2. FTIR spectra (a), TGA/DTG curves (b) and XRD spectra (c) of carbon samples before leaching using starting mixtures of lignin-NaCl, lignin-NaOH and lignin-NaOH-NaCl (Paper I), FTIR spectra (d) of carbon samples before leaching using mixtures of lignin-KOH (F2007) and lignin-KOH-KCl (PRED1) (Paper II).

FTIR peaks related to carbonates (1423 , 1426 cm^{-1} and 832 , 876 cm^{-1}) were observed for active carbons before leaching of the carbonized samples prepared by NaOH and NaOH-NaCl (Fig. 4.2a) (Featherstone et al., 1984). The X-ray diffraction peaks of the standard Na_2CO_3 pattern (ICSD98-008-0985) were also found in samples obtained by NaOH-NaCl (Fig. 4.2c). Moreover, the characteristic peak of Na_2CO_3 thermal decomposition at 835 $^{\circ}\text{C}$ was also observed on the DTG curve (Fig. 4.2b) (Kim et al., 2001). These findings

allow assuming the possible formation of sodium carbonate from sodium hydroxide during the carbonization stage.

The carbonized samples of the starting mixtures containing lignin-KOH-KCl (sample PRED1) were studied in a similar way to sodium-contained mixtures using FTIR (Figure 4.2d) and XRD (Figure 4.5a, next section). The results are presented in Paper II. Furthermore, water-washing samples were analysed (Paper III). The sample PRED1 was prepared at 900 °C according to the optimal conditions defined in the present studies of Paper II. Peaks assigned to the carbonates were not found on the FTIR spectra of the sample PRED1 prepared at 900 °C using lignin-KOH-KCl unlike the sample prepared using only KOH at 700 °C (878 and 1402 cm^{-1}). Moreover, X-ray diffraction peaks of potassium carbonate were not found on the XRD spectra (Fig. 4.5a, next section). Consequently, potassium carbonate was not found in the solid mixture of the carbonized lignin-KOH-KCl mixture. On the other hand, 21–24% of potassium carbonate was found by potentiometric titration in the resulting washing water sample containing KOH and K_2CO_3 after carbonization at 950 °C (results from Paper III). Therefore, potassium carbonate is formed, but it was only detected in the washing water sample and was not found in the solid sample. In addition to that, the elemental potassium was observed visually after the carbonization process of the sample PRED1 (Figure 4.3).

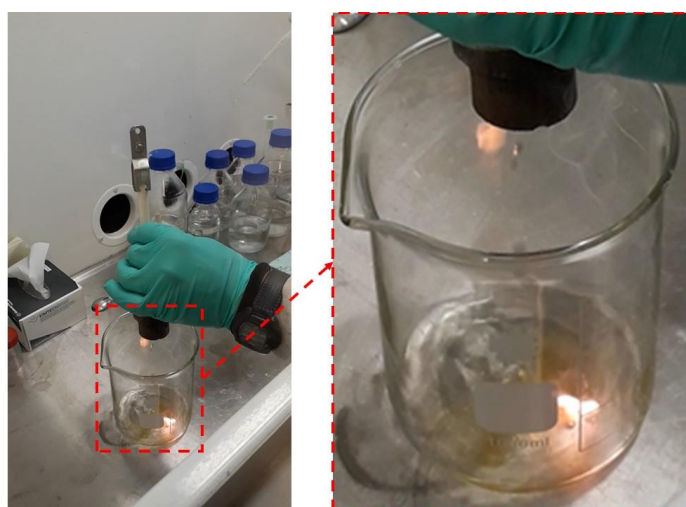


Figure 4.3. The observed metallic potassium formed inside the insulation plugs of the tube furnace.

In the accordance with the aforementioned outcomes, it can be deduced that the alkali metal carbonate (Na or K) is formed at the temperature range of 700–950 °C. Elemental potassium was also visually observed for the lignin-KOH-KCl mixture prepared at 900–950 °C. Potassium carbonate is the resultant product of the chemical reactions (1.5), (1.9) and (1.10), while elemental potassium is the product of the chemical reactions (1.4), (1.5),

(1.7), (1.8) and (1.11). Thus, all of these reactions are possible. However, it is still difficult to estimate the exact chemical reaction pathway using only the information of the resultant solid products (i.e. K_2CO_3 and K).

For this purpose, the evolved gases were analysed using mass spectrometry (Fig 4.4 b,d). Furthermore, differential thermal analysis was employed to evaluate the thermal behaviour of the process (endothermic or exothermic nature). To analyze the evolved gases and the thermal behaviour of the lignin-KOH-KCl mixture, DTA-MS analysis was applied. Figure 4.4 shows DTA, DTG curves (left side) and MS (right side) peaks of lignin (Fig.4.4a,b) and a mixture of lignin-KOH-KCl (Fig. 4.4c,d). Based on the literature, the following gaseous products evolved during the pyrolysis, and/or gasification was analyzed using MS (Alcañiz-Monge & Illán-Gómez, 2008; Faix et al., 1988; Sams & Shadman, 1986; Wigmans et al., 1983): H_2 ($m/z=2$), CH_3^+ ($m/z=15$), CH_4 or O^+ ($m/z=16$), H_2O ($m/z=18$), CO or $H_2C=CH_2$ ($m/z=28$), CO_2 ($m/z=44$).

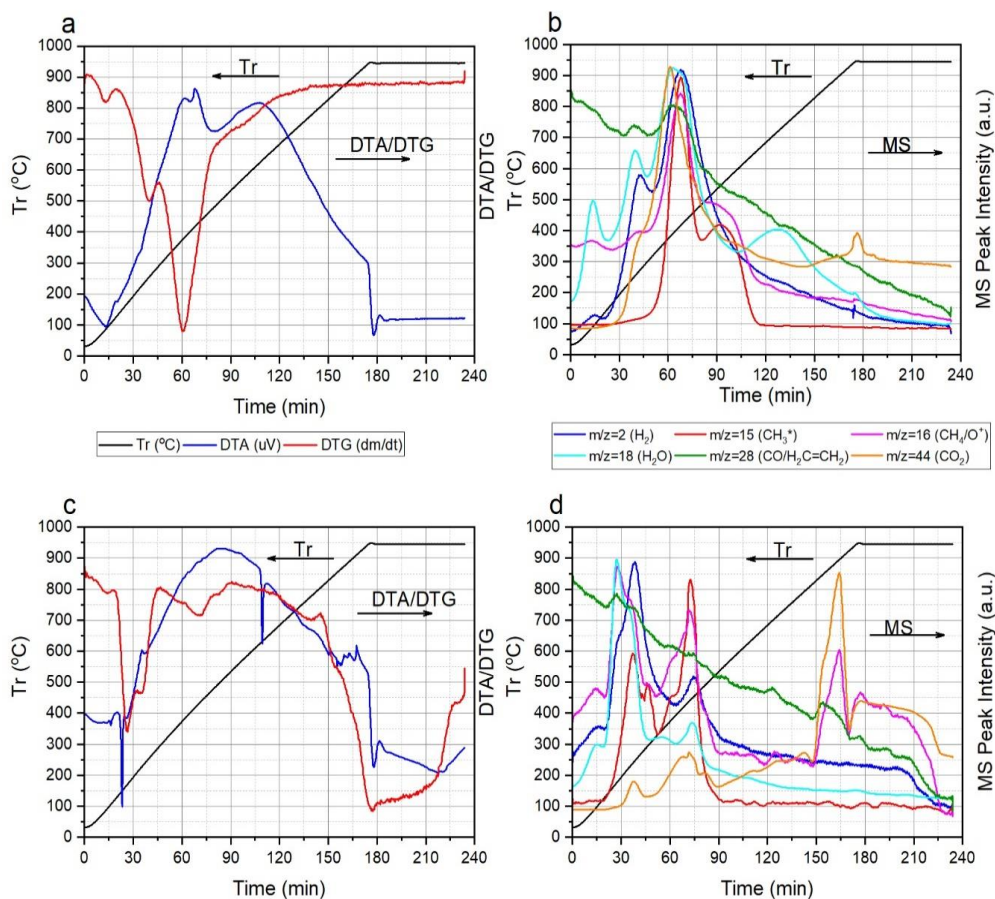
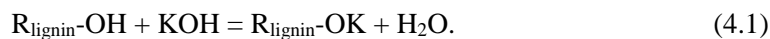


Figure 4.4. DTA, DTG and MS spectra of lignin (a,b) and lignin-KOH-KCl (c,d).

To understand how lignin behaves in the entire process temperature range without KOH and KCl, the lignin sample was analyzed for comparison because it has no added chemicals. Figure 4.4a and b show the DTA, DTG (Fig. 4.4a) and MS of evolved gases (Fig. 4.4b) of lignin. Figure 4.4a demonstrates a DTG peak at 100 °C related to vaporized water, two other DTG peaks and one shoulder related to the mass loss that occurred at carbonization of lignin at 250, 400 and 600 °C, respectively. Figure 4.2a also shows one endothermic DTA peak at 100 °C associated with heat consumption for water vaporization, and two exothermic DTA peaks related to the heat release due to carbonization of lignin at 400 and 600 °C, respectively. Figure 4.4b shows that the gases that evolved at 150–600 °C are related to the thermal decomposition of lignin with the most appreciable release of gas at 350–450 °C, which is accompanied by the most severe mass loss at a similar temperature (Faix et al., 1988). The small release of CO₂ at 950 °C could be explained by the decomposition of potassium carbonate, which is a common component of ash (Knudsen et al., 2004). However, the mass loss (DTG) or heat flow (DTA) was not observed probably because its content in lignin is negligible.

In Figure 4.4, the DTG, DTA curves (Fig.4.4c) and MS spectra of gaseous products (Fig.4.4d) are demonstrated for the lignin-KOH-KCl mixture. Water evaporates at 50–145 °C with related mass loss (DTG), endothermic valley (DTA) and a small MS peak of H₂O. The strong and sharp endothermic peak is observed at 150 °C. The shape, sharpness, absence of mass loss and endothermic nature of the peak suggests that the melting occurred at this temperature. But lignin does not possess a clear melting point at this temperature range and the KOH-KCl mixture melts at a significantly higher temperature. However, it is well-known that phenolic hydroxyls of lignin interact with KOH with the formation of phenoxides (phenolates) (Azarov, V.I., Burov, A.V., and Obolenskaya, 1999):



Moreover, the reactions of destruction and condensation have led to lignin softening in the presence of alkali (results of Paper I). Therefore, it can be assumed that the melting at 150 °C is associated with the melting of lignin phenoxides and products of destruction/condensation.

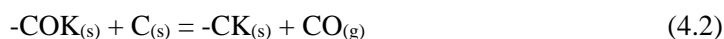
Next to the peak of melting, there are two significant DTG peaks at 170–235 °C and 440 °C, with the most essential gas formation observed on mass spectra (Fig. 4.4d) due to lignin carbonization. Note that there is an appreciable release of water at 170 °C due to lignin condensation in the presence of alkali (Azarov, V.I., Burov, A.V., and Obolenskaya, 1999; Faix et al., 1988). The DTA curve in Fig. 4.4c shows one big exothermic peak from 175 °C to the isothermal range related to exothermic lignin carbonization. There are two small endotherms at 175 and 235 °C related to the corresponding mass loss.

There is a sharp and strong endothermic peak in the fusion of the eutectic mixture of potassium hydroxide and potassium chloride at 630 °C. The mass loss and gas evolution

were not observed at this temperature. This value is lower compared to the database value (690–700 °C) (FACT Database, 2022). This might be because either the conditions are different, the composition of the eutectic mixture is different (contaminated with phenoxides) or the amount of KCl can also be consumed for some chemical interactions with lignin and the amount of KOH became higher leading to the melting point reduction of the eutectic mixture (Knudsen et al., 2004).

Starting from 800 °C to the end of the process (isothermal 950 °C), a significant mass loss is observed with the biggest DTG peak (Fig.4.4c) and the corresponding release of CO₂ and O⁺ followed by CO. As mentioned above, redox reactions take place. The potassium of KOH is reduced to atomic potassium, which is the product of these reactions. The elemental potassium is in a gas phase at these conditions (boiling point is 759 °C). KOH could also be transformed into a potassium carbonate (reactions (1.5), (1.9) and (1.10)). In support of K₂CO₃ formation, the small DTA peak at 900±2.5 °C is related to its melting in similar conditions in the N₂ or CO₂ atmosphere (Lehman et al., 1998). Gaseous products such as CO₂ and CO are observed in mass spectra at a temperature above 800 °C (Fig.4.4d). These could be products of the chemical reactions (1.1)–(1.4), (1.7) and (1.11). However, the evolved gases of reactions (1.1), (1.3) and (1.4) also consist of H₂O and H₂, which are not observed in these mass spectra. Therefore, these reactions are questionable in this case. Only chemical reactions (1.2), (1.7) and (1.11) show the evolution of CO. Meanwhile, carbon dioxide is not evolved together with CO according to the (1.1)–(1.11) reactions as it is observed on MS spectra (Fig.4.4d). Moreover, these reactions cannot explain the formation of atomic O⁺. The formation of CH₄ (m/z=16) is highly unlikely since it is usually accompanied by a free radical CH₃· that is not observed on MS (Fig. 4.4d) (Faix et al., 1988). In addition, chemical reactions (1.1)–(1.11) were studied for materials that mainly consist of carbon, unlike lignin with an aromatic structure containing various functional groups. Therefore, there should be an additional source of CO₂ and O⁺.

According to previous studies, functional groups of charcoal and wood, including phenolic hydroxyls of lignin could interact with KOH, K₂CO₃ and KCl with a formation of atomic potassium (Hashimoto et al., 1986; Johansen et al., 2011; Knudsen et al., 2004; Okuno et al., 2005; Sams & Shadman, 1986; Wigmans et al., 1983). Taking into account the chemical reaction (4.1) of potassium phenoxide formation, the interaction between -COK and char could be possible (Ehrburger et al., 1986; Mims & Pabst, 1983; Sams & Shadman, 1986):



The char of reaction (4.3) is the product of lignin carbonization and its amount above 500 °C is significant. Atomic potassium and CO₂ could also originate from a chemical reaction (Hashimoto et al., 1986; Okuno et al., 2005; Wigmans et al., 1983):

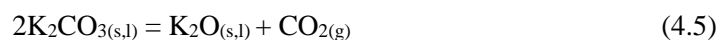


where C(O) is an oxygen-containing functional group, M(O) is –COK and M is K in the present case.

Both CO and CO₂ are evolved according to reactions (4.2) and (4.4) without the formation of H₂O or H₂ and therefore possible in the present case since CO and CO₂ are observed in mass spectra while H₂O and H₂ are not observed (Fig.4.4d). It is worth noting that potassium chloride could also be a source of phenoxides (reaction (4.1)) and therefore involved in the chemical reactions (4.2)–(4.4) (Johansen et al., 2011; Knudsen et al., 2004; Okuno et al., 2005).

However, chemical reactions (4.2) and (4.4) do not explain the formation of O⁺ (m/z=16), which is observed in mass spectra with appreciable intensity (Fig.4.2d). According to the general culture, KOH easily interacts with CO₂ with a formation of K₂CO₃ (reaction (1.9)). One can see in MS (Fig.4.2b) that the essential amount of CO₂ is formed during lignin carbonization, which can further interact with KOH through the chemical reaction (1.9). Thus, potassium carbonate can also be formed by chemical reaction (1.9), whose DTA melting peak is observed at 900±2.5 °C (Lehman et al., 1998). Moreover, according to the results mentioned above, potassium carbonate was found in the washing water samples and detected by FTIR and XRD in the solid sample of carbon before leaching.

In light of the previous literature findings, the potassium carbonate does decompose with a formation of potassium oxide and carbon dioxide (Knudsen et al., 2004):



The formed K₂O in turn decomposes with a formation of atomic potassium and oxygen, which can be detected as O⁺ (m/z=16) in mass spectra (Fig.4.2d) (Knudsen et al., 2004; Simmons et al., 1977):



Chemical reaction (4.5) is an additional source of carbon dioxide as well as reaction (4.4) and probably the main chemical reaction pathway of CO₂ formation rather than chemical reaction (4.4) since it is accompanied by chemical reaction (4.6). In other words, CO₂ is formed starting from 800 °C due to the potassium carbonate decomposition that was formed by the interaction of KOH and CO₂ (reaction (1.9)). Chemical reaction (4.6) explains the formation of O⁺, which further allows assuming a reaction pathway through chemical reactions (4.5) and (4.6). Moreover, a wide endothermic DTA peak is observed at 800–880 °C, and the process starts right after the melting of K₂CO₃ (at 910 °C) has occurred with a heat consumption that further supports the assumed reactions (4.5) and (4.6) that are also endothermic (Simmons et al., 1977).

Based on the abovementioned results and previous studies, it can be assumed that metallic potassium and CO₂ could originate from the decomposition of potassium carbonate, which, in turn, was formed by the interaction between alkali and CO₂ of lignin carbonization (chemical reactions (4.5) and (4.6)). Also, the formation of atomic potassium, as well as CO and CO₂, could be justified by the carbon gasification where oxygen-containing functional groups are involved (chemical reaction (4.2)–(4.4)). CO formation is also possible through chemical reactions (1.2), (1.7) and (1.11).

All in all, the chemical reaction pathway could be summarized in Table 4.2 (below). The elemental potassium that is responsible for the micropores' origin is formed through the decomposition of potassium carbonate that is formed in situ from potassium hydroxide and evolved CO₂ during lignin carbonization. In addition to that, elemental potassium could be reduced from the phenoxides of lignin.

Table 4.2. Possible chemical reactions of lignin-KOH-KCl mixture at 30-950 °C.

Temperature (°C)	Chemical reaction or physical process	Number
30-150	$H_2O_{(sorbed)} = H_2O_{(g)}$	-
	$R_{lignin}-OH + KOH = R_{lignin}-OK + H_2O$	(4.1)
	$R_{lignin}-OH + KCl = R_{lignin}-OK + HCl$	(4.7)
150	$R-OK_{(s)} = R-OK_{(l)}$	-
Starting at 150	Lignin = Char + Gases (<i>incl. CO₂</i>) + Liquid + Tar	-
	$2KOH + CO_2 = K_2CO_3 + H_2O$	(1.9)
630	$(KOH-KCl)_{(s)} = (KOH-KCl)_{(l)}$	(4.1)
Starting at 800	$K_2CO_{3(s,l)} = K_2O_{(s,l)} + CO_{2(g)}$	(4.5)
	$K_2CO_{3(s,l)} + 2C_{(s)} = 2K_{(g)} + 3CO_{(g)}$	(1.11)
	$C + CO_2 = 2CO$	(1.2)
	$2K_2O = 4K_{(g)} + 2O_{2(g)}$	(4.6)
	$K_2O + C = 2K + CO$	(1.7)
	$-COK_{(s)} + C_{(s)} = -CK_{(s)} + CO_{(g)}$	(4.2)
	$-CK_{(s)} = K_{(g)} + C_{(s)}$	(4.3)
$C(O) + M(O) = M + CO_2$	(4.4)	

Self-templating

Another possible role of alkali is self-templating. Inorganic particles of NaOH or KOH may create pores or channels similar in size to their particles (Marsh & Rodríguez-Reinoso, 2006a). In particular, the macropore formation could be assumed through the self-templating mechanism by KOH grains (Li et al., 2014; W. Zhang et al., 2015). The SEM image in Paper II shows macropores before leaching (Figure 4.5d) and after leaching (Figure 4.6a–e) of active carbons, which probably originated from KOH grains since their size is larger than the observed KCl crystals (Fig 4.5b,c). The grains of KOH were not found in samples before leaching since potassium hydroxide had been evaporated and decomposed, leaving macropores from the sample during the

carbonization process. Consequently, alkali could also be responsible for the formation of macropores through self-templating.

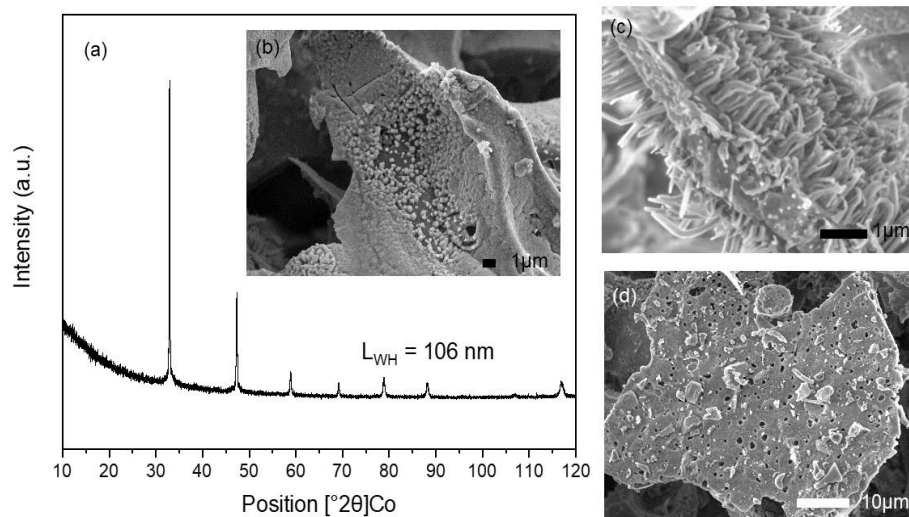


Figure 4.5. Superactive carbon before leaching: XRD spectra indicating KCl diffraction peaks (a); SEM images: KCl crystals (b), KCl dendrite-like structures (c), KCl formations around macropores (d) (Paper II).

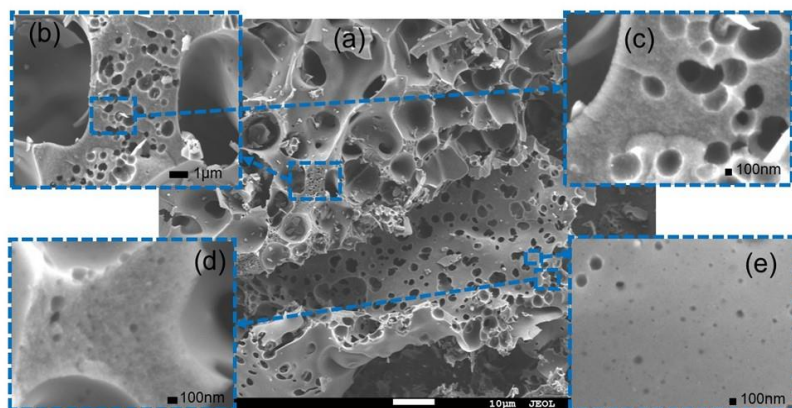


Figure 4.6. Superactive carbon after leaching: SEM micrographs (a)-(e) (Paper II).

4.2.2 The role of salt

NaCl and KCl could be the template of macropores since their crystal size is the same as the macropore size. In Paper I, XRD and SEM crystal sizes of NaCl (70 and 50–100 nm, respectively) are of the same order as NLDFT and SEM macropore sizes of 63.2 and 40–80 nm, respectively. A similar template mechanism was observed for the KOH-KCl mixture (Paper II). In Figure 4.5b, the cubic KCl crystals have the same size as macropores, which are about 100 nm. There are also amorphous dendrite-like shapes of KCl whose size (the base of the dendrite) is comparable to macropores (Fig.4.5c) (Broström et al., 2013; Wang & Tan, 2019). Therefore, the NaCl or KCl template origin of macropores could be assumed to be similar to the alkali self-templating mechanism.

In addition, NaCl or KCl could interact with phenolic hydroxyls of lignin with a formation of phenoxides (Yin et al., 2020):



Moreover, there is also possible catalytic gasification of carbon in which NaCl or KCl are involved (Arnold & Hill, 2019). Potassium chloride is a more active gasification catalyst than NaCl (Veraa & Bell, 1978). The sample prepared using a KOH-NaCl mixture demonstrated a reduced surface area (2435 m²/g), unlike the sample (2938±42 m²/g) that was prepared by KOH-KCl under the same process conditions (Paper II). Therefore, there might be a catalytic effect of NaCl and KCl, and samples prepared using KCl salt are more ‘activated’ because of the higher catalytic activity of the latter. The salt is not only a template. Consequently, the role of salt in the porous structure formation is self-templating, and it contributes as a catalyst. Furthermore, NaCl or KCl could be an additional source of the elemental alkali metal through the phenoxide formation.

4.2.3 A synergy between salt and alkali

As discussed above, a high surface area of active carbons could be achieved using salt and the alkali at a reduced amount of the latter (Table 4.1). To find out the underlying efficiency of the method, the possible synergy between potassium hydroxide and potassium chloride is discussed here.

In papers I and II, the formation of micropores on the walls of macropores was assumed based on experimental findings that are in agreement with the previous studies (Morishita et al., 2010). Thus, macropores provide additional places for micropores, and therefore the surface area is increased. In the present case, the salt template creates the additional formation of macropores, which further facilitates reduced alkali consumption for self-templating, and more alkali could be contributed to the metallic potassium formation, which is an origin of micropores (i.e. surface area). This mechanism is schematically presented in Figure 4.7. Moreover, the catalytic effect of the salt template of micropores genesis could be enhanced by alkali. In particular, the activity of the catalyst for gasification is reinforced if its melting point is decreased due to the wetting behaviour

(Hüttinger & Minges, 1985; Veraa & Bell, 1978). In the case of the KOH-KCl mixture, the melting point of the eutectic mixture is below the melting point of sole KCl, and therefore the enhanced catalytic effect of KCl takes place.

Consequently, the synergy between alkali and a salt template could be explained by the additional macropore formation via the salt template and promoted salt catalytic activity due to the reduced melting point of the eutectic mixture KOH-KCl.

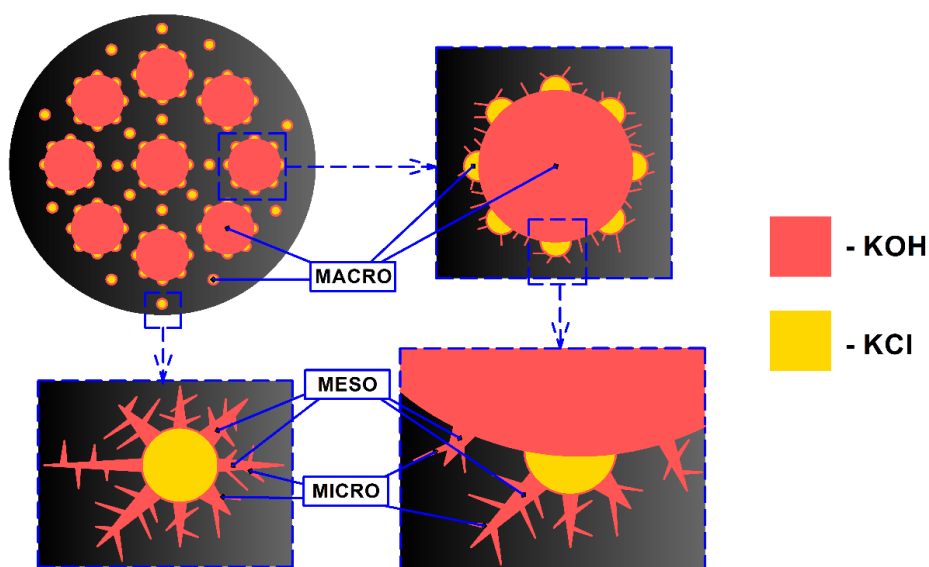


Figure 4.7. Scheme of the pore origin using KOH and KCl simultaneously (Paper II).

4.3 Influence of chemical ratio, temperature and time on the porosity origin and yield of the prepared active carbons

4.3.1 Parameters which promote the most developed porosity and yield at the minimized consumption of alkali

The porous structure of active carbon as well as its yield are a function of many parameters: precursor type and its structure; chemicals used, impregnation or direct mixing, leaching conditions, chemical ratio, temperature, time, etc. Parameters that could be methodically controlled and have the strongest effect on the properties of the obtained carbon are temperature A ($^{\circ}\text{C}$), time B (min) and chemical ratio C (g/g) (Fierro et al., 2007).

In Paper I, the influences of these three factors on the surface area and yield of carbons prepared by NaOH-NaCl-lignin mixtures were studied. Applying the response surface method (RSM), the dependence of surface area and yield from the chemical ratio, temperature and time can be described mathematically. More specifically, the surface area of the process using lignin-NaOH-NaCl mixtures in a temperature range of 530–870 °C, a chemical ratio of 0.16–1.84 g/g and a time of 10–110 minutes does fit the quadratic model. The strongest influence on the surface area is demonstrated by the temperature with the highest regression coefficient of 272. Meanwhile, the chemical ratio and time possess a decreased effect on the surface area as well as having lower regression coefficients of 137 and 51, respectively. In other words, the extent of the effect of process factors on the surface area is reduced in the following order: temperature A > chemical ratio C > time B. The BET surface area quadratic model at $R^2=0.992$ and $p \ll 0.05$ is:

$$\text{BET} = 765 + 272A + 51B + 137C + 22AB + 74AC + 29BC + 22A^2 - 19B^2 - 53C^2 \quad (4.8)$$

The opposite situation is observed for the yield. According to the linear model, the yield decreases at the increased chemical ratio, temperature and time. It is worth noting that the most pronounced influence on yield is the chemical ratio because its regression coefficient demonstrates the most negative value (-6.61) followed by temperature (3.13) and time (-0.61). The yield linear model at $R^2=0.971$ and $p \ll 0.05$ is:

$$\text{Yield} = 37.48 - 3.13A - 0.60B - 6.61C \quad (4.9)$$

The process obeys the general rule: the higher the chemical ratio, temperature and time, the higher the porosity and the lower the yield (Fierro et al., 2007; Yue & Economy, 2017). This is explained by the progressive burn-off of carbon matter that promotes porosity development due to pore formation and the simultaneous yield decrease due to carbon matter consumption.

Using the desirability function, the optimal parameters to achieve the highest yield and surface area at the minimized chemical ratio (i.e. alkali consumption) can be derived (Harrington, 1965). These parameters are presented in Table 4.1 in the previous section, which includes a comparison with the literature data. According to the optimal conditions, to produce an active carbon sample with a surface area of 998 m²/g and a yield of 37%, the NaOH-NaCl-lignin mixture was prepared at a ratio of 0.24–0.36:1 g/g, at 870 °C for 47 minutes.

Similarly, the samples of active carbon were prepared at a higher chemical ratio (3 g/g) using KOH-KCl-lignin mixtures. The results are presented in Paper II. The surface area increases with the increase in the KOH amount in the KOH-KCl mixture, followed by the temperature increase. The regression coefficients of the SSA linear model are positive:

505 and 486 for the KOH amount and temperature, respectively. The model at $R^2=0.980$ and $p<<0.05$ is:

$$SSA = 2064 + 486A + 505B + 191AB \quad (4.10)$$

The yield decreases as the temperature and KOH amount increase. Temperature has the strongest influence on yield. The regression coefficients of the yield linear model are negative: -11.18 and -6.92 for the temperature and KOH amount, respectively. The model at $R^2=0.966$ and $p<<0.05$ is:

$$\text{Yield} = 41.77 - 11.18A - 6.92B - 6.34AB \quad (4.11)$$

where A is temperature ($^{\circ}\text{C}$), B is amount of KOH in the KOH/KCl mixture (g/g). The models described by equations (4.10) and (4.11) are valid in the framework of temperatures between 700 and 900 $^{\circ}\text{C}$ and between 0.3 and 1.5 g/g of KOH in the total 3 g/g of the KOH-KCl mixture. The optimal parameters derived from the obtained linear equations are KOH=1g/g, KCl=2g/g and $t=900$ $^{\circ}\text{C}$. These parameters allow producing active carbon having 2938 m^2/g of surface area at 29% of yield. It is worth noting that active carbon of high surface area (> 2500 m^2/g) can be produced at a 3–4 times lower amount of potassium hydroxide than the previously reported methods. The comparison with the literature information is presented in Table 4.3 (Paper II). In addition, parameters that promote the largest surface area and yield at the minimized consumption of alkali have been identified.

Table 4.3. The comparison of carbons having a high surface area.

Reference	(Otowa et al., 1993)	(Lozano-Castelló et al., 2001)	(Fierro et al., 2007)	This study
SSA, m^2/g	3100	3290	3100	2938
KOH amount, g/g	4	4	3	1
V_{micro} , cm^3/g	-	-	1.5	0.92
V_{total} , cm^3/g	1.5	1.45	1.7	1.29
Precursor	Petroleum coke	Spanish anthracite	Kraft lignin	Hydrolysis lignin

For comparison, the values of surface areas presented in Table 4.3 are higher than the maximum theoretical surface area of carbonaceous material of 2630 m^2/g , which is estimated from only one infinite graphene layer (Kaneko et al., 1992). However, this limit is not valid for active carbons since these materials possess irregular structures and cannot be considered well-ordered graphites.

4.3.2 Pore size control by varied process parameters

Among other properties, the adsorption performance of active carbon also depends on its pore size. Therefore, the possibility to control the size of pores is necessary to tune the carbon properties for the desired applications (Romanos et al., 2011). The experimental plan of Paper II also allows controlling pore size. In particular, the amount of KOH and temperature influence pore size distribution. Meanwhile, the effect of time was also investigated. In Figure 4.8, the NLDFT pore size distribution and physisorption isotherms are demonstrated for the active carbon samples prepared by varied KOH amounts, different temperatures and varied times. At 700 °C, homogeneous pore size distribution was observed, indicating the most probable micropore size of 1 nm followed by less intense peaks of 1.3 and 1.6 nm for active carbons prepared using varied KOH amounts of 0.3, 0.9 and 1.5 g/g, respectively. The physisorption isotherms of the samples prepared at 700 °C and 0.3 or 0.9 g/g of KOH amount coincide with Type I of microporous

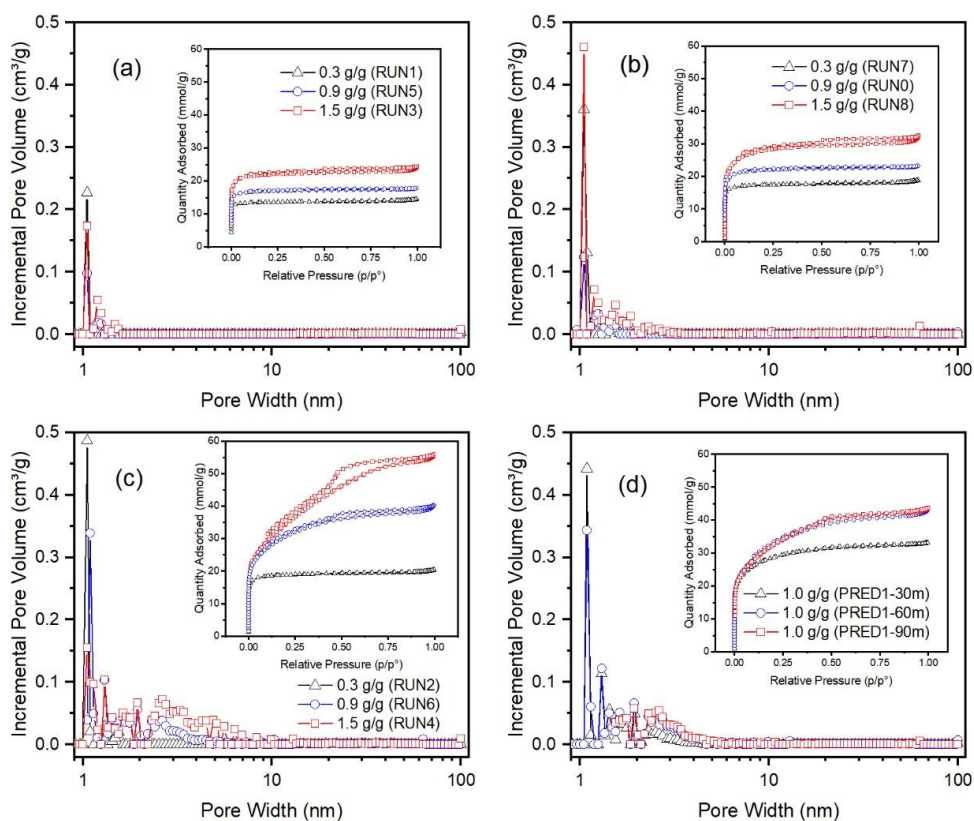


Figure 4.8. NLDFT pore size distribution and N₂ adsorption-desorption isotherms (insets) of superactive carbons prepared at different constant temperatures by varied KOH amounts: 700 °C (a), 800 °C (b), 900 °C (c); samples prepared at constant temperature and (900 °C) and KOH amount (1.0 g/g) by varied dwell time (d) (Paper II).

materials with no adsorption hysteresis. Meanwhile, the sample prepared at 700 °C and 1.5 g/g of KOH represents obscure adsorption hysteresis that could be attributed to mesopores or supermicropores (Sing, 2013; Thommes et al., 2015). However, peaks of mesopores are not observed in the NLDFT pore size distribution. Consequently, samples prepared at 700 °C are microporous showing micropore enlargement with the increasing amount of KOH.

At 800 °C, a diverse micropore size of 1–2 nm with the most significant peak at 1 nm is observed. The presence of supermicropores (> 1.7 nm) became noticeable for the sample prepared using 0.9 and 1.5 g/g of KOH. In addition, the sample prepared using 1.5 g/g demonstrates the mesopores formation that results in adsorption hysteresis due to capillary condensation. NLDFT shows peaks of mesopores with sizes of 2–3 nm. Thus, with an increase in temperature from 700 to 800 °C, the micropore expansion became more pronounced, and more supermicropores are formed. Moreover, some micropores are fused into mesopores. A similar tendency was observed related to the KOH amount increase – the pore size increases as well.

At 900 °C, micropore enlargement became more noticeable and incremental pore volume of micropores with a size over 1 nm is higher. At a target temperature of 900 °C and KOH amount of 0.9 and 1.5 g/g, the active carbon samples became micro-/mesoporous with a characteristic ascended curvature of N₂ physisorption isotherms at relative pressure $p/p^0 < 0.4$, desorption hysteresis type IV and peaks of NLDFT pore size distribution at 2–10 nm (Kruk et al., 1997; Thommes et al., 2015). The samples prepared at 0.3 g/g of KOH whatever target temperature was used (700, 800 or 900 °C) remain microporous.

The influence of time on structural properties was also evaluated. Figure 4.8d demonstrates NLDFT pore size distribution and adsorption isotherms of the samples produced at an unvaried amount of KOH (1 g/g) and target temperature (900 °C). The time was varied: 30, 60 and 90 min. There is almost no effect of a time increase (from 60 to 90 minutes) on the adsorbed nitrogen amount, isotherm shape and pore size distribution. Meanwhile, the reduced time to 30 min reduces the nitrogen uptake, and the pore size distribution became uniform. In this fashion, the increase in process time has a negligible influence on textural properties whilst decreased time reduces the adsorbed amount of nitrogen and diversity of pore size distribution. In other words, decreased time might prevent pore enlargement.

Consequently, with increasing temperature, KOH amount and time, the average pore size increases as well as nitrogen uptake. Among dominating micropores, supermicropores and mesopores are formed. As already discussed, burn-off is promoted by the increase in these two parameters, which results in developed porosity. Time has a negligible effect, but its decrease might facilitate uniformity of pore size distribution. All in all, by varying the KOH amount in the KOH-KCl mixture, temperature and time, the desired pore size can be achieved.

4.4 Techno-economic assessment of the production of the superactive carbon and its benefit for the water treatment process

4.4.1 Techno-economic assessment

To show the potential of producing superactive carbon on a bigger scale than the laboratory scale, a techno-economic assessment was accomplished. Toward this aim, a simplified process scheme, estimation of CAPEX, OPEX and MSP are discussed here. In addition, chemical recovery in the process is also accounted for this TEA.

The process diagram of the SAC production is discussed in this section and shown in Figure 3.1. The amount of lignin, chemicals, water, nitrogen and consumed energy is provided for one ton of the produced carbon (i.e. the product). Lignin from the silo (1) is transferred to the ball mill (2) where it is grinded with potassium hydroxide and potassium chloride. The amount of lignin is 3.7 t/t based on 27% of the yield. Taking into account the recovery degree (Table 4.4), the consumption of KOH and KCl is 0.32 and 0.18 t/t, respectively. The obtained lignin-KOH-KCl mixture is supplied to the furnace (3) where it is carbonized at 900–950 °C for 60 minutes in the nitrogen atmosphere. This process is continuous. The amount of nitrogen, 0.036 t/t, is fed to the furnace from the gas tank (13). In the cooler (4), to neutralize the formed elemental potassium, the nitrogen flow is mixed with water vapour. The leaching of chemicals from the produced carbon is carried out in the washing tank (5). The carbon is separated from the solution by solid-liquid separation (6). The solution containing chemicals is supplied to the dryer (12). After that, chemicals are transferred to a ball mill (2) where fresh chemicals are added according to the losses of 10% and 5% of KOH and KCl, respectively. The carbon after dewatering (6) goes through pelletization (7) and is dried (8) with a subsequent screening (9) for further storage (10) and packaging (11). To produce energy, the side products of the carbonization are burned in the combustor (14). The side products are pyrogas, condensed liquid and lignin tar. The flue gas from the incineration is cleaned using the cyclone (15). The overall heat consumption for the operation is 23.43 GJ/t or 6.51 MWh/t as well as consumed energy for carbonization (19.28 GJ/t), water vaporization of drying (12.93 GJ/t) minus heat release of the burned side products (8.78 GJ/t). Heat losses of 10% were assumed for this estimation. The values of lignin, chemicals, water and energy consumption are presented in Table 4.4.

Table 4.4. Consumptions of lignin, chemicals, water and energy.

Consumable	Quantity/t(product)	Cost per unit (EUR)
Hydrolysis lignin (t)	3.70	161.11 (Stavropoulos & Zabaniotou, 2009)
KOH (t)	0.32	331.83 (Alibaba, 2022b)
KCl (t)	0.18	330.50 (Alibaba, 2022a)
N ₂ (t)	0.036	2 500.00 (Vanreppelen et al., 2011)
Water (t)	1.01	5.00 (Bangalore Ashok et al., 2018)
Heat (MWh)	6.51	23.06 (Statistics Finland, 2022)
Electricity (MWh)	3.19	23.06 (Statistics Finland, 2022)

Active carbon having a high surface area is produced in this study using KCl and KOH at a significantly reduced amount of the latter compared to the previously reported methods (Table 4.3). From the process economics standpoint, chemicals used in the process should be recovered. For this purpose, KOH and KCl are regenerated. According to the activation mechanism, potassium hydroxide is transformed to atomic potassium and potassium carbonate through several chemical reactions (see Chapter 4.2). By the interaction with water, elemental potassium can be converted back to potassium hydroxide. The recovery degree of the potassium hydroxide and potassium carbonate mixture is 90±6% containing 24±1% of potassium carbonate. The values are in agreement with previous research findings (Ehrburger et al., 1986; Hilton et al., 2012; Montes & Hill, 2018; Yuan et al., 2012). It is worth noting that the presence of 24±1% of K₂CO₃ in KOH+K₂CO₃ does not significantly influence the final property of the superactive carbon. More specifically even a 100% substitution of KOH by K₂CO₃ results similar surface area of 2295-2690 m²/g and yield of 19-37% (Ponomarev, 2020). Therefore, contamination of potassium carbonate in the recovered chemicals will not negatively effect the properties of the obtained superactive carbon. Since potassium chloride is relatively inert compared to potassium hydroxide, its composition remains the same and its recovery degree is also high at about 94%. The results are summarized in Table 4.5. Using the values of the recovery degree, chemical consumption per one ton of the obtained carbon can be calculated.

Table 4.5. Recovery degree of the used chemicals.

Component	Recovery degree (%)
KOH+K ₂ CO ₃	91 ± 6
K ₂ CO ₃ of (KOH+K ₂ CO ₃)	23.9 ± 0.7
K ⁺	94 ± 3
Cl ⁻	94 ± 2

For the varied product capacity of 0.5-5.0 kt/y, the CAPEX ranges between 4.17 and 20.91 MEUR. The values are in agreement with the literature (Choy et al., 2005; Fingolo et al., 2020; Ko et al., 2004; Lima et al., 2008; Ng et al., 2003; Vanreppelen et al., 2011). The OPEX for these product capacities is in the range of 1.11–9.30 MEUR. The MSP decreases as the production capacity increases. For the product capacity of 0.5 kt/y, the MSP would be 4.36 kEUR/t. Meanwhile, the prices are 3.82, 3.39 and 2.93 for the production capacities of 1.0, 2.0 and 5.0 kt/y, respectively. The values of CAPEX, OPEX and MSP for the varied product capacity are summarized in Table 4.6.

Table 4.6. CAPEX, OPEX and MSP for the varied product capacity.

Capacity (kt/y)	CAPEX (MEUR)	OPEX (MEUR/y)	MSP (kEUR/t)
0.5	4.17	1.11	4.36
1.0	6.78	2.08	3.82
2.0	11.01	3.95	3.39
5.0	20.91	9.30	2.93

These values are higher than the price of commercial active carbon, which ranges from 1.0–2.5 kEUR/t and has a surface area of 500–1500 m²/g (Girods et al., 2009). However, the higher price of active carbon produced in the process designed here is justified since active carbon produced in this way possesses a higher surface area of over 2500 m²/g. Moreover, adopting the price-per-area approach (1000 m²/g = 2.0 kEUR/t), active carbon having a surface area of 2938 m²/g (Table 4.3) can be sold at almost 6 kEUR/t, which is substantially lower than the 4.36–2.93 kEUR/t in this study (Fingolo et al., 2020; Stavropoulos & Zabaniotou, 2009). Therefore, active carbon having a large surface area > 2500 m²/g produced by this method could be sold at an attractive price, and the method is promising for full-scale application.

4.4.2 Benefit for the water treatment process

Active carbon of high adsorptive capacity facilitates its reduced amount to treat the water. However, the large surface area does not obligatorily indicate high adsorptive capacity. To prove that active carbon of high surface area produced by the method of this study also possesses a high adsorptive capacity for NOM, it was tested with real water samples. Furthermore, for comparison purposes, the adsorptive capacity for NOM of commercial active carbon samples was estimated. The benefit of the use of high surface area carbon for the water treatment process was calculated.

Two water samples were used. The initial concentration of water samples #1 and #2 was between 4.6 and 3.4 mgTOC/L. The adsorptive capacity of the commercial active carbon (CAC) Norit Hydrodarco having a surface area of 560 m²/g is 48 and 39 mgTOC/g for water samples #1 and #2, respectively. The values are in agreement with the typical values of commercial active carbons, which range from 10–70 mg/L (Roberts & Summers, 1982). Meanwhile, the active carbon of high surface area (SAC), prepared in this study, demonstrated the adsorptive capacity of 906 and 620 mgTOC/g for water samples #1 and #2, respectively. The values are dozens of times higher compared to the values of the commercial active carbon. Thus, active carbon of a high surface area also demonstrates a high adsorptive capacity for NOM. The results of calculations are presented in Figure 4.9 and Table 4.7.

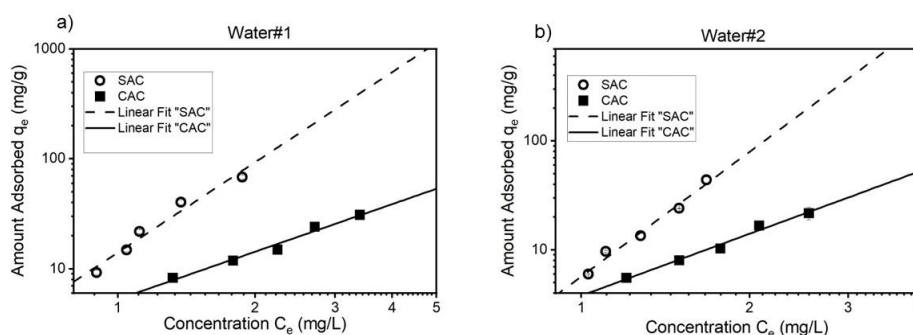


Figure 4.9. Natural organic matter (NOM) adsorption isotherms (a) and (b) of the commercial active carbon (CAC) and superactive carbon (SAC) (Paper III).

Applying the TOC limit of 2.0 mg/L (based on EU regulations, see 98/93/EC) and the inlet concentration of TOC (4.6 mgTOC/L), the dose to treat 1 m³ of water sample #1 using commercial active carbon is 0.184 kg/m³. Similarly, 0.101 kg/m³ is needed to treat water #2 since the inlet concentration is lower (3.4 mgTOC/L). Meanwhile, if active carbon prepared in this study is used for water treatment, the needed consumption of the adsorbent is significantly reduced and equals 0.028 and 0.018 kg/m³ to treat water #1 and #2, respectively. The average market price adopting the price-per-area approach or vendors' quotations, the price for active carbon having a surface area of around 500 m²/g is around 1 kEUR/t. Using the values of the needed dose and conventional active carbon price, the costs to treat water #1 and #2 are 18 and 10 EUR-cent/m³, respectively. As discussed above, active carbon of a high surface area prepared in this study could be sold at the price of 2.93–4.36 kEUR/t. Despite the higher selling price, since the adsorptive capacity is higher, which in turn promotes a substantial dose reduction, the costs to treat water #1 and #2 are 8–12 and 5–8 EUR-cent/m³. Consequently, the process savings of the use of active carbon having a high surface area are substantial – 34–55% for water #1

and 23–48% for water #2. Thus, there is a benefit to the water treatment process. The results are summarized in Table 4.7.

Table 4.7. Characteristics of water samples, CAC and SAC adsorptive capacities and parameters for the benefit evaluation of SAC for the water treatment.

Water sample	Water#1		Water#2	
	CAC	SAC	CAC	SAC
Initial concentration C ₀ , (mgTOC/L)	4.64 ± 0.06	4.6 ± 0.1	3.42 ± 0.00	3.4 ± 0.1
pH-initial	7.84	7.75	7.76	7.83
pH-final	8-8.55	7.8	8.1-9.0	7.8
Adsorptive capacity q (mgTOC/g- Carbon)	48 ± 1	906 ± 78	38.82	619 ± 83
Price, EUR/kg	1.00	2.93-4.36	1.00	2.93-4.36
Dose, kg/m ³	1.84·10 ⁻¹	2.80·10 ⁻²	1.01·10 ⁻¹	1.79·10 ⁻²
Costs (EUR-cent/m ³)	18	8-12	10	5-8
Costs savings (%)	-	34-55%	-	23-48%

5 Conclusion and future perspectives

In this study, using the mixture of lignin-NaOH-NaCl and lignin-KOH-KCl, the active carbons with high surface area and a diverse porous structure were produced with a substantially reduced amount of the alkali. The main activation pathway shows that alkali is the source of elemental potassium, which is responsible for the micropores' origin formed through the decomposition of potassium carbonate that is formed in situ from potassium hydroxide and evolved CO₂ during lignin carbonization. Furthermore, elemental potassium could be reduced from the oxygen-containing functional groups of lignin (e.g. phenoxides). Alkali could also be responsible for the formation of macropores through self-templating. The role of salt in the porous structure formation is self-templating, and there is a contribution as a catalyst. Moreover, NaCl or KCl could be an additional source of the elemental alkali metal through the phenoxide formation. A salt and alkali synergy could be explained by the additional formation of macropore via the salt template and promoted salt catalytic activity due to the reduced melting point of the eutectic mixture KOH-KCl. Parameters that promote the highest surface area (2938 m²/g) and yield (29%) at the minimized amount of alkali (1 g/g) have been defined. The parameters are t=900 °C, time=60 min, KOH=1 g/g and KCl=2 g/g. It is worth noting that active carbon with such a high surface area could be obtained at a substantial decrease in the amount of KOH, which is 3 to 4 times less than with the previous methods. By increasing or decreasing the KOH amount in the KOH-KCl mixture, the temperature and the time, the desired pore size can be achieved. The diversity of pore size increases as these parameters increase, and vice versa. Active carbon, having a high surface area of over 2500 m²/g produced by this method, could be sold at a competitive price (2.93–4.36 kEUR/t), and the method is promising for full-scale application. In addition, chemicals could be recovered after the process. The process savings for water purification are substantial – between 23% and 55% compared to commercial active carbon. Thus, there is a benefit to the water treatment process.

The method could be extended to different raw materials in addition to hydrolysis lignin. For example, precursors could be charcoal, fossil coal, wood, peat, etc. The effect of the starting material type and structure on the mechanism of activation as well as the porosity development could be studied. The benefit of active carbon having a high surface area prepared by this method could also be evaluated for different applications such as supercapacitors, gas storage, batteries, etc. In addition to that, the process might be scaled up and simulated in a continuous mode.

References

- Amer Alcañiz-Monge, J., & Illán-Gómez, M. J. (2008). Insight into hydroxides-activated coals: Chemical or physical activation? *Journal of Colloid and Interface Science*, 318(1), 35–41. <https://doi.org/https://doi.org/10.1016/j.jcis.2007.10.017>
- Alibaba. (2022a). *Potassium Chloride Price*. Alibaba.com
- Alibaba. (2022b). *Potassium Hydroxide Price*. www.alibaba.com
- Ando, N., Matsui, Y., Kurotobi, R., Nakano, Y., Matsushita, T., & Ohno, K. (2010). Comparison of natural organic matter adsorption capacities of super-powdered activated carbon and powdered activated Carbon. *Water Research*, 44(14), 4127–4136. <https://doi.org/10.1016/j.watres.2010.05.029>
- Arnold, R. A., & Hill, J. M. (2019). Catalysts for gasification: a review. *Sustainable Energy & Fuels*, 3(3), 656–672. <https://doi.org/10.1039/C8SE00614H>
- Azarov, V.I., Burov, A.V., and Obolenskaya, A. V. (1999). *Khimiya drevesiny i sinteticheskikh polimerov (Chemistry of Wood and Synthetic Polymers)*. SPbLTA.
- Bangalore Ashok, R. P., Oinas, P., Lintinen, K., Sarwar, G., Kostainen, M. A., & Österberg, M. (2018). Techno-economic assessment for the large-scale production of colloidal lignin particles. *Green Chemistry*, 20(21), 4911–4919. <https://doi.org/10.1039/C8GC02805B>
- Boos, D. (1970). *ELECTROLYTIC CAPACITOR HAVING CARBON PASTE ELECTRODES* (Patent No. US3536963A).
- Box, G. E. P., & Wilson, K. B. (1951). On the Experimental Attainment of Optimum Conditions. *Journal of the Royal Statistical Society. Series B (Methodological)*, 13(1), 1–45.
- Broström, M., Enestam, S., Backman, R., & Mäkelä, K. (2013). Condensation in the KCl–NaCl system. *Fuel Processing Technology*, 105, 142–148. <https://doi.org/10.1016/j.fuproc.2011.08.006>
- Brunauer, S., Emmett, P. H., & Teller, E. (1938). Adsorption of Gases in Multimolecular Layers. *Journal of the American Chemical Society*, 60(2), 309–319. <https://doi.org/10.1021/ja01269a023>
- Cao, Y., Wang, X., Gu, Z., Fan, Q., Gibbons, W., Gadhamshetty, V., Ai, N., & Zeng, G. (2018). Potassium chloride templated carbon preparation for supercapacitor. *Journal of Power Sources*, 384(February), 360–366. <https://doi.org/10.1016/j.jpowsour.2018.02.079>

- Choy, K. K. H., Barford, J. P., & McKay, G. (2005). Production of activated carbon from bamboo scaffolding waste—process design, evaluation and sensitivity analysis. *Chemical Engineering Journal*, 109(1), 147–165. <https://doi.org/10.1016/j.cej.2005.02.030>
- Chudakov, M. I. (1983). *Promushlennoe Ispolzovanie Lignina (Industrial Applications of Lignin)*. Lesnaya Promyshlennost.
- Dousek, F. P., & Jansta, J. (1975). Kinetics of electrochemical corrosion of polytetrafluorethylene by alkali metal amalgams. *Electrochimica Acta*, 20(1), 1–6. [https://doi.org/10.1016/0013-4686\(75\)85036-5](https://doi.org/10.1016/0013-4686(75)85036-5)
- Dousek, F. P., Jansta, J., Dubinin, M. M., Kadlets, O., Kataeva, L. I., & Onusaitis, B. A. (1975). Inhomogeneous micropore structures and adsorption properties of carbon adsorbents. 9. Microporous adsorbents with maximum development of the micropore volume. *Bulletin of the Academy of Sciences of the USSR, Division of Chemical Science*, 20(1), 849–854. <https://doi.org/10.1007/BF00957042>
- Dubinin, M. M. (1960). The Potential Theory of Adsorption of Gases and Vapors for Adsorbents with Energetically Nonuniform Surfaces. *Chemical Reviews*, 60(2), 235–241. <https://doi.org/10.1021/cr60204a006>
- Dubinin, M.M., Radushkevich, L.V. (1947). On the equation of the characteristic curve for active coals. *Doklady Akademii Nauk SSSR [Reports of the Academy of Sciences of the USSR]*, 4(4), 331–334.
- Ehrburger, P., Addoun, A., Addoun, F., & Donnet, J.-B. (1986). Carbonization of coals in the presence of alkaline hydroxides and carbonates: Formation of activated carbons. *Fuel*, 65(10), 1447–1449. [https://doi.org/10.1016/0016-2361\(86\)90121-3](https://doi.org/10.1016/0016-2361(86)90121-3)
- Evstigneyev, E. I., Yuzikhin, O. S., Gurinov, A. A., Ivanov, A. Y., Artamonova, T. O., Khodorkovskiy, M. A., Bessonova, E. A., & Vasilyev, A. V. (2016). Study of Structure of Industrial Acid Hydrolysis Lignin, Oxidized in the H₂O₂-H₂SO₄ System. *Journal of Wood Chemistry and Technology*, 36(4), 259–269. <https://doi.org/10.1080/02773813.2015.1137945>
- FACT Database. (2022). *KCl-KOH phase diagram*. http://www.crct.polymtl.ca/fact/phase_diagram.php?file=KCl-KOH.jpg&dir=FTsalt
- Faix, O., Jakab, E., Till, F., & Székely, T. (1988). Study on low mass thermal degradation products of milled wood lignins by thermogravimetry-mass-spectrometry. *Wood Science and Technology*, 22(4), 323–334. <https://doi.org/10.1007/BF00353322>

- Featherstone, J. D. B., Pearson, S., & LeGeros, R. Z. (1984). An Infrared Method for Quantification of Carbonate in Carbonated Apatites. *Caries Research*, 18(1), 63–66. <https://doi.org/10.1159/000260749>
- FEECO International. (2022). *Activated Carbon: A Growing Market of Opportunity*. <https://feeco.com/activated-carbon-a-growing-market-of-opportunity/>
- Fierro, V., Torné-Fernández, V., & Celzard, A. (2007). Methodical study of the chemical activation of Kraft lignin with KOH and NaOH. *Microporous and Mesoporous Materials*, 101(3), 419–431. <https://doi.org/10.1016/j.micromeso.2006.12.004>
- Fingolo, A. C., Klein, B. C., Rezende, M. C. A. F., Silva e Souza, C. A., Yuan, J., Yin, G., Bonomi, A., Martinez, D. S. T., & Strauss, M. (2019). Techno-Economic Assessment and Critical Properties Tuning of Activated Carbons from Pyrolyzed Sugarcane Bagasse. *Waste and Biomass Valorization*. <https://doi.org/10.1007/s12649-019-00774-y>
- Fingolo, A. C., Klein, B. C., Rezende, M. C. A. F., Silva e Souza, C. A., Yuan, J., Yin, G., Bonomi, A., Martinez, D. S. T., & Strauss, M. (2020). Techno-Economic Assessment and Critical Properties Tuning of Activated Carbons from Pyrolyzed Sugarcane Bagasse. *Waste and Biomass Valorization*, 11(8), 1–13. <https://doi.org/10.1007/s12649-019-00774-y>
- Girods, P., Dufour, A., Fierro, V., Rogaume, Y., Rogaume, C., Zoulalian, A., & Celzard, A. (2009). Activated carbons prepared from wood particleboard wastes: Characterisation and phenol adsorption capacities. *Journal of Hazardous Materials*, 166(1), 491–501. <https://doi.org/10.1016/j.jhazmat.2008.11.047>
- Grand View Research. (2022). *Activated Carbon Market Size*. <https://www.grandviewresearch.com/industry-analysis/activated-carbon-market>
- Gurvich, L. G. (1915). No Title. *Zhurnal Rus. Fiz.-Khimicheskago Obshchestva.*, 805–827.
- Harrington, E. C. (1965). The desirability function. *Industrial Quality Control*, 21(10), 494–498.
- Hashimoto, K., Miura, K., Xu, J.-J., Watanabe, A., & Masukami, H. (1986). Relation between the gasification rate of carbons supporting alkali metal salts and the amount of oxygen trapped by the metal. *Fuel*, 65(4), 489–494. [https://doi.org/10.1016/0016-2361\(86\)90038-4](https://doi.org/10.1016/0016-2361(86)90038-4)
- Hayashi, J., Uchibayashi, M., Horikawa, T., Muroyama, K., & Gomes, V. G. (2002). Synthesizing activated carbons from resins by chemical activation with K₂CO₃. *Carbon*, 40(15), 2747–2752. [https://doi.org/10.1016/S0008-6223\(02\)00151-3](https://doi.org/10.1016/S0008-6223(02)00151-3)

- Hilton, R., Bick, P., Tekeei, A., Leimkuehler, E., Pfeifer, P., & Suppes, G. J. (2012). Mass Balance and Performance Analysis of Potassium Hydroxide Activated Carbon. *Industrial & Engineering Chemistry Research*, 51(26), 9129–9135. <https://doi.org/10.1021/ie301293t>
- Hüttinger, K. J., & Minges, R. (1985). Catalytic water vapour gasification of carbon: Importance of melting and wetting behaviour of the 'catalyst.' *Fuel*, 64(4), 491–494. [https://doi.org/10.1016/0016-2361\(85\)90083-3](https://doi.org/10.1016/0016-2361(85)90083-3)
- Hüttinger, K. J., & Minges, R. (1986). Influence of the catalyst precursor anion in catalysis of water vapour gasification of carbon by potassium: 1. Activation of the catalyst precursors. *Fuel*, 65(8), 1112–1121. [https://doi.org/10.1016/0016-2361\(86\)90179-1](https://doi.org/10.1016/0016-2361(86)90179-1)
- Jansta, J., Dousek, F. P., & Patzelová, V. (1975). Low temperature electrochemical preparation of carbon with a high surface area from polytetrafluoroethylene. *Carbon*, 13(5), 377–380. [https://doi.org/10.1016/0008-6223\(75\)90005-6](https://doi.org/10.1016/0008-6223(75)90005-6)
- Jiménez, V., Sánchez, P., de Lucas, A., Valverde, J. L., & Romero, A. (2009). Influence of the nature of the metal hydroxide in the porosity development of carbon nanofibers. *Journal of Colloid and Interface Science*, 336(1), 226–234. <https://doi.org/10.1016/J.JCIS.2009.03.049>
- Johansen, J. M., Jakobsen, J. G., Frandsen, F. J., & Glarborg, P. (2011). Release of K, Cl, and S during Pyrolysis and Combustion of High-Chlorine Biomass. *Energy & Fuels*, 25(11), 4961–4971. <https://doi.org/10.1021/ef201098n>
- Johns, M. M., Marshall, W. E., & Toles, C. A. (1999). The effect of activation method on the properties of pecan shell-activated carbons. *Journal of Chemical Technology & Biotechnology*, 74(11), 1037–1044. [https://doi.org/10.1002/\(SICI\)1097-4660\(199911\)74:11<1037::AID-JCTB160>3.0.CO;2-O](https://doi.org/10.1002/(SICI)1097-4660(199911)74:11<1037::AID-JCTB160>3.0.CO;2-O)
- Kaneko, K., Ishii, C., Ruike, M., & Kuwabara, H. (1992). Origin of superhigh surface area and microcrystalline graphitic structures of activated carbons. *Carbon*, 30(7), 1075–1088. [https://doi.org/10.1016/0008-6223\(92\)90139-N](https://doi.org/10.1016/0008-6223(92)90139-N)
- Kim, J., Lee, Y., & Lee, H. (2001). *Decomposition of Na₂CO₃ by Interaction with SiO₂ in Mold Flux of Steel Continuous Casting*. 41(2), 116–123.
- Knudsen, J. N., Jensen, P. A., & Dam-Johansen, K. (2004). Transformation and Release to the Gas Phase of Cl, K, and S during Combustion of Annual Biomass. *Energy & Fuels*, 18(5), 1385–1399. <https://doi.org/10.1021/ef049944q>
- Ko, D. C. K., Mui, E. L. K., Lau, K. S. T., & McKay, G. (2004). Production of activated carbons from waste tire – process design and economical analysis. *Waste Management*, 24(9), 875–888. <https://doi.org/10.1016/j.wasman.2004.03.006>

- Kruk, M., Dufour, B., Celer, E. B., Kowalewski, T., Jaroniec, M., & Matyjaszewski, K. (2005). Synthesis of mesoporous carbons using ordered and disordered mesoporous silica templates and polyacrylonitrile as carbon precursor. *Journal of Physical Chemistry B*, *109*(19), 9216–9225. <https://doi.org/10.1021/jp045594x>
- Kruk, M., Jaroniec, M., & Sayari, A. (1997). Application of Large Pore MCM-41 Molecular Sieves To Improve Pore Size Analysis Using Nitrogen Adsorption Measurements. *Langmuir*, *13*(23), 6267–6273. <https://doi.org/10.1021/la970776m>
- Lehman, R. L., Gentry, J. S., & Glumac, N. G. (1998). Thermal stability of potassium carbonate near its melting point. *Thermochimica Acta*, *316*(1), 1–9. [https://doi.org/10.1016/S0040-6031\(98\)00289-5](https://doi.org/10.1016/S0040-6031(98)00289-5)
- Li, M., Liu, C., Cao, H., Zhao, H., Zhang, Y., & Fan, Z. (2014). KOH self-templating synthesis of three-dimensional hierarchical porous carbon materials for high performance supercapacitors. *Journal of Materials Chemistry A*, *2*(36), 14844–14851. <https://doi.org/10.1039/C4TA02167C>
- Liang, T.-T., Yamada, Y., Yoshizawa, N., Shiraishi, S., & Oya, A. (2001). Preparation of porous carbon by defluorination of poly(tetrafluoroethylene) and the effect of γ -irradiation on the polymer. *Chemistry of Materials*, *13*(9), 2933–2939. <https://doi.org/10.1021/cm010184w>
- Lillo-Ródenas, M. A., Cazorla-Amorós, D., & Linares-Solano, A. (2003). Understanding chemical reactions between carbons and NaOH and KOH: An insight into the chemical activation mechanism. *Carbon*, *41*(2), 267–275. [https://doi.org/10.1016/S0008-6223\(02\)00279-8](https://doi.org/10.1016/S0008-6223(02)00279-8)
- Lima, I. M., McAloon, A., & Boateng, A. A. (2008). Activated carbon from broiler litter: Process description and cost of production. *Biomass and Bioenergy*, *32*(6), 568–572. <https://doi.org/10.1016/j.biombioe.2007.11.008>
- Lozano-Castelló, D., Lillo-Ródenas, M. A., Cazorla-Amorós, D., & Linares-Solano, A. (2001). Preparation of activated carbons from Spanish anthracite: I. Activation by KOH. *Carbon*, *39*(5), 741–749. [https://doi.org/10.1016/S0008-6223\(00\)00185-8](https://doi.org/10.1016/S0008-6223(00)00185-8)
- Maciá-Agulló, J. A., Moore, B. C., Cazorla-Amorós, D., & Linares-Solano, A. (2004). Activation of coal tar pitch carbon fibres: Physical activation vs. chemical activation. *Carbon*, *42*(7), 1367–1370. <https://doi.org/10.1016/j.carbon.2004.01.013>
- Marsh, H., Crawford, D., O'Grady, T. M., & Wennerberg, A. (1982). Carbons of high surface area. A study by adsorption and high resolution electron microscopy. *Carbon*, *20*(5), 419–426. [https://doi.org/10.1016/0008-6223\(82\)90042-2](https://doi.org/10.1016/0008-6223(82)90042-2)
- Marsh, H., & Rodríguez-Reinoso, F. (2006a). Activated Carbon. In *Activated Carbon*. <https://doi.org/10.1016/B978-0-08-044463-5.X5013-4>

- Marsh, H., & Rodríguez-Reinoso, F. (2006b). *CHAPTER 2 - Activated Carbon (Origins)* (H. Marsh & F. B. T.-A. C. Rodríguez-Reinoso, Eds.; pp. 13–86). Elsevier Science Ltd. <https://doi.org/10.1016/B978-008044463-5/50016-9>
- Marsh, H., & Rodríguez-Reinoso, F. (2006c). *CHAPTER 5 - Activation Processes (Thermal or Physical)* (H. Marsh & F. B. T.-A. C. Rodríguez-Reinoso, Eds.; pp. 243–321). Elsevier Science Ltd. <https://doi.org/10.1016/B978-008044463-5/50019-4>
- Marsh, H., & Rodríguez-Reinoso, F. (2006d). *CHAPTER 6 - Activation Processes (Chemical)* (H. Marsh & F. B. T.-A. C. Rodríguez-Reinoso, Eds.; pp. 322–365). Elsevier Science Ltd. <https://doi.org/10.1016/B978-008044463-5/50020-0>
- Matranga, K. R., Myers, A. L., & Glandt, E. D. (1992). Storage of natural gas by adsorption on activated carbon. *Chemical Engineering Science*, *47*(7), 1569–1579. [https://doi.org/10.1016/0009-2509\(92\)85005-V](https://doi.org/10.1016/0009-2509(92)85005-V)
- Matsuoka, K., Yamagishi, Y., Yamazaki, T., Setoyama, N., Tomita, A., & Kyotani, T. (2005). Extremely high microporosity and sharp pore size distribution of a large surface area carbon prepared in the nanochannels of zeolite Y. *Carbon*, *43*(4), 876–879. <https://doi.org/10.1016/j.carbon.2004.10.050>
- McEnaney, B. (2002). Properties of Activated Carbons. In *Handbook of Porous Solids* (pp. 1828–1863). <https://doi.org/doi:10.1002/9783527618286.ch24b>
- Merchant, A. A., & Petrich, M. A. (1993). Pyrolysis of scrap tires and conversion of chars to activated carbon. *AIChE Journal*, *39*(8), 1370–1376. <https://doi.org/10.1002/aic.690390814>
- Mims, C. A., & Pabst, J. K. (1983). Role of surface salt complexes in alkali-catalysed carbon gasification. *Fuel*, *62*(2), 176–179. [https://doi.org/10.1016/0016-2361\(83\)90193-X](https://doi.org/10.1016/0016-2361(83)90193-X)
- Montes, V., & Hill, J. M. (2018). Activated carbon production: Recycling KOH to minimize waste. *Materials Letters*, *220*, 238–240. <https://doi.org/10.1016/j.matlet.2018.03.019>
- Mordor Intelligence. (2022). *Activated Carbon Market - Growth, Trends, COVID-19 Impact, and Forecasts (2022 - 2027)*. <https://www.mordorintelligence.com/industry-reports/activated-carbon-market>
- Morishita, T., Soneda, Y., Tsumura, T., & Inagaki, M. (2006). Preparation of porous carbons from thermoplastic precursors and their performance for electric double layer capacitors. *Carbon*, *44*(12), 2360–2367. <https://doi.org/10.1016/j.carbon.2006.04.030>

- Morishita, T., Tsumura, T., Toyoda, M., Przepiórski, J., Morawski, A. W., Konno, H., & Inagaki, M. (2010). A review of the control of pore structure in MgO-templated nanoporous carbons. *Carbon*, 48(10), 2690–2707. <https://doi.org/10.1016/j.carbon.2010.03.064>
- Newcombe, G. (2006). Chapter 8 - Removal of natural organic material and algal metabolites using activated carbon. In G. Newcombe & D. B. T.-I. S. and T. Dixon (Eds.), *Interface Science in Drinking Water Treatment* (Vol. 10, pp. 133–153). Elsevier. [https://doi.org/10.1016/S1573-4285\(06\)80077-3](https://doi.org/10.1016/S1573-4285(06)80077-3)
- Ng, C., Marshall, W. E., Rao, R. M., Bansode, R. R., & Losso, J. N. (2003). Activated carbon from pecan shell: process description and economic analysis. *Industrial Crops and Products*, 17(3), 209–217. [https://doi.org/10.1016/S0926-6690\(03\)00002-5](https://doi.org/10.1016/S0926-6690(03)00002-5)
- Nishihara, H., & Kyotani, T. (2012). *Chapter 10 - Zeolite-Templated Carbon – Its Unique Characteristics and Applications* (J. M. D. B. T.-N. C. A. Tascón, Ed.; pp. 295–322). Elsevier. <https://doi.org/10.1016/B978-0-08-097744-7.00010-7>
- O’Grady, T. M., & Wennerberg, A. N. (1986). High-Surface-Area Active Carbon. In *Petroleum-Derived Carbons* (Vol. 303, pp. 20–302). American Chemical Society. <https://doi.org/doi:10.1021/bk-1986-0303.ch020>
- Okada, K., Yamamoto, N., Kameshima, Y., & Yasumori, A. (2003). Porous properties of activated carbons from waste newspaper prepared by chemical and physical activation. *Journal of Colloid and Interface Science*, 262(1), 179–193. [https://doi.org/10.1016/S0021-9797\(03\)00107-3](https://doi.org/10.1016/S0021-9797(03)00107-3)
- Okuno, T., Sonoyama, N., Hayashi, J., Li, C.-Z., Sathe, C., & Chiba, T. (2005). Primary Release of Alkali and Alkaline Earth Metallic Species during the Pyrolysis of Pulverized Biomass. *Energy & Fuels*, 19(5), 2164–2171. <https://doi.org/10.1021/ef050002a>
- Otowa, T., Nojima, Y., & Miyazaki, T. (1997). Development of KOH activated high surface area carbon and its application to drinking water purification. *Carbon*, 35(9), 1315–1319. [https://doi.org/10.1016/S0008-6223\(97\)00076-6](https://doi.org/10.1016/S0008-6223(97)00076-6)
- Otowa, T., Tanibata, R., & Itoh, M. (1993). Production and adsorption characteristics of MAXSORB: High-surface-area active carbon. *Gas Separation & Purification*, 7(4), 241–245. [https://doi.org/10.1016/0950-4214\(93\)80024-Q](https://doi.org/10.1016/0950-4214(93)80024-Q)
- Ou, L., Dou, C., Yu, J.-H., Kim, H., Park, Y.-C., Park, S., Kelley, S., & Lee, E. Y. (2021). Techno-economic analysis of sugar production from lignocellulosic biomass with utilization of hemicellulose and lignin for high-value co-products. *Biofuels, Bioproducts and Biorefining*, 15(2), 404–415. <https://doi.org/10.1002/bbb.2170>

- Perrich, J. R. (1981). *Activated Carbon Adsorption For Wastewater Treatment* (1st ed.). CRC Press. <https://doi.org/10.1201/9781351069465>
- Peters, M. S., Timmerhaus, K. D., & West, R. E. (2003). *Plant Design and Economics for Chemical Engineers* (5th ed.). McGraw-Hill.
- Ponomarev, N. P., (2020). *Method for producing active carbon* (Patent No. FI20205673A1).
- Qiao, W., Yoon, S.-H., & Mochida, I. (2006). KOH Activation of Needle Coke to Develop Activated Carbons for High-Performance EDLC. *Energy & Fuels*, 20(4), 1680–1684. <https://doi.org/10.1021/ef050313l>
- Rabinovich, M. L. (2014). Lignin by-products of soviet hydrolysis industry: resources, characteristics, and utilization as a fuel. *Cellulose Chemistry and Technology*, 48(7–8), 613–631.
- Rabinovich, M. L., Fedoryak, O., Dobeles, G., Andersone, A., Gawdzik, B., Lindström, M. E., & Sevastyanova, O. (2016). Carbon adsorbents from industrial hydrolysis lignin: The USSR/Eastern European experience and its importance for modern biorefineries. *Renewable and Sustainable Energy Reviews*, 57(January), 1008–1024. <https://doi.org/10.1016/j.rser.2015.12.206>
- Randtke, S. J., & Snoeyink, V. L. (1983). Evaluating GAC adsorptive capacity. *Journal AWWA*, 75(8), 406–413. <https://doi.org/10.1002/j.1551-8833.1983.tb05177.x>
- Ravikovitch, P. I., Vishnyakov, A., Russo, R., & Neimark, A. V. (2000). Unified Approach to Pore Size Characterization of Microporous Carbonaceous Materials from N₂, Ar, and CO₂ Adsorption Isotherms. *Langmuir*, 16(5), 2311–2320. <https://doi.org/10.1021/la991011c>
- Roberts, P. V., & Summers, R. S. (1982). Performance of granular activated carbon for total organic carbon removal. *Journal (American Water Works Association)*, 74(2), 113–118.
- Rodríguez-Reinoso, F., & Molina-Sabio, M. (1992). Activated carbons from lignocellulosic materials by chemical and/or physical activation: an overview. *Carbon*, 30(7), 1111–1118. [https://doi.org/10.1016/0008-6223\(92\)90143-K](https://doi.org/10.1016/0008-6223(92)90143-K)
- Romanos, J., Beckner, M., Rash, T., Firlej, L., Kuchta, B., Yu, P., Suppes, G., Wexler, C., & Pfeifer, P. (2011). Nanospace engineering of KOH activated carbon. *Nanotechnology*, 23(1), 15401. <https://doi.org/10.1088/0957-4484/23/1/015401>
- Ros, A., Lillo-Ródenas, M. A., Fuente, E., Montes-Morán, M. A., Martín, M. J., & Linares-Solano, A. (2006). High surface area materials prepared from sewage

- sludge-based precursors. *Chemosphere*, 65(1), 132–140. <https://doi.org/10.1016/j.chemosphere.2006.02.017>
- Rouquerol, F., Rouquerol, J., Sing, K. S. W., Maurin, G., & Llewellyn, P. (2014). *I - Introduction* (F. Rouquerol, J. Rouquerol, K. S. W. Sing, P. Llewellyn, & G. B. T.-A. by P. and P. S. (Second E. Maurin, Eds.; pp. 1–24). Academic Press. <https://doi.org/10.1016/B978-0-08-097035-6.00001-2>
- Rouquerol, J., Llewellyn, P., & Rouquerol, F. (2007). *Is the bet equation applicable to microporous adsorbents?* 49–56. [https://doi.org/10.1016/S0167-2991\(07\)80008-5](https://doi.org/10.1016/S0167-2991(07)80008-5)
- Sadakata, M., Takahashi, K., Saito, M., & Sakai, T. (1987). Production of fuel gas and char from wood, lignin and holocellulose by carbonization. *Fuel*, 66(12), 1667–1671. [https://doi.org/10.1016/0016-2361\(87\)90360-7](https://doi.org/10.1016/0016-2361(87)90360-7)
- Sams, D. A., & Shadman, F. (1986). Mechanism of potassium-catalyzed carbon/CO₂ reaction. *AIChE Journal*, 32(7), 1132–1137. <https://doi.org/10.1002/aic.690320710>
- Shao, J., Ma, F., Wu, G., Dai, C., Geng, W., Song, S., & Wan, J. (2017). In-situ MgO (CaCO₃) templating coupled with KOH activation strategy for high yield preparation of various porous carbons as supercapacitor electrode materials. *Chemical Engineering Journal*, 321, 301–313. <https://doi.org/10.1016/j.cej.2017.03.092>
- Simmons, L. L., Lowden, L. F., & Ehlert, T. C. (1977). A mass spectrometric study of potassium carbonate and potassium oxide. *The Journal of Physical Chemistry*, 81(8), 706–709. <https://doi.org/10.1021/j100523a005>
- Sing, K. S. W. (2013). Adsorption by Active Carbons. In *Adsorption by Powders and Porous Solids: Principles, Methodology and Applications: Second Edition* (2nd ed.). Elsevier Ltd. <https://doi.org/10.1016/B978-0-08-097035-6.00010-3>
- Statistics Finland. (2022). *Energy prices*. https://www.stat.fi/til/ehi/2021/03/ehi_2021_03_2021-12-09_tau_002_en.html
- Stavropoulos, G. G., & Zabaniotou, A. A. (2009). Minimizing activated carbons production cost. *Fuel Processing Technology*, 90(7), 952–957. <https://doi.org/10.1016/j.fuproc.2009.04.002>
- Tanaike, O., Yoshizawa, N., Hatori, H., Yamada, Y., Shiraishi, S., & Oya, A. (2002a). Mesoporous carbon from poly(tetrafluoroethylene) defluorinated by sodium metal. *Carbon*, 40(3), 457–459. [https://doi.org/10.1016/S0008-6223\(01\)00289-5](https://doi.org/10.1016/S0008-6223(01)00289-5)
- Tanaike, O., Yoshizawa, N., Hatori, H., Yamada, Y., Shiraishi, S., & Oya, A. (2002b). Preparation and Characterization of Porous Carbons By Defluorination of Ptfе with

- Alkali Metals - Effect of Alkali Metals on the Porous Structure -. *Molecular Crystals and Liquid Crystals*, 388(1), 45–50. <https://doi.org/10.1080/10587250215275>
- Thommes, M., Cychosz, K. A., & Neimark, A. V. (2012). *Chapter 4 - Advanced Physical Adsorption Characterization of Nanoporous Carbons* (J. M. D. B. T.-N. C. A. Tascón, Ed.; pp. 107–145). Elsevier. <https://doi.org/10.1016/B978-0-08-097744-7.00004-1>
- Thommes, M., Kaneko, K., Neimark, A. V., Olivier, J. P., Rodriguez-Reinoso, F., Rouquerol, J., & Sing, K. S. W. (2015). Physisorption of gases, with special reference to the evaluation of surface area and pore size distribution (IUPAC Technical Report). *Pure and Applied Chemistry*, 87(9–10), 1051–1069. <https://doi.org/10.1515/pac-2014-1117>
- Vanreppelen, K., Kuppens, T., Thewys, T., Carleer, R., Yperman, J., & Schreurs, S. (2011). Activated carbon from co-pyrolysis of particle board and melamine (urea) formaldehyde resin: A techno-economic evaluation. *Chemical Engineering Journal*, 172(2), 835–846. <https://doi.org/10.1016/j.cej.2011.06.071>
- Veraa, M. J., & Bell, A. T. (1978). Effect of alkali metal catalysts on gasification of coal char. *Fuel*, 57(4), 194–200. [https://doi.org/10.1016/0016-2361\(78\)90116-3](https://doi.org/10.1016/0016-2361(78)90116-3)
- Wang, Y., & Tan, H. (2019). Condensation of KCl(g) under varied temperature gradient. *Fuel*, 237, 1141–1150. <https://doi.org/10.1016/j.fuel.2018.10.046>
- Wennerberg, A., & O'Grady, T. (1978). *ACTIVE CARBON PROCESS AND COMPOSITION* (Patent No. 4082694).
- Wigmans, T., Elfring, R., & Moulijn, J. A. (1983). On the mechanism of the potassium carbonate catalysed gasification of activated carbon: the influence of the catalyst concentration on the reactivity and selectivity at low steam pressures. *Carbon*, 21(1), 1–12. [https://doi.org/10.1016/0008-6223\(83\)90150-1](https://doi.org/10.1016/0008-6223(83)90150-1)
- Williamson, G. K., & Hall, W. H. (1953). Discussion of the Theories of Line Broadening. *Acta Metallurgica*, 1, 22. [https://doi.org/10.1016/0001-6160\(53\)90006-6](https://doi.org/10.1016/0001-6160(53)90006-6)
- Xu, C. C., Dessbesell, L., Zhang, Y., & Yuan, Z. (2021). Lignin valorization beyond energy use: has lignin's time finally come? *Biofuels, Bioproducts and Biorefining*, 15(1), 32–36. <https://doi.org/10.1002/bbb.2172>
- Yahya, M. A., Al-Qodah, Z., & Ngah, C. W. Z. (2015). Agricultural bio-waste materials as potential sustainable precursors used for activated carbon production: A review. *Renewable and Sustainable Energy Reviews*, 46, 218–235. <https://doi.org/10.1016/j.rser.2015.02.051>

- Yin, L., Leng, E., Fang, Y., Liu, T., Gong, X., & Zhou, J. (2020). Effects of KCl, KOH and K₂CO₃ on the pyrolysis of C β -O type lignin-related polymers. *Journal of Analytical and Applied Pyrolysis*, 147, 104809. <https://doi.org/10.1016/j.jaap.2020.104809>
- Yuan, M., Kim, Y., & Jia, C. Q. (2012). Feasibility of recycling KOH in chemical activation of oil-sands petroleum coke. *The Canadian Journal of Chemical Engineering*, 90(6), 1472–1478. <https://doi.org/10.1002/cjce.20671>
- Yue, Z., & Economy, J. (2017). 4 - Carbonization and activation for production of activated carbon fibers. In J. Y. B. T.-A. C. F. and T. Chen (Ed.), *Woodhead Publishing Series in Textiles* (pp. 61–139). Woodhead Publishing. <https://doi.org/10.1016/B978-0-08-100660-3.00004-3>
- Zhang, T., Walawender, W. P., & Fan, L. T. (2010). Grain-based activated carbons for natural gas storage. *Bioresource Technology*, 101(6), 1983–1991. <https://doi.org/10.1016/j.biortech.2009.10.046>
- Zhang, W., Lin, H., Lin, Z., Yin, J., Lu, H., Liu, D., & Zhao, M. (2015). 3 D Hierarchical Porous Carbon for Supercapacitors Prepared from Lignin through a Facile Template-Free Method. *ChemSusChem*, 8(12), 2114–2122. <https://doi.org/10.1002/cssc.201403486>
- Zhihang, Y., Zhihua, X., Daofang, Z., Chen, W., Zhang, T., Huang, Y., Gu, L., Deng, H., & Danqi, T. (2017). Box-Behnken design approach towards optimization of activated carbon synthesized by co-pyrolysis of waste polyester textiles and MgCl₂. *Applied Surface Science*, 427, 340–348. <https://doi.org/10.1016/j.apsusc.2017.08.241>

Publication I

Ponomarev, N.P. and Sillanpää, M.
**Combined chemical-templated
activation of hydrolytic lignin for producing porous carbon**

Reprinted with permission from

Industrial

Crops and Products

Vol. 135, pp. 30-38, 2019

© 2019, Elsevier



Contents lists available at ScienceDirect

Industrial Crops & Products

journal homepage: www.elsevier.com/locate/indcrop

Combined chemical-templated activation of hydrolytic lignin for producing porous carbon

Nikolai Ponomarev*, Mika Sillanpää

Department of Green Chemistry, School of Engineering Science, Lappeenranta-Lahti University of Technology LUT, Sammonkatu 12, FI-50130, Mikkeli, Finland



ARTICLE INFO

Keywords:

Lignin
Activated carbon
Template
NaCl

ABSTRACT

Chemical activation and template method using lignin have been considered efficient for producing microporous activated carbon. However, the limited accessibility of micropores and significant chemical consumption hinder the application of aforementioned methods. In order to save attractive properties of both activation routes and to overcome environmental impact, novel combined chemical-templated activation was investigated. A mixture of NaOH and NaCl was employed to produce carbon, which possessed high surface area and versatile porous structure. The process was optimised and described by mathematical models using the response surface method (RSM). The BET surface area and yield were selected as output performances (responses), whilst temperature, time and chemical ratio were chosen as variable inputs (factors). Macropore sizes were of the same NaCl crystal size confirmed by XRD and SEM indicating a template mechanism. Micropore origin was suggested by chemical reactions between NaOH and carbon with a formation of Na_2CO_3 confirmed by XRD standard patterns and corresponding FTIR peaks. According to RSM design, the most significant factor is chemical ratio for both responses. The experimental data of the BET surface area is in a good validity of the quadratic model, while yield matched the linear model well according to the ANOVA test. In this study, porous carbon was produced by new method overcoming the major challenges of templated and chemical activation and brings added value of lignin.

1. Introduction

Research into the production of activated carbon has attracted substantial attention. Activated carbon is a material with a versatile porous structure, using carbon-rich starting materials such as wood, coconut shells and cellulose (Sing, 2014). Activated carbon has found ubiquitous applications in many fields such as wastewater treatment and drinking water production (Boehm, 1994), separation and purification (Marsh and Rodríguez-Reinoso, 2006), catalysis and electronic manufacturing (Frackowiak and Béguin, 2001).

The widespread implementation of activated carbon is hindered because of expensive raw materials. In order to overcome this problem, waste materials were employed for activated carbon production (Zhihang et al., 2017). Lignin has attracted recent attention as a precursor for producing carbon materials (Culebras et al., 2018; Dalton et al., 2019). Being a side product of the paper and hydrolysis industries, lignin can be also a beneficial raw material for activated carbon. Among plant polymers, lignin has superior properties such as high carbon yield, availability and cost-efficiency (Torné-Fernández et al., 2009). Moreover, there are around 95 million tonnes of waste hydrolytic lignin in a post-Soviet Union area, causing environmental

problems and requiring utilisation (Evstigneyev et al., 2016).

Physical activation of carbon using water steam is the most common industrial process of activated carbon production (Fu et al., 2013). However, physical activation has some drawbacks, in particular quite high activation temperatures and the need for preliminary pyrolysis of biomass before activation. For this reason, chemical activation has attracted attention enabling the process in a single step. For example, ZnCl_2 , H_3PO_4 , K_2CO_3 (Hayashi et al., 2000); KOH and NaOH (Fierro et al., 2007) have been employed for the chemical activation of carbon. The environmental impact is the impending factor of application chemical agents such as ZnCl_2 and H_3PO_4 . Despite the straightforwardness of alkali activation, the price of the final product is still high due to significant chemical consumption.

One of the newest approaches is templated activation. In this case, an inorganic template is used. The templates could be zeolites (Matsuoka et al., 2005) or mesoporous silica (Kruk et al., 2005). The solution of polymer penetrates into the template structure, then polymerisation occurs and the obtained composite is carbonised. After carbonisation, the template is removed using acid to obtain a template-like porous structure. An ordered micropore or mesopore structure tends to emerge through this method. The disadvantages are expensive

* Corresponding author.

E-mail addresses: nikolai.ponomarev@lut.fi, pnn92@mail.ru (N. Ponomarev).<https://doi.org/10.1016/j.indcrop.2019.03.050>

Received 8 February 2019; Received in revised form 18 March 2019; Accepted 21 March 2019

Available online 19 April 2019

0926-6690/© 2019 The Authors. Published by Elsevier B.V. This is an open access article under the CC BY-NC-ND license (<http://creativecommons.org/licenses/by-nc-nd/4.0/>).

starting materials (zeolites or silica), the use of oil-based polymers and the application of strong mineral acids. Moreover, the obtained templated microporous carbons have limited accessibility of micropores due to lack of macropores (Morishita et al., 2010). Magnesium oxide or calcium carbonate were successfully applied for the template to produce carbons with a high surface area avoiding aforementioned drawbacks (Shao et al., 2017). A successful attempt was made to use KCl template-activated carbon with consequent CO₂ activation (Cao et al., 2018).

Understanding the activation mechanism and pore origin is crucial for activated carbon production. Some information on the activation mechanism using NaOH was obtained indicating interaction between the carbon and activation agent (Lillo-Ródenas et al., 2003). The mechanism of template pore formation was well described pointing out inherited pore size from crystalline size (Morishita et al., 2006). However, combined chemical-templated activation has never been studied and evaluation of the mechanism is necessary.

One-Variable-At-a-Time (OVAT) was used widely for optimisation of activated carbon production. However, OVAT requires many experiments to properly evaluate the effect of input variables (factors) on output performance (response) (Torné-Fernández et al., 2009). Moreover, factors and responses are not described statistically by a mathematical model in the case of OVAT. Response surface methodology (RSM) was employed for optimisation of activated carbon production (Nieto-Delgado and Rangel-Mendez, 2011). RSM allows the creation of mathematical models with a minimum number of experimental runs and the evaluation of statistical validation using the ANOVA test. Also, the assessment of the multiple responses can be done using a desirability function in simultaneous optimisation. For instance, temperature, time and ratio are variable inputs while BET surface and yield are multiple responses typically selected for optimisation of activated carbon production (Das and Mishra, 2017).

The main objective of the present work was to develop a sustainable process in order to obtain carbon with versatile porous texture that is useful in various applications. Lignin was selected for activated carbon production as a cost-efficient source. To overcome the main limitations of the common activation processes, the novel combined chemical-templated activation was investigated. In order to gain insight into the pore origin, the activation mechanism was studied. For the optimisation of the process and its mathematical description, the RSM method was employed, further leading to increased efficiency and providing a better understanding of the process.

2. Materials and methods

2.1. Materials

The raw material for activated carbon was industrial acid hydrolytic lignin from coniferous wood. A lignin fraction of 200 µm of with 8.5% moisture content was used for experiments without any modifications. All chemicals were supplied by Sigma-Aldrich, were of analytical grade and used as received. The nitrogen for inert atmosphere and porosity analysis was of 99.999% purity. Commercial steam-activated carbon Norit EA 0.5–1.5 was used for the hardness comparison.

2.2. Preparation

In a typical experiment, 21.86 g of lignin (20.00 g of dry matter) was mixed with a solution containing 72.0 mL of water, 12.00 g of NaCl and 8.00 g of NaOH. The obtained mixture was let to swell for an hour at room temperature, then was extruded and dried at 130 °C for 16 h. The received dried material was ground and granules of size 1–2 mm were collected. Afterwards, the material was pyrolysed in a tubular furnace in a N₂ inert atmosphere at 800 °C for 60 min. The temperature, time and NaOH/NaCl-to-lignin ratio were also varied according to experimental design (Table 1). The flow of N₂ and heating rate were constant

Table 1
Factors and responses of experimental design.

Run	Factors			Responses	
	A Temperature (°C)	B Time (min)	C Ratio ^a (g/g)	Y ₁ BET (m ² /g)	Y ₂ Yield (%)
0 (1)	700 (0)	60 (0)	1.00 (0)	738	37.25
0 (2)	700 (0)	60 (0)	1.00 (0)	735	37.25
0 (3)	700 (0)	60 (0)	1.00 (0)	736	37.33
1	600 (-1)	30 (-1)	0.50 (-1)	393	48.00
2	800 (1)	30 (-1)	0.50 (-1)	802	42.22
3	600 (-1)	90 (1)	0.50 (-1)	412	46.67
4	800 (1)	90 (1)	0.50 (-1)	873	41.20
5	600 (-1)	30 (-1)	1.50 (1)	454	33.30
6	800 (1)	30 (-1)	1.50 (1)	1120	29.00
7	600 (-1)	90 (1)	1.50 (1)	553	33.30
8	800 (1)	90 (1)	1.50 (1)	1346	25.70
9	532 (-1.682)	60 (0)	1.00 (0)	384	41.50
10	868 (1.682)	60 (0)	1.00 (0)	1210	29.83
11	700 (0)	9.5 (-1.682)	1.00 (0)	600	39.00
12	700 (0)	110.5 (1.682)	1.00 (0)	768	37.50
13	700 (0)	60 (0)	0.16 (-1.682)	325	49.01
14	700 (0)	60 (0)	1.84 (1.682)	846	29.11

^a NaOH/NaCl-to-lignin mass ratio.

and equal to 0.5 L/min and 5 °C/min, respectively. After pyrolysis, the inorganic part was leached from the material using 0.1 mol/L of HCl. The material was isolated from the solution using a Buchner funnel and washed several times until it had a neutral pH. Then the product was dried at 130 °C for 16 h.

2.3. Characterisation

The functional groups of the material were studied using Fourier transform infrared spectroscopy (FTIR) on a Bruker Vertex 70. The crystalline structure of the material was evaluated using X-ray powder diffraction (XRD) on a high-resolution PANalytical diffractometer. The scans were recorded employing Co Kα radiation at a voltage of 40 kV from 10° to 100° 2θ angles. The crystalline size was calculated using XRD data applying the Williamson-Hall (W-H) method (Williamson and Hall, 1953). The surface area, pore size distribution, micro and total pore volume were derived from the data of the N₂ adsorption-desorption isotherm obtained by Tristar® II Plus. The surface area was calculated using the Brunauer, Emmett and Teller (BET) theory (Brunauer et al., 1938) applying the recommended procedure for microporous materials (Rouquerol et al., 2007). Pore size distribution and micropore volume were evaluated using the non-local density functional theory (NLDFT) (Ravikovitch and Neimark, 2001) applying the “N₂ @ 77 on Carbon Slit Pores” kernel provided by the software of Tristar® II Plus. The micropore volume was also calculated using the Dubinin-Radushkevich equation (Dubinin and Radushkevich, 1947). The total volume of pores was calculated at p/p* = 0.99. The structure of the material was studied employing scanning electron microscopy (SEM) on a Hitachi S-4800. Thermogravimetric analyses (TGA) were performed on a NETZSCH TG thermal analyser at a heating rate 5 °C/min from 23 °C to 1000 °C. The yield was calculated using values of raw material and final product masses, respectively. The Vickers hardness of granules was evaluated using INNOVATEST Micro-Vickers Hardness Tester 423 A at a load 100 g for a dwell time 10 s.

2.4. Process optimization

The process variables such as target temperature A (°C), residence time B (min) and NaOH/NaCl-to-lignin ratio C (g/g) were considered as factors. The factors were analysed using the response surface method (RSM) (Box and Wilson, 1951). Three levels of factors, including zero

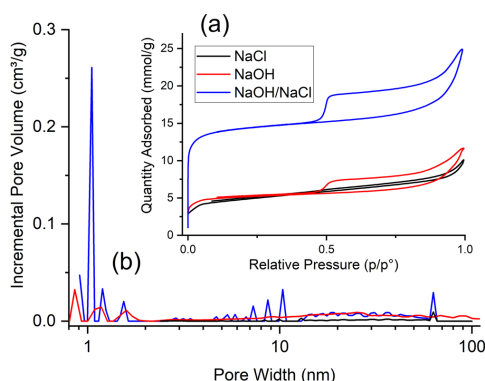


Fig. 1. N₂ adsorption-desorption isotherms (a) and NLDFT pore size distribution (b) of carbons prepared at 800 °C using lignin-NaCl, lignin-NaOH and lignin-NaOH/NaCl.

Table 2
Texture properties and yield of carbons prepared using various amounts of NaOH and/or NaCl.

C Ratio (g/g)		BET (m ² /g)	V _{micro} ^a (cm ³ /g)	V _{total} ^b (cm ³ /g)	Yield (%)
NaOH	NaCl				
0.0	0.5	421	0.14	0.30	44.16
0.5	0.0	456	0.15	0.35	38.67
0.5	0.5	1307	0.43	0.74	32.50

^a Micropore volume is calculated by DR equation.
^b Total volume of pores is calculated at p/p° = 0.99.

level, were ascribed to each parameter. The minimum, zero and maximum levels are temperatures of 600, 700 and 800 °C; time 30, 60 and 90 min; NaOH/NaCl-to-lignin ratio 0.5, 1.0 and 1.5 g/g. The BET surface area Y₁ (m²/g) and yield Y₂ (%) were selected as responses for process optimisation. To evaluate the reproducibility and validity of experimental findings, three repetitions were performed on a zero level. The design of experiments is demonstrated in Table 1. Experimental data were analysed by RSM using Design Expert 11 software, and ANOVA analysis was performed to evaluate the adequacy of the models.

3. Results and discussion

3.1. Carbon texture

Fig. 1a shows the adsorption isotherms and of carbons prepared after the use of NaOH, NaCl and NaOH/NaCl. The structure properties of obtained carbons are also presented in Table 2. Adsorption isotherms are described according to the IUPAC report (Thommes et al., 2015). The isotherm curvature of carbon prepared from the mixture of lignin-NaCl exhibits composite type I,II assigned to micro- macroporous materials. Carbon prepared using lignin-NaOH demonstrated an isotherm shape of microporous materials with a characteristic plateau starting at a point above 0.1 p/p°. Activated carbons produced from kraft lignin using NaOH or KOH activation are associated with microporous materials (Fierro et al., 2007). The isotherm of carbon prepared using a mixture of NaOH and NaCl coincided with combined isotherm type I, II, since enhanced N₂ uptake is observed at pressures below 0.1 p/p° associated with micropore filling, while the ascended curvature of the plateau is inherent in macropores. The adsorption hysteresis of carbon prepared using only NaOH is attributed to the H4 type and accompanied with isotherms I or composite type I, II indicating incomplete filling of macropores with pore condensate. The hysteresis loop of carbon prepared using only NaCl is associated with the isotherm type II of macroporous materials. The adsorption capacities of carbons prepared using only NaCl or NaOH are similar whereas the N₂ uptake of carbons prepared using NaOH/NaCl mixture is more pronounced.

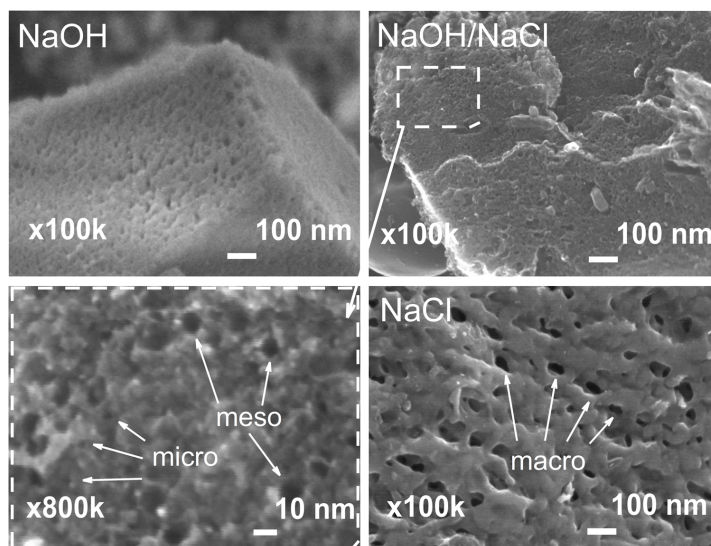


Fig. 2. SEM images of carbons prepared using lignin-NaOH, lignin-NaOH/NaCl and lignin-NaCl.

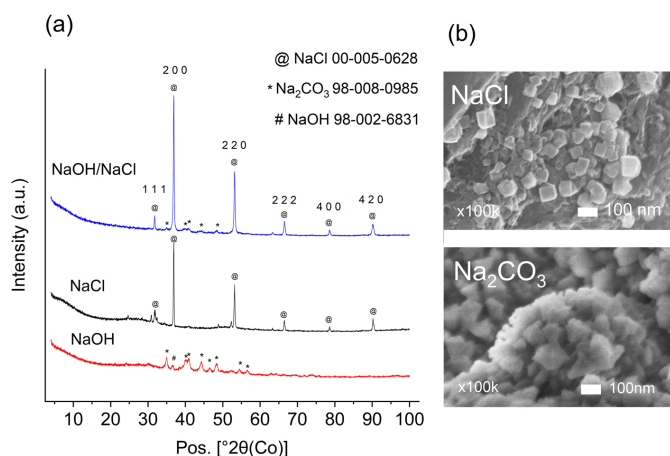


Fig. 3. XRD spectra (a) and SEM micrographs (b) of samples prepared using NaCl, NaOH or NaOH/NaCl before leaching.

Table 3

The crystal size of NaCl and pore size of carbons prepared using NaCl or NaOH/NaCl.

Reagent	NaCl	NaCl/NaOH
XRD crystal size ^a (nm)	69.48	70.02
SEM crystal size ^b (nm)	50-100	50-100
NLDFT macropore size ^c (nm)	63.2	63.2
SEM macropore size ^d (nm)	40-80	40-80

^a Calculated by the W-H method using the following diffraction peaks: 111, 200, 220, 222, 400, 420 (Fig. 3a).

^b Observed NaCl crystals on SEM micrograph (Fig. 3b).

^c The most significant peak of macropores obtained by NLDFT pore size distribution (Fig. 1b).

^d Observed macropore size on SEM micrograph (Fig. 2).

The texture properties of carbons prepared using various mixtures are summarized in Table 2. The samples prepared using only NaOH or NaCl have a relatively similar total volume of pores and BET surface area, while carbon prepared using a mixture of NaOH/NaCl demonstrated significantly higher values. The BET surface area and micropore volume of carbon prepared using NaOH/NaCl are larger than the

NaOH- or NaCl-activated carbons. This observation can be explained by additional micropore formation on macropore walls that contributed to the enlargement of BET surface area. (Morishita et al., 2010). The aforementioned micro- and macroporosity of carbons lead to the largest total pore volume of carbons prepared using NaOH/NaCl. The total pore volume of carbon prepared using NaCl is caused by micro and macropore formation, while, in the case of NaOH microporosity, mainly deals with its origin.

Due to lack of chemical interaction between NaCl and carbon, NaCl leads to the largest carbon yield, whereas NaOH-activated carbon demonstrated reduced yield assumed to be because of the possible chemical reaction between NaOH and carbon. In the case of composite NaOH/NaCl mixture, the lowest yield is supposed by the additional NaCl catalytic effect of thermal degradation (Müller-Hagedorn et al., 2003). In other words, the catalytic effect of NaCl is possible for both mixtures containing NaCl, but in case of NaOH/NaCl, it brings added effect alongside chemical interaction between NaOH and carbon that allow assuming the reason of the lowest yield for NaOH/NaCl mixture.

In addition, the NaOH/NaCl composite mixture has a remarkable effect on the porous texture of prepared carbon. The results suggest different origin of porous structure depending on the used chemical.

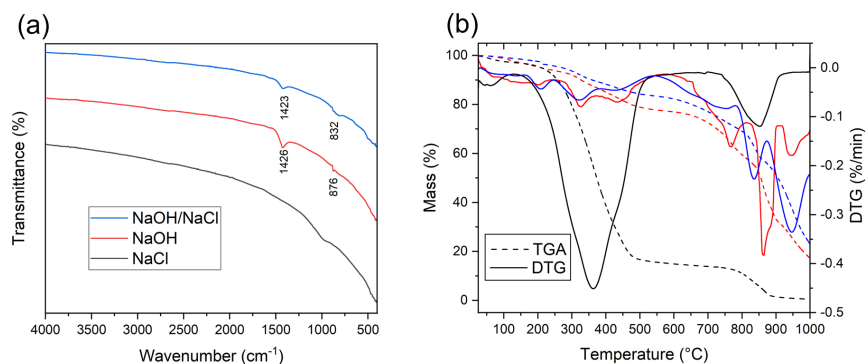


Fig. 4. FTIR spectra of pyrolysed carbons before leaching (a) and TGA/DTG curves (b) of samples before pyrolysis using NaCl, NaOH and NaOH/NaCl.

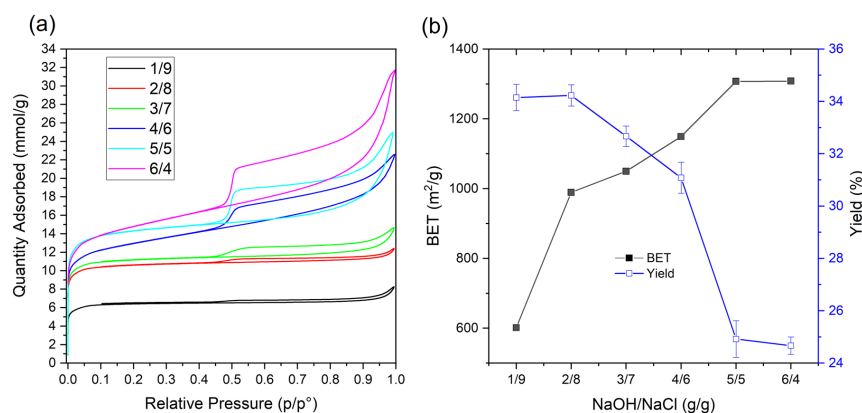


Fig. 5. N₂ adsorption-desorption isotherms (a); BET and yield (b) of prepared carbons using various NaOH/NaCl ratio at C = 1.0 g/g.

Table 4
Structure properties of prepared carbons using various NaOH/NaCl ratio.

NaOH/NaCl (g/g)	BET (m ² /g)	V _{micro} ^a (cm ³ /g)	V _{meso} ^b (cm ³ /g)	V _{total} ^c (cm ³ /g)	Yield (%)
1/9	601	0.19	0.05	0.25	34.15
2/8	989	0.32	0.05	0.37	34.23
3/7	1050	0.34	0.10	0.44	32.67
4/6	1150	0.37	0.30	0.67	31.08
5/5	1307	0.43	0.31	0.74	24.92
6/4	1308	0.41	0.54	0.95	24.67

^a Micropore volume is calculated by DR equation.

^b Mesopore volume is calculated as the difference between V_{total} and V_{micro}.

^c Total volume of pores is calculated at p/p° = 0.99.

3.2. The origin of pores

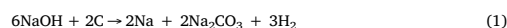
3.2.1. The role of NaCl

As discussed above, the NaCl contributes to macropore formation. According to previous research, oxides (Morishita et al., 2006) or KCl (Cao et al., 2018) crystals dispersed in carbon matrix could be a source of pores of similar size. These studies suggest a template mechanism of pore using NaCl. To clarify the assumed origin of pores, the pore size was evaluated using NLDFT pore-size distribution (Fig. 1b) and SEM micrographs (Fig. 2), while NaCl crystal size was calculated by the W-H method using XRD data (Fig. 3a). Both sizes, of pores and crystals, obtained by the NLDFT and XRD methods, were also visually compared with sizes observed on SEM micrographs (Figs. 2 and 3b). The NLDFT pore-size distribution (Fig. 1b) exhibits the peak at 63.2 nm, a size that is indexed to macropores according to IUPAC classification. In Fig. 3 and in Table 3, NaCl crystal size derived from information on corresponding XRD peaks can be seen crystals observed on the SEM micrograph have a similar size of macropores observed in Fig. 2, regardless of the use of NaOH. Therefore, we can assume the template role of NaCl in the process of pore formation.

3.2.2. The role of NaOH

Among the macropores, a considerable amount of micropores and some mesopores of carbons prepared using NaOH/NaCl are defined by NLDFT pore size distribution (Fig. 1b) in good agreement with the SEM micrographs (Fig. 2). NaOH-activated carbon exhibits micropores while the lack of NaCl leads to the absence of macropores, which are not observed on the SEM images (Fig. 2 NaOH). The most probable pores of NaOH-activated carbons whatever use of NaCl, defined by NLDFT

analyses are micropores (Fig. 1b). In a high-resolution SEM micrograph (Fig. 2), micropores of a size around 2 nm can also be found. Micropores could be formed by the following chemical reactions (Lillo-Ródenas et al., 2003):



The product of assumed chemical reaction (1) is sodium carbonate that can be detected by analytical methods. The characteristic peaks of Na₂CO₃ are found in the XRD spectra of samples prepared using NaOH (Fig. 3a). The corresponding peaks of Na₂CO₃ are indexed to reference number ICSD98-008-0985 of the standard XRD pattern of sodium carbonate. The SEM micrograph of the sample prepared using NaOH before leaching shows a different structure compare to samples containing NaCl. The formed crystal shapes are inherent in sodium carbonate. The peaks at 1423, 1426 cm⁻¹ and 832, 876 cm⁻¹ attributed to carbonates (Da Cunha et al., 2014) are found on FTIR spectra (Fig. 4a) and the thermal decomposition of Na₂CO₃ starting at 835 °C (Kim et al., 2001) is observed as a strong peak on the DTG curve (Fig. 4b). In support of micropores origin, chemical reactions (1) and (2) could be assumed since the formation of Na₂CO₃ is confirmed by the abovementioned analytical methods. The formation of mesopores of size 7–10 nm (Fig. 2) can also be explained by the assumed chemical reactions, since the NaCl crystals corresponding to mesopores size are not observed on SEM and not derived from XRD data. Consequently, the template origin of mesopores is questionable while chemical formation is more probable.

3.3. Effect of NaOH/NaCl ratio

As discussed earlier NaOH and NaCl have a significant effect on porous structure. The influence of various NaOH/NaCl ratios on carbon texture is worth studying. The adsorption isotherms of carbons prepared using different NaOH-to-NaCl ratios are presented in Fig. 5a.

Starting from ratios of 1/9 to 3/7, adsorption isotherms exhibit Type I of microporous materials. With an increase NaOH presence from 4/6 to 6/4, the isotherms showed an ascended curvature and pronounced hysteresis H4 more intrinsic in composite isotherm I, II, indicating the development of the porous structure. In particular, the slope of the isotherm and hysteresis H4 type pointed to macropore formation, while the plateau starting at low p/p° is attributed to micropores network. The micropore volume and total volume significantly increased starting from a 4/6 ratio and leading to an enlarged BET

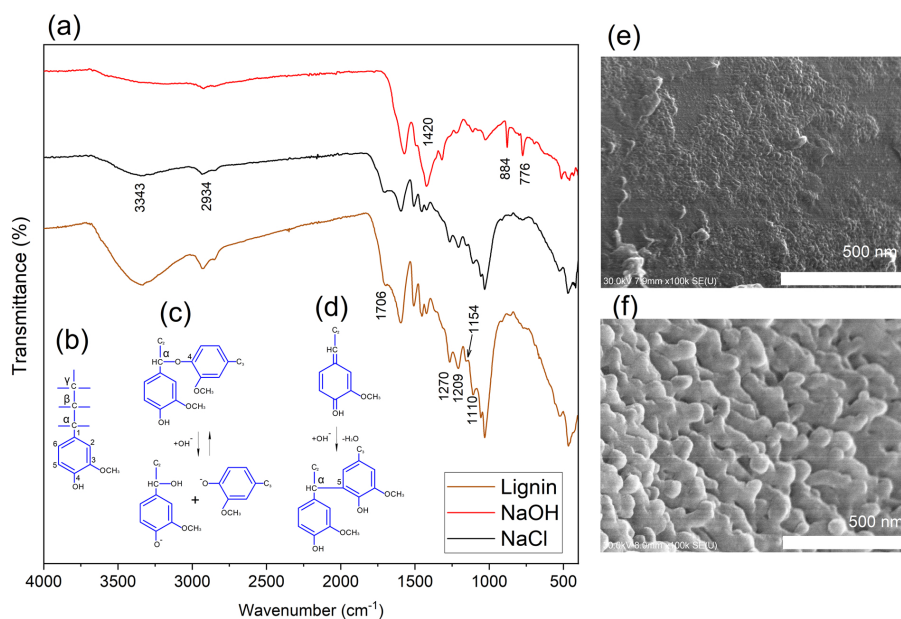


Fig. 6. The FTIR spectra of raw lignin, dried mixtures of lignin-NaCl and lignin-NaOH (a); guaiacylpropane unit (b); reactions of destruction (c) and condensation (d) of lignin in alkaline media; SEM images of lignin-NaOH (e) and lignin-NaCl (f) mixtures.

Table 5
Regression coefficients in coded units and statistical validations of models.

Factor/Response	BET Surface area	Yield
Model	Quadratic	Linear
Intercept	765.36	37.48
A ^a	272.21	-3.13
B ^b	51.25	-0.60
C ^c	136.94	-6.61
AB	22.32	-
AC	73.62	-
BC	29.43	-
A ²	21.51	-
B ²	-18.51	-
C ²	-53.28	-
Standard deviation	3.44 (m ² /g)	0.03 (%)
R-squared	0.992	0.971
Model F-value	87.15	135.43
Model p-value	< 0.0001	< 0.0001

^a Temperature.

^b Time.

^c Ratio.

surface area (Table 4). It is noteworthy that, total pore volume increases with increased NaOH since assumed interactions (1) and (2) induce carbon burn-off with further formation of macropores (Fierro et al., 2007). Meanwhile, micropore volume also increases assuming possible additional micropore formation on macropore walls (Morishita et al., 2010) so, according to Fig. 5a and Table 4, carbons prepared using NaOH-to-NaCl ratios from 1/9 to 3/7 are assigned to microporous materials, while samples prepared using 4/6 to 6/4 ratios are also significantly meso-macroporous.

The effect of the NaOH-to-NaCl ratio versus BET surface area and yield is presented in Fig. 5b. As NaOH content increase, BET surface also increases while yield decreases since the carbon was consumed for

void formation via presumed reactions (1) or (2). According to the results presented on Fig. 5b and Table 4, the largest BET surface and pore volume at moderate yield are attributed to 4/6 NaOH-to-NaCl ratio. Moreover, the meso- and macropores are more intrinsic starting from a 4/6 ratio that is beneficial to the accessibility of micropores, so a 4/6 ratio is selected for further experiments.

It can be seen that carbons prepared using only NaCl (Fig. 1a) are ascribed to macroporous materials and, even when an insignificant amount of NaOH was added (ratio 1/9, Fig. 5a), micropores appeared. This can be explained by the chemical interaction between lignin and NaOH, which is discussed in the next section “Interaction between lignin and NaOH”.

3.4. The interaction between lignin and NaOH

The chemical reactions of lignin in alkali media could sufficiently affect the porous structure of the obtained carbon. The reactions of destruction and condensation are peculiar to lignin in the presence of NaOH. Condensation is more inherent in coniferous lignin compared to deciduous lignin. In the present case, the origin of the used lignin is coniferous wood that can be confirmed by a characteristic FTIR peak at 1270 cm⁻¹ (Fig. 6a) indexed to a guaiacylpropane unit (Fig. 6b) (Azarov et al., 1999). In particular, reactions of destruction are caused by split-off α -O-4 or β -O-4 bonds (Fig. 6c) and condensation can occur in α -5 position (Fig. 6d) (Azarov et al., 1999). The strong peaks located at 3343 cm⁻¹ and 2934 cm⁻¹ are assigned to stretching vibrations of OH- and C-H in -CH₃ or -CH₂-, respectively. Significant changes are observed the following peaks: 1706 cm⁻¹ - aromatic C-H_n stretching (Yang et al., 2007); 1270 cm⁻¹ -C-O-C stretching of the aryl-alkyl ether bond (Yang et al., 2007); 1209 cm⁻¹ -C-O stretching of the guaiacyl ring (Azarov et al., 1999); 1154 cm⁻¹ and 1110 cm⁻¹ - stretching vibrations in the guaiacylpropane unit (Azarov et al., 1999).

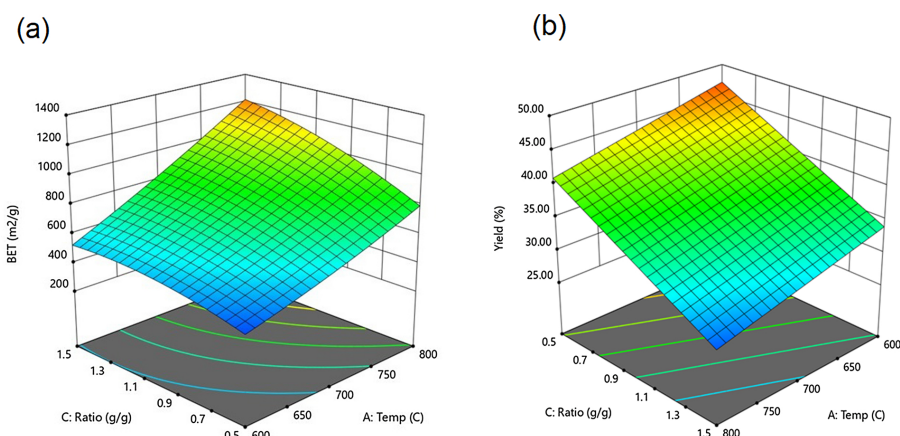


Fig. 7. Three-dimensional responses of BET surface area (a) and yield (b).

Table 6

The values of responses at optimal factors using desirability function.

Optimal factors and responses	BET (m ² /g)	Yield (%)
Temperature A (°C)	868	
Time B (min)	47	
Ratio C (g/g)	0.6	
Predicted response	1009	37.8
Obtained response	998	37.4
Standard deviation	5	0.3

Table 7

The comparison of obtained activated carbon with previously reported KOH- and NaOH-activated carbons.

Activation agent	KOH	NaOH	NaOH/NaCl (only NaOH)
Ratio (g/g)	1	1	0.60 (0.24)
Temperature (°C)	700	700	868
Time (min)	60	60	47
N ₂ flow (mL/min)	200	200	500
Heating rate (°C/min)	5.0	5.0	5.0
BET (m ² /g)	1100	1100	998
Yield (%)	50	40	37.4
Reference	(Fierro et al., 2007)	(Fierro et al., 2007)	This study

The mentioned changes are assigned to linkages, which take part in the reactions of destruction (Fig. 6c) and condensation (Fig. 6d). The peaks at 1420 cm⁻¹, 884 cm⁻¹ and 776 cm⁻¹ could be indexed to formed carbonate by CO₂ captured from air (Da Cunha et al., 2014).

SEM micrographs exhibit the textural changes of lignin-NaOH (Fig. 6e) and lignin-NaCl (Fig. 6f) mixtures before pyrolysis. It can be seen that the sample of lignin-NaOH has a smooth surface whereas roughness and a porous structure are observed for lignin-NaCl. These differences are explained by possible interaction between the NaOH and lignin via the assumed aforementioned interactions (Fig. 6c, d).

The thermal degradation (see TGA/DTG, Fig. 4b) at around 200–210 °C is assigned to cleavage of α-O-4 or β-O-4 linkages (Balat, 2008). The peaks at 325 °C and 365 °C could be attributed to splitting off aliphatic chains and destruction of carbon-carbon linkage C_α-C_β (Azarov et al., 1999). It is noteworthy that, for the sample containing NaCl, a peak at 200–210 °C is not observed while, for the sample containing NaOH there are peaks at 200–210 °C, indicating possible

interaction (Fig. 6c, d). The temperature difference of carbon-carbon C_α-C_β cleavages starting at 325 °C for samples containing NaOH and at 365 °C for NaCl samples can be also induced by possible effect of NaOH. In support of inference, the peak at 435 °C cleavage in the aryl-aryl bonds at 435 °C (Balat, 2008) is only observed for samples containing NaOH, pointing to the influence of NaOH on the lignin structure.

Interestingly, the FTIR peaks of lignin are not observed for pyrolysed carbons (Fig. 4a) whether or not NaOH or NaCl was used, indicating the essential degradation of lignin and the formation of a carbon-like structure.

The granulation capability of lignin-NaOH mixture can be explained by suggested interactions. In particular, reactions of condensation may contribute to granulation without binder. The comparison of Vickers hardness for NaOH-activated carbon and commercial activated carbon Norit is presented in Supplementary Material S1. NaOH-activated carbon exhibits higher values of Vickers hardness (44.61 kgf/mm²) compared to commercial activated carbon Norit (23.11 kgf/mm²). However, it was not possible to granulate lignin-NaCl mixture without binder due to lack of aforementioned interactions (Fig. 6c, d). In the case of activated carbon using lignin-NaOH/NaCl mixture, the granules were not sufficiently hard to evaluate via the Vickers test because the presence of macropores significantly reduces the hardness of the material (Nieto-Delgado and Rangel-Mendez, 2011).

3.5. Process optimisation

The process optimisation of activated carbon production using NaOH/NaCl mixture was performed according to the experimental design (Table 1). The NaOH/NaCl ratio was discussed in the previous section "Effect of NaOH/NaCl ratio" and the optimal 4/6 ratio was used for process optimisation among varied factors. The regression coefficients of each response and values of statistical validity are presented in Table 5.

It can be seen from Table 5 that the standard deviation of three repetitions on a zero level (Table 1) are negligible for both responses indicating remarkable reproducibility. The R-squared of responses approaches unity since the difference between the predicted and experimental values are negligible. The model F-value of 87.15 and 135.43 for BET surface area and yield, respectively implies that the models are significant since there is only a 0.01% chance of this occurring because of noise. The model p-value below 0.05 indicates that the model terms are significant, whereas, for BET and yield models, the p-values are far

below 0.05 (Table 5). In addition, according to the abovementioned statistical validations, the experimental data of BET surface area is in good agreement with the quadratic model while yield does fit a linear model.

The regression coefficients of the BET model increase with an increase factor values. By contrast, the yield decreases while factors increase that can be concluded from the negative values of regression coefficients. The factor of the NaOH/NaCl-to-lignin ratio (C) is the most essential factor since the regression coefficient values are the highest. The influence of temperature (A) on responses is also significant, while time (B) demonstrates the weakest effect. Fig. 7 exhibits the steep curvature of three-dimensional responses (BET and yield) of temperature (A) and ratio (C). It is noteworthy that, the maximum cannot be achieved for both responses because while one response increases, the other decreasing. More specifically, the maximum BET surface area appears at 800 °C and 1.5 g/g, while the maximum yield is observed at the minimum temperature 600 °C and 0.5 g/g of ratio.

This behaviour is in a good agreement with previously reported results (Fierro et al., 2007) and (Zhihang et al., 2017) indicating that increase factors has a positive effect on the BET surface whereas the influence on yield is negative. The increase of ratio, temperature and time lead to an enlarged surface area since the formation of porous texture is occurred in the same manner (chemical reaction (1) and (2)). Meanwhile, the yield decreases due to the transformation of micropores to meso- and macropores with further void formation.

According to the obtained mathematical models for BET surface area and yield, the optimal values of factors can be predicted. To maximise both responses simultaneously, a desirability function D was used (Harrington, 1965):

$$D = (d_1 \cdot d_2 \cdot \dots \cdot d_n)^{\frac{1}{n}} = \left(\prod_{i=1}^n d_i \right)^{\frac{1}{n}} \quad (3)$$

where d_i is a response and n is a number of responses.

Table 6 shows predicted and obtained responses at optimal factors. Activated carbons prepared at optimal factors in three repetitions to evaluate reproducibility and the difference between predicted and obtained values are negligible, additionally indicating the validity of the model.

The large value of BET surface area can be achieved at moderate yield using optimal conditions defined by RSM design. To demonstrate the outstanding features of this method, a comparison with previously reported NaOH- or KOH-activated carbon using kraft lignin was made (Fierro et al., 2007) (Table 7).

The BET surface area of obtained activated carbon is more or less the same while the chemical ratio is much lower. Moreover, NaOH consumption is four times lower than with the previously reported method. The discrepancies in yield can be explained by the increased consumption of N_2 flow used in experiments.

4. Conclusion

The new affordable NaOH/NaCl mixture was successfully used as an activation agent for activated carbon production using hydrolytic lignin. The application of NaOH/NaCl allows a reduction in NaOH consumption for the activation, contributing to the cost-efficiency of the obtained carbon. A large BET surface area was achieved while the yield was kept at a moderate level using this method. The mechanism of activation has been proposed and confirmed by analytical techniques. In particular, NaCl promotes the template mechanism of macropore formation, while NaOH is responsible for the microporous structure through chemical reactions. The results of adsorption isotherms, NLDFT pore-size distribution, XRD crystal size and SEM images coincide and corroborate the assumed mechanism. The NaOH/NaCl ratio was studied indicating developed micro- meso- and macroporosity with an increase NaOH content. Based on structural changes for samples

containing NaOH, which were observed by FTIR, SEM and TGA, the interaction of lignin and NaOH is assumed and could influence the porous structure of the obtained carbon. Optimisation using RSM design has been performed and the quadratic model fits the experimental data of the BET surface area, whereas yield is in a good agreement with the linear model according to the ANOVA test. The predicted values of BET area and yield using a desirability function are well matched with the obtained values also indicating the adequacy of the model.

In addition, the carbon obtained using NaOH/NaCl mixture and hydrolytic lignin demonstrated coinciding textural properties compared to previously reported NaOH- or KOH-activated carbons. Meanwhile, accessibility to micropores has been greatly developed through macropores created by the NaCl template. Moreover, NaOH consumption using this method was significantly reduced leading to extension of this method to industrial application.

Acknowledgments

This work was supported by the Finnish innovation funding Business Finland [6886/31/2017]. We appreciate Professor Khanita Kamwilaisak from Khon Kaen University for valuable comments for the manuscript. We thank Dr Oleksii Sozinov and Dr Denys Musienko from Lappeenranta-Lahti University of Technology LUT for the meaningful discussions concerning X-Ray diffraction. We also thank anonymous reviewers for useful comments and suggestions that improve the quality of the manuscript.

Appendix A. Supplementary data

Supplementary material related to this article can be found, in the online version, at doi:<https://doi.org/10.1016/j.indcrop.2019.03.050>.

References

- Azarov, V.I., Burov, A.V., Obolenskaya, A.V., 1999. Khimiya drevesiny i sinteticheskikh polimerov (Chemistry of Wood and Synthetic Polymers). SPbLTA, St.Petersburg. Khimiya drevesiny i sinteticheskikh polimerov (Chemistry of Wood and Synthetic Polymers). SPbLTA, St.Petersburg.
- Balat, M., 2008. Mechanisms of thermochemical biomass conversion processes. Part 1: reactions of pyrolysis. Energy Sources Part A Recover. Util. Environ. Eff. 30, 620–635. <https://doi.org/10.1080/15567030600817258>.
- Boehm, H.P., 1994. Some aspects of the surface chemistry. Carbon 32, 759–769. [https://doi.org/10.1016/0008-6223\(94\)90031-0](https://doi.org/10.1016/0008-6223(94)90031-0).
- Box, G.E.P., Wilson, K.B., 1951. On the experimental attainment of optimum conditions. J. R. Stat. Soc. Ser. B 13, 1–45.
- Brunauer, S., Emmett, P.H., Teller, E., 1938. Adsorption of gases in multimolecular layers. J. Am. Chem. Soc. 60, 309–319. <https://doi.org/10.1021/ja01269a023>.
- Cao, Y., Wang, X., Gu, Z., Fan, Q., Gibbons, W., Gadhamshetty, V., Ai, N., Zeng, G., 2018. Potassium chloride templated carbon preparation for supercapacitor. J. Power Sources 384, 360–366. <https://doi.org/10.1016/j.jpowsour.2018.02.079>.
- Culebras, M., Beaucamp, A., Wang, Y., Clauss, M.M., Frank, E., Collins, M.N., 2018. Biobased structurally compatible polymer blends based on lignin and thermoplastic elastomer polyurethane as carbon Fiber precursors. ACS Sustain. Chem. Eng. 6, 8816–8825. <https://doi.org/10.1021/acssuschemeng.8b01170>.
- Da Cunha, D.L., Pereira, G.F.C., Felix, J.F., Albino Aguiar, J., De Azevedo, W.M., 2014. Nanostructured hydrocerussite compound (Pb₂(CO₃)₂(OH)₂) prepared by laser ablation technique in liquid environment. Mater. Res. Bull. 49, 172–175. <https://doi.org/10.1016/j.materresbull.2013.08.030>.
- Dalton, N., Lynch, R.P., Collins, M.N., Culebras, M., 2019. Thermoelectric properties of electrospun carbon nanofibres derived from lignin. Int. J. Biol. Macromol. 121, 472–479. <https://doi.org/10.1016/j.ijbiomac.2018.10.051>.
- Das, S., Mishra, S., 2017. Box-Behnken statistical design to optimize preparation of activated carbon from Limonia acidissima shell with desirability approach. J. Environ. Chem. Eng. 5, 588–600. <https://doi.org/10.1016/j.jece.2016.12.034>.
- Dubinin, M.M., Radushkevich, L.V., 1947. On the equation of the characteristic curve for active coals. Dokl. Akad. Nauk SSSR 4, 331–334 [Reports Acad. Sci. USSR].
- Evstigneyev, E.I., Yuzikhin, O.S., Gurinov, A.A., Ivanov, A.Y., Artamonova, T.O., Khodorovskiy, M.A., Bessonova, E.A., Vasilyev, A.V., 2016. Study of structure of industrial acid hydrolysis lignin, oxidized in the H₂O₂-H₂SO₄ system. J. Wood Chem. Technol. 36, 259–269. <https://doi.org/10.1080/02773813.2015.1137945>.
- Fierro, V., Torné-Fernández, V., Celzard, A., 2007. Methodical study of the chemical activation of Kraft lignin with KOH and NaOH. Microporous Mesoporous Mater. 101, 419–431. <https://doi.org/10.1016/j.micromeso.2006.12.004>.
- Frackowiak, E., Béguin, F., 2001. Carbon materials for the electrochemical storage of energy in capacitors. Carbon 39, 937–950. [https://doi.org/10.1016/S0008-6223\(00](https://doi.org/10.1016/S0008-6223(00)

- 00183-4.
- Fu, K., Yue, Q., Gao, B., Sun, Y., Zhu, L., 2013. Preparation, characterization and application of lignin-based activated carbon from black liquor lignin by steam activation. *Chem. Eng. J.* 228, 1074–1082. <https://doi.org/10.1016/j.cej.2013.05.028>.
- Harrington, E.C., 1965. The desirability function. *Ind. Qual. Control* 21, 494–498.
- Hayashi, J., Kazehaya, A., Muroyama, K., Watkinson, A.P., 2000. Preparation of activated carbon from lignin by chemical activation. *Carbon* 38, 1873–1878. [https://doi.org/10.1016/S0008-6223\(00\)00027-0](https://doi.org/10.1016/S0008-6223(00)00027-0).
- Kim, J., Lee, Y., Lee, H., 2001. Decomposition of Na_2CO_3 by interaction with SiO_2 in mold flux of steel continuous casting. *ISIJ Int.* 41, 116–123.
- Kruk, M., Dufour, B., Celer, E.B., Kowalewski, T., Jaroniec, M., Matyjaszewski, K., 2005. Synthesis of mesoporous carbons using ordered and disordered mesoporous silica templates and polyacrylonitrile as carbon precursor. *J. Phys. Chem. B* 109, 9216–9225. <https://doi.org/10.1021/jp045594x>.
- Lillo-Ródenas, M.A., Cazorla-Amorós, D., Linares-Solano, A., 2003. Understanding chemical reactions between carbons and NaOH and KOH: an insight into the chemical activation mechanism. *Carbon* N. Y. 41, 267–275. [https://doi.org/10.1016/S0008-6223\(02\)00279-8](https://doi.org/10.1016/S0008-6223(02)00279-8).
- Marsh, H., Rodríguez-Reinoso, F., 2006. Activated carbon. *Activated Carbon*. <https://doi.org/10.1016/B978-0-08-044463-5.X5013-4>.
- Matsuoka, K., Yamagishi, Y., Yamazaki, T., Setoyama, N., Tomita, A., Kyotani, T., 2005. Extremely high microporosity and sharp pore size distribution of a large surface area carbon prepared in the nanochannels of zeolite Y. *Carbon* N. Y. 43, 876–879. <https://doi.org/10.1016/j.carbon.2004.10.050>.
- Morishita, T., Soneda, Y., Tsumura, T., Inagaki, M., 2006. Preparation of porous carbons from thermoplastic precursors and their performance for electric double layer capacitors. *Carbon* N. Y. 44, 2360–2367. <https://doi.org/10.1016/j.carbon.2006.04.030>.
- Morishita, T., Tsumura, T., Toyoda, M., Przepiórski, J., Morawski, A.W., Konno, H., Inagaki, M., 2010. A review of the control of pore structure in MgO-templated nanoporous carbons. *Carbon* N. Y. 48, 2690–2707. <https://doi.org/10.1016/j.carbon.2010.03.064>.
- Müller-Hagedorn, M., Bockhorn, H., Krebs, L., Müller, U., 2003. A comparative kinetic study on the pyrolysis of three different wood species. *J. Anal. Appl. Pyrolysis* 68–69, 231–249. [https://doi.org/10.1016/S0165-2370\(03\)00065-2](https://doi.org/10.1016/S0165-2370(03)00065-2).
- Nieto-Delgado, C., Rangel-Mendez, J.R., 2011. Production of activated carbon from organic by-products from the alcoholic beverage industry: surface area and hardness optimization by using the response surface methodology. *Ind. Crops Prod.* 34, 1528–1537. <https://doi.org/10.1016/j.indcrop.2011.05.014>.
- Ravikovitch, P.I., Neimark, A.V., 2001. Characterization of micro- and mesoporosity in SBA-15 materials from adsorption data by the NLDFT method. *J. Phys. Chem. B* 105, 6817–6823. <https://doi.org/10.1021/jp010621u>.
- Rouquerol, J., Llewellyn, P., Rouquerol, F., 2007. Is the bet equation applicable to microporous adsorbents? In: Llewellyn, P.L., Rodríguez-Reinoso, F., Rouquerol, J., Seaton, N. (Eds.), *COPS-7: Characterization of Porous Solids VII, Studies in Surface Science and Catalysis*. Elsevier, Amsterdam, pp. 49–56. [https://doi.org/10.1016/S0167-2991\(07\)80008-5](https://doi.org/10.1016/S0167-2991(07)80008-5).
- Shao, J., Ma, F., Wu, G., Dai, C., Geng, W., Song, S., Wan, J., 2017. In-situ MgO (CaCO_3) templating coupled with KOH activation strategy for high yield preparation of various porous carbons as supercapacitor electrode materials. *Chem. Eng. J.* 321, 301–313. <https://doi.org/10.1016/j.cej.2017.03.092>.
- Sing, K.S.W., 2014. Adsorption by active carbons. *Adsorption by Powders and Porous Solids*. Elsevier, pp. 321–391. <https://doi.org/10.1016/B978-0-08-097035-6.00010-3>.
- Thommes, M., Kaneko, K., Neimark, A.V., Olivier, J.P., Rodríguez-Reinoso, F., Rouquerol, J., Sing, K.S.W., 2015. Physisorption of gases, with special reference to the evaluation of surface area and pore size distribution (IUPAC Technical Report). *Pure Appl. Chem.* 87, 1051–1069. <https://doi.org/10.1515/pac-2014-1117>.
- Torné-Fernández, V., Mateo-Sanz, J.M., Montané, D., Fierro, V., 2009. Statistical optimization of the synthesis of highly microporous carbons by chemical activation of kraft lignin with NaOH. *J. Chem. Eng. Data* 54, 2216–2221. <https://doi.org/10.1021/je800827n>.
- Williamson, G.K., Hall, W.H., 1953. Discussion of the theories of line broadening. *Acta Metall.* 1, 22. [https://doi.org/10.1016/0001-6160\(53\)90006-6](https://doi.org/10.1016/0001-6160(53)90006-6).
- Yang, H., Yan, R., Chen, H., Lee, D.H., Zheng, C., 2007. Characteristics of hemicellulose, cellulose and lignin pyrolysis. *Fuel* 86, 1781–1788. <https://doi.org/10.1016/j.fuel.2006.12.013>.
- Zhihang, Y., Zhihua, X., Daofang, Z., Chen, W., Zhang, T., Huang, Y., Gu, L., Deng, H., Danqi, T., 2017. Box-Behnken design approach towards optimization of activated carbon synthesized by co-pyrolysis of waste polyester textiles and MgCl_2 . *Appl. Surf. Sci.* 340–348. <https://doi.org/10.1016/j.apsusc.2017.08.241>.

Publication II

Ponomarev, N.P. and Kallioinen, M.
**Synergy between alkali activation
and a salt template in superactive carbon production from lignin**

Reprinted with permission from
Nanotechnology
Vol. 32, 2021
© 2021, IOP Publishing

Synergy between alkali activation and a salt template in superactive carbon production from lignin

Nikolai P Ponomarev*  and Mari Kallioinen

Department of Separation Sciences, School of Engineering Science, Lappeenranta-Lahti University of Technology LUT, Sammonkatu 12, FI-50130 Mikkeli, Finland

E-mail: nikolai.ponomarev@lut.fi and pnn92@mail.ru

Received 9 September 2020, revised 2 November 2020

Accepted for publication 12 November 2020

Published 2 December 2020



CrossMark

Abstract

Due to growing demand, the performance of traditional active carbon is insufficient. An innovative solution is superactive carbon with an ultra-high surface area as high as $3000 \text{ m}^2 \text{ g}^{-1}$. However, this material is very costly due to the considerable amount of alkali used in its manufacturing. To obtain superactive carbon from lignin, KOH and KCl were used simultaneously. The method was thoroughly studied to describe the mechanism of pore origin and control the pore size. Because of synergy between KOH and KCl, superactive carbon with an ultra-high surface area ($2938 \pm 42 \text{ m}^2 \text{ g}^{-1}$) was obtained at essentially diminished KOH consumption (1 g g^{-1}) in contrast to previously reported methods. The process was optimised using the response surface method. The pore size can be tuned by varying the amount of KOH and temperature. Observed synergy enabled reduced alkali consumption, overcoming the barrier to widespread implementation of superactive carbon.

Supplementary material for this article is available [online](#)

Keywords: activated carbon, KOH, KCl, lignin

(Some figures may appear in colour only in the online journal)

1. Introduction

Active carbon is a well-known porous solid material with a diverse porous structure and large specific surface area (SSA). There are a variety of applications of active carbon from wastewater treatment to energy storage materials [1]. Active carbon is produced from carbonaceous materials through physical or chemical activation [2]. SSA is a crucial characteristic of active carbon and it is typically between 500 and $1500 \text{ m}^2 \text{ g}^{-1}$ for commercial samples. The cutting edge product is superactive carbon that possesses an ultra-high surface

area up to $3000 \text{ m}^2 \text{ g}^{-1}$ [3]. The ultra-high surface area is beneficial for various applications. For instance, in drinking water purification the adsorption of sodium hypochlorite and chloroform was substantially increased by increasing the surface area [4]. The capacitance of supercapacitors using materials with high surface area is also better than conventional active carbon [5–7]. The increased SSA of superactive carbon is also advantageous for gas storage systems, since a larger volume of natural gas can be adsorbed [8]. As can be seen from these examples, the use of superactive carbon is beneficial in many applications and its use can decrease the needed amount of adsorbent, enabling more sustainable processes. However, improvements to increase the sustainability of the manufacturing process of superactive carbon are still needed.

Superactive carbon was first produced by the AMOCO company (Standard Oil Company) in 1978 by KOH activation using petroleum coke as a raw material [9]. The

* Author to whom any correspondence should be addressed.

 Original content from this work may be used under the terms of the [Creative Commons Attribution 4.0 licence](#). Any further distribution of this work must maintain attribution to the author(s) and the title of the work, journal citation and DOI.

superactive carbon of AMOCO is now produced by the Kansai Coke and Chemicals Company under the brand name MAXSORB® [10]. The unique aspect of the process is the use of significant excess of potassium hydroxide per gram of starting material (3–4 g g⁻¹). The superactive carbons produced in the process have a surface area greater than 3000 m² g⁻¹ and rich in micropores. The genesis of a microporous structure is conducted through the interaction of potassium hydroxide with carbon matter, yielding the formation of the corresponding carbonate at temperatures below 700 °C and metallic potassium over 700 °C [11]. The metallic potassium is assumed to be responsible for the origin of micropores through intercalation and by following an expansion of the graphite layers [12]. The micropores and mesopores are generated on the walls of the macropores, which in turn are formed through the self-template of KOH grains [13, 14]. Superactive carbon possesses a versatile porous structure necessary for industrial applications but, since a large amount of KOH is consumed in the process, the material is not affordable and, for most applications, traditional steam-activated carbon is used because of its low price, despite the superior properties of superactive carbon. Studies aiming to reduce alkali consumption in the process of superactive carbon production are therefore essential for technological applications.

Ordered porous carbon can be produced using the so-called template method. A zeolite template is used as a carbon replica for the synthesis of highly ordered porous material with a surface area of 2000–4000 m² g⁻¹ [15]. The polymer solution penetrates the zeolite structure with subsequent carbonisation. The resultant composite contains zeolite and carbon. The zeolite template is removed by leaching using strong mineral acid, and an exact carbon replica is obtained. The template carbon possesses an ordered microporous structure underlying an ultra-high SSA but, for the adsorption applications, a diverse porous structure, containing both mesopores and macropores is needed, and the ordered microporous structure of the template carbon is not porous enough [16]. Moreover, since the raw materials are usually synthetic zeolites and polymers coupled with leaching by a strong acid, the zeolite template carbon is an expensive material with limited applications compared to conventional activated carbon.

There are very few reports that have demonstrated the use of affordable templates for carbon materials with or without subsequent physical or chemical activation [17–19]. However, the reported materials do not possess an ultrahigh surface area. Our previous studies revealed a new method for producing microporous carbon by the simultaneous use of NaCl as a template and NaOH as an activator [20]. This method enables production of an active carbon at reduced alkali consumption, but the obtained carbon has a surface area in the range of conventional activated carbon and far below, in contrast to the ultrahigh surface area of the superactive carbon prepared by KOH activation or the zeolite template method.

(Super)active carbon can be made on any carbonaceous materials. The availability and affordability of the potential

raw material should be taken into account. The carbon content in the raw material is also important because the higher the carbon content in the raw material, the higher the potential yield of the product. Examples of raw materials for superactive carbons are petroleum coke [10], Spanish anthracite [21] and kraft lignin [22]. Lignin, as the second most abundant plant polymer after cellulose and having substantial carbon content over 50%, is an advantageous choice among a variety of raw materials [23]. It is also a by-product of the paper industry and ethanol production from wood. Lignin that originates from the kraft process is called kraft or alkali lignin. It is produced, for example, by the LignoBoost® process through precipitation of lignin from black liquor using acid and CO₂ [24]. Despite the straightforwardness of the process, the availability of kraft lignin is still quite limited due to several applications that utilise it and the limited volumes and numbers of commercial-scale producers. Another example of industrial lignin is hydrolysis lignin. This material is a by-product of ethanol production through the hydrolysis of wood carbohydrates. In this process, the carbohydrate part of the wood is hydrolysed for subsequent fermentation while the aromatic part (lignin) remains almost the same. Usually, the hydrolysis lignin is incinerated to produce energy, but the use of lignin for a valuable product like superactive carbon is beneficial compared to incineration. In particular, the price of active carbon is 2–7 times higher than the price of energy obtained after the incineration of lignin [25]. Moreover, there are over 95 million tonnes of lignin waste deposits from the biomass hydrolysis process in post-Soviet republics, leading to environmental problems, so their utilisation is required [26]. Accordingly, hydrolysis lignin is an advantageous raw material for the manufacturing of superactive carbon.

The aim of this study is to intensify the production of superactive carbon by applying the synergy between KOH activation and a KCl template. To optimise the process and obtain superactive carbon at maximum surface area and product yield at minimised alkali consumption, the response surface method (RSM) was applied [27]. Since the control of pore size is important for industrial applications, the tuning of pore size distribution was methodically conducted [28, 29]. In addition, the mechanism of pore formation was investigated revealing the synergy of KOH activation and the KCl template.

2. Materials and methods

2.1. Materials

The raw material is coniferous hydrolysis lignin with a moisture content of 6%. The chemicals such as KOH, K₂CO₃, KCl and NaCl (Sigma-Aldrich) were of analytical purity and dried in a vacuum at 105 °C to remove moisture before use. Deionised water was used to wash the obtained carbon. The nitrogen gas was 99.9999% purity.

2.2. Methods

2.2.1. Producing superactive carbon. The lignin was mixed with KOH and KCl in a mortar. The amount of KOH in the KOH/KCl mixture varied between 0.3 and 1.5 g g⁻¹ while the amount of KCl was 2.7–1.5 g g⁻¹ for each experimental run. The total lignin-to-KOH/KCl ratio was constant at 3 g g⁻¹. The obtained mixture was transferred to a tube furnace and heated at 5 °C min⁻¹ to the target temperatures of 700 °C, 800 °C and 900 °C. Carbonisation was maintained at target temperature for 60 min, and was conducted under nitrogen flow of 21 min⁻¹. Afterwards, the composite of carbon and chemicals was mixed with water. The chemicals were dissolved by washing several times in a Bucher funnel until neutral pH in the washing water was obtained. The produced carbon was dried in a vacuum at 105 °C for 16 h.

For comparison, the KOH-activated carbon (Sample F2007) was prepared according to the procedure adopted from literature [22]. In particular, KOH was mixed with lignin at a ratio of 3.0 g g⁻¹; heated at a ramp rate of 5 °C min⁻¹ to a target temperature of 700 °C and the temperature was maintained for 60 min. The produced carbon was washed several times in water until a neutral pH was obtained in the water. At the same heating rate and dwell time, for the comparison purpose, the carbon sample was prepared at 900 °C by using a mixture of 1.5 g of K₂CO₃ and 1.5 g of KCl (Sample RUN4-K₂CO₃). In the same manner, the carbon sample was obtained by mixing 1.0 g of KOH and 2.0 g of NaCl (Sample PRED1-NaCl). The effect of time (30, 60 and 90 min) was evaluated at 900 °C and KOH/KCl amount was 1.0/2.0 g g⁻¹ (Samples PRED1-30m, PRED1-60m and PRED1-90m).

2.2.2. Optimisation. The process was optimised using the RSM [27] by varying two factors: temperature (*A*, °C) and the amount of KOH in the KOH/KCl mixture (*B*, g g⁻¹). Minimum, zero and maximum levels were assigned to each factor: 700 °C, 800 °C and 900 °C for temperature and; 0.3, 0.9 and 1.5 g g⁻¹ for KOH amount. The characteristics of the produced carbon such as SSA (m² g⁻¹) and yield (Yield, %) were selected as responses. To evaluate the reproducibility, the samples were prepared in triplicate at zero level and optimal conditions. The adequacy of the obtained mathematical model was validated by ANOVA analysis.

2.2.3. Characterisation. The produced carbon was studied using N₂ physisorption on a Tristar[®] II Plus, Micromeritics. The characterisation was based on N₂ adsorption–desorption isotherms. The values of SSA were estimated using the Brunauer, Emmett and Teller theory [30], applying the recommended procedure for microporous solids [31]. The total pore volume was calculated at $p/p^0 = 0.99$. The micropore volume was calculated using the Dubin–Radushkevich equation [32]. The pore size distribution was plotted using non-local density functional theory (NLDFT) for carbon slit-like pores [33]. X-ray powder diffraction was used to investigate the ordered structures of the materials on a high-resolution PANalytical diffractometer. The spectra were

recorded from 10° to 120° 2θ degrees applying Co Kα radiation at a voltage of 40 kV. Crystal size was calculated using data from the corresponding diffraction peaks applying the Williamson–Hall method (W–H) [34]. Fourier transform infrared (FTIR) spectroscopy was performed on a Bruker Vertex 70 spectrometer. Scanning electron microscopy (SEM) images were obtained with a JEOL JSM-7900 scanning electron microscope, which was equipped with an energy dispersive x-ray spectrometer (EDS). Transmission electron microscopy (TEM) images were produced with a Hitachi H-7600 transmission electron microscope. Raman spectra were taken with a Horiba HR800 UV (Jobin/Yvon).

3. Results and discussion

3.1. Comparison of NaOH/NaCl and KOH/KCl mixtures

The samples were prepared according to the optimal conditions specified in table 1 of the previously studied method [20]. As seen in this table 1, the use of the mixture KOH/KCl resulted in a larger surface area and greater pore volume than the use of NaOH/NaCl. Figure 1 (the inset) shows the N₂ adsorption/desorption isotherms of the prepared carbons using different starting mixtures. Both of samples demonstrated intrinsic isotherm type I for microporous materials, but the carbon prepared using the NaOH/NaCl mixture demonstrates the hysteresis H4 that could be ascribed to the formed mesopores [35]. The shapes of the isotherm and adsorption hysteresis are attributed to the progressive carbon burn-off that leads to the fusion of micropores into mesopores [3]. On the NLDFT pore size distribution (figure 1, the inset), the peaks of meso- and macropores are strong for samples prepared using sodium-contained mixtures in contrast to samples prepared using KOH/KCl. Those prepared using KOH/KCl are more microporous while carbons prepared using NaOH/NaCl contain higher amounts of mesopores and macropores. Since the SSA mainly originates from micropores, it is greater for samples prepared using KOH/KCl due to a smaller number of meso- and macropores. This phenomenon can be explained by the assumption that KOH is favourable for micropores origin, while NaOH is responsible for the fusion between micropores into mesopores due to the above-mentioned burn-off [22]. Consequently, since potassium is a more active alkali metal than sodium, the mixture consisting of KOH and KCl is more effective in producing active carbon [36].

3.2. Ultra-high surface area

Since the KOH/KCl mixture is more efficient than the sodium-contained mixture, it was selected for further studies, to produce superactive carbon. At a modest chemical ratio, KOH/KCl-to-lignin of 0.6 g g⁻¹, a larger surface area can be achieved. To obtain carbon with ultra-high surface area by this method at minimum alkali consumption and the highest product yield, the RSM method was employed [27]. In the case of KOH activation, to obtain superactive carbons, the

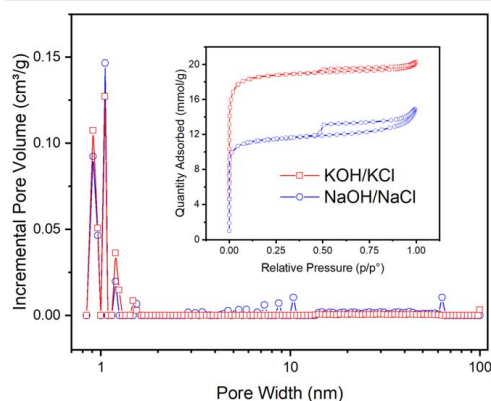


Figure 1. NLDFT pore size distribution and N_2 adsorption/desorption isotherms (the inset) of prepared carbons using the mixture of MOH/MCl ($M = Na, K$).

Table 1. Comparison of porous carbons prepared using NaOH/NaCl and KOH/KCl mixtures.

Alkaline metal	Na	K
MOH/MCl-to-lignin ($g\ g^{-1}$)	0.24/0.36	
Target temperature ($^{\circ}C$)	868	
Dwell time (min)	47	
SSA ($m^2\ g^{-1}$)	998 ± 5	1765 ± 35
V_{micro} ($cm^3\ g^{-1}$)	0.34 ± 0.01	0.58 ± 0.01
V_{total} ($cm^3\ g^{-1}$)	0.44 ± 0.00	0.61 ± 0.01
Reference	[20]	This study

chemical ratio should be between 3 and $4\ g\ g^{-1}$ [10, 22], so for all the experiments the chemical ratio (KOH/KCl-to-lignin, $g\ g^{-1}$) was maintained constant at $3.0\ g\ g^{-1}$. The formation of metallic potassium from KOH is a major activation pathway for an ultra-high surface area [11]. Metallic potassium is produced at temperatures over $700\ ^{\circ}C$ [10, 11], so the temperature regime from $700\ ^{\circ}C$ to $900\ ^{\circ}C$ was selected. Since the dwell time is a less significant factor for producing porous carbon, it was constantly kept at 60 min [20]. Based on the aforementioned information, only two factors were controlled in the experimental plan: KOH amount and target temperature.

At first, the experiments were performed at zero level (RUN0(1–3)). It can be seen that a large surface area ($2012 \pm 28\ m^2\ g^{-1}$) can be achieved at moderate alkali consumption. The maximum theoretical carbon yield from lignin is 55% [37], so the product yield ($41.51 \pm 0.59\%$) is quite high at zero level. The purpose of the zero level is also to evaluate the reproducibility of the method. Three repetitions were performed indicating good reproducibility. At a minimum level (RUN1), carbon was produced with a moderate value for the SSA ($1262\ m^2\ g^{-1}$), which is appropriate for the conventional active carbon. The results tallied well with the previous results when the alkali consumption was

very low [20]. The highest value of product yield (54.41%) was achieved at RUN1 which is close to the maximum theoretical value. The results on a minimum level revealed very modest alkali consumption ($0.3\ g\ g^{-1}$) while the surface area is satisfactory for typical active carbons. Moreover, the carbon yield was much higher, exceeding 54% in contrast to the 18% yield of steam-activated carbon with a surface area of $750\text{--}800\ m^2\ g^{-1}$ [38]. On a maximum level (RUN4), an ultrahigh surface area was gained ($3236\ m^2\ g^{-1}$) at the lowest carbon yield (15.58%), but the results at maximum level demonstrated the possibility to produce superactive carbon with a SSA exceeding $3000\ m^2\ g^{-1}$ at a KOH amount of $1.5\ g\ g^{-1}$ versus the $3.0\ g\ g^{-1}$ of the previously reported KOH-activated carbon using kraft lignin [22].

Overall, eight experimental runs were completed. The matrix (table 2) shows that by increasing the amount of alkali and target temperature, the surface area increases, while the yield decreases, which is the usual situation for active carbon production. This approach enables describing the process mathematically within the studied parameters using hydrolysis lignin as a starting material. Using the experimental plan (table 2), the equation of the process can be derived. For the surface area, the mathematical model of the process represents the linear equation:

$$SSA = 2064 + 486A + 505B + 191AB, \quad (1)$$

where the value of 2064 is an intercept; A and B are the process factors—temperature ($^{\circ}C$) and KOH amount ($g\ g^{-1}$), respectively.

The most essential factor for the SSA is the amount of KOH, while temperature also has a significant influence. According to the equation, all the regression coefficients are positive indicating increasing surface area with an increased level of KOH and temperature. This is also clear from the experimental plan.

The product yield can be described by the following equation:

$$Yield = 41.77 - 11.18A - 6.92B - 6.34AB. \quad (2)$$

In this case, the regression coefficients are negative. The yield values decrease as target temperature and the amount of added KOH increase. The most substantial factor for the product yield in this process is a target temperature in contradistinction to the chemical ratio for the method using NaCl/NaOH mixture [20]. This feature can be elucidated on by the assumption that NaOH leads to more intense burn-off of carbon matter, unlike KOH [22].

The above-mentioned attributes are inherent in porous carbon production [22]. With increasing temperature and KOH amount, the SSA increases while the yield decreases. KOH is an active component inducing erosion, etching and void formation that lead to surface area enlargement and at the same time yield reduction. The increase in temperature is accompanied by the progressive burn-off the carbon bulk with development of the surface area and loss of yield.

The statistical validations for the mathematical models obtained are shown in table 3. According to the ANOVA test, the experimental responses coincide with the predicted

Table 2. Experimental plan for producing superactive carbon by varying the amount of KOH (g g^{-1}) and target temperature ($^{\circ}\text{C}$).

Sample	A t ($^{\circ}\text{C}$)		B KOH (g g^{-1})		KCl (g g^{-1})	Response	
	Coded	Not coded	Coded	Not coded		SSA ($\text{m}^2 \text{g}^{-1}$)	Yield (%)
RUN0(1)	0	800	0	0.90	2.10	1984	42.25
RUN0(2)	0	800	0	0.90	2.10	2001	41.67
RUN0(3)	0	800	0	0.90	2.10	2050	40.60
RUN1	-1	700	-1	0.30	2.70	1262	54.41
RUN2	1	900	-1	0.30	2.70	1769	44.84
RUN3	-1	700	1	1.50	1.50	1964	50.51
RUN4	1	900	1	1.50	1.50	3236	15.58
RUN4-K ₂ CO ₃	1	900	1	1.50 (K ₂ CO ₃)	1.50	2690	31.03
RUN5	-1	700	0	0.90	2.10	1585	51.78
RUN6	1	900	0	0.90	2.10	2722	29.18
RUN7	0	800	-1	0.30	2.70	1640	48.53
RUN8	0	800	1	1.50	1.50	2500	40.18
PRED1-30m	1	900	0.17	1.00	2.00	2515	32.94
PRED1-60m	1	900	0.17	1.00	2.00	2938	28.96
PRED1-90m	1	900	0.17	1.00	2.00	3009	25.41
PRED1-NaCl	1	900	0.17	1.00	2.00 (NaCl)	2435	30.08

Table 3. Statistical validation of obtained mathematical models.

	Equation (1): SSA ($\text{m}^2 \text{g}^{-1}$)	Equation (2): Yield (%)
Standard deviation	22	0.69
R^2	0.9798	0.9664
p -value	<0.0001	<0.0001
F -value	112.98	67.05

responses in equations (1) and (2). More specifically, R -squared is close to unity while the p -values are far below 0.05, indicating that the models are significant and in agreement with experimental data. The model F -values of 112.98 and 67.05 for the surface area and carbon yield, respectively, also imply that the models are valid. Moreover, the intercepts of equations (1) and (2) are close to the corresponding average values of surface area and the yield at zero level further proving the adequacy of the models obtained. The aforementioned linear equations can therefore be employed for the prediction of the desired values for SSA and yield. In other words, the optimal parameters of the KOH amount and target temperature can be estimated by the models to achieve the highest SSA and yield.

The ultra-high surface area of $3236 \text{ m}^2 \text{g}^{-1}$ was achieved by this method (Sample RUN4). Nevertheless, from the economic point of view, the superactive carbon should be produced at the highest possible yield saving the ultra-high surface area. The RSM method allows optimising the method using the obtained mathematical models (equations (1) and (2)). The prediction was made with the aim of achieving the largest surface area at the highest carbon yield. The purpose was also to minimise the KOH amount since only this chemical is consumed through chemical reactions with carbon. After optimisation, carbon (PRED1-60m) using the optimal

process parameters ($t(^{\circ}\text{C}) = 900$; $\text{KOH}(\text{g g}^{-1}) = 1.00$) possesses an ultra-high surface area of $2938 \pm 42 \text{ m}^2 \text{g}^{-1}$ at a good yield of $28.96 \pm 0.69\%$. Moreover, the alkali consumption was considerably reduced (only 1 g g^{-1}). The optimal conditions can be also used for any other carbonaceous material to produce superactive carbon.

Despite the time is a less significant factor, the effect of time was studied at optimum parameters (table 2, Samples: PRED1-30m, PRED1-60m and PRED1-90m). Compared to the sample PRED1-60m, the carbon prepared for 30 min has a reduced surface area of $2515 \text{ m}^2 \text{g}^{-1}$ and a slightly increased yield of 32.94% while sample prepared for 90 min has almost the same surface area of $3009 \text{ m}^2 \text{g}^{-1}$ at a reduced yield of 25.41%. Therefore, since the carbon prepared at optimal conditions and for 60 min has the highest values of surface area and yield (Sample PRED1 60 min), the dwell time was correctly selected.

Table 4 shows the comparison between the superactive carbons prepared by this method with carbons from literature prepared by KOH activation. In contrast to the superactive carbons prepared by only KOH activation, the studied material prepared using KOH + KCl also resulted in an ultra-high surface area, comparable total pore volume and micropore volume. However, the required KOH consumption using this method is 3–4 times less than those in literature methods. Since the porous carbon with an ultra-high surface area was yielded at a diminished amount of KOH, the new method has a significant advantage compared to the previously reported methods for producing superactive carbons (table 4).

3.3. Pore size control

The experimental plan (table 2) allows methodically conducting pore size control. The effects of varying KOH amount and temperature on the pore size distribution and N_2 adsorption–desorption isotherms were investigated (figure 2). Figures 2(a)–(c) show the effect of increasing KOH amount at

Table 4. The comparison of superactive carbons.

Reference	MAXSORB® [10]	[21]	[22]	This study ^a
SSA ($\text{m}^2 \text{g}^{-1}$)	3100	3290	3100	2938 ± 42
KOH amount (g g^{-1})	4	4	3	1
V_{micro} ($\text{cm}^3 \text{g}^{-1}$)	—	—	1.5	0.92 ± 0.00
V_{total} ($\text{cm}^3 \text{g}^{-1}$)	1.5	1.45	1.7	1.29 ± 0.01
Raw material	Petroleum coke	Spanish anthracite	Kraft lignin	Hydrolysis lignin

^a The values were obtained in triplicates.

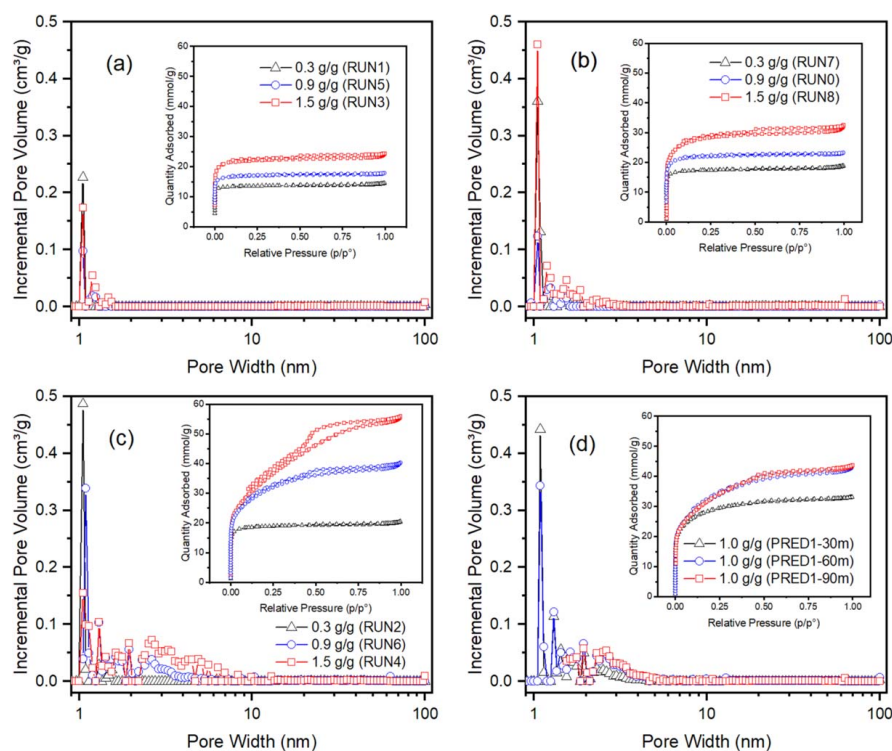


Figure 2. NLDFT pore size distribution and N_2 adsorption–desorption isotherms (the insets) of superactive carbons prepared at different constant temperatures by varied KOH amount: 700 °C (a), 800 °C (b), 900 °C (c); samples prepared at constant temperature and (900 °C) and KOH amount (1.0 g g^{-1}) by varied dwell time (d).

constant temperatures of 700 °C, 800 °C and 900 °C. The adsorption isotherms (the insets) show that the quantity of adsorbed N_2 increases with increasing KOH amount. The pore size distribution shows uniformity at 700 °C, indicating the strongest peak assigned to the size of 1 nm and two others of 1.3 and 1.6 nm. Also, the adsorption isotherms are attributed to type I for microporous materials, which are in good agreement with pore size distribution. However, only for sample RUN3 there hysteresis type IV, which can probably be attributed to capillary condensation or pore blocking in mesopores [35]. At increased temperatures of 800 °C and 900 °C, a wide micropore size distribution is observed. At a

temperature of 800 °C, the micropore size is 1–2 nm with the most probable pore size of 1 nm. At the highest KOH consumption (RUN8), a small number of mesopores is also generated. Moreover, the hysteresis is also observed only for this sample (RUN8) attributed to mesopores. At a temperature of 900 °C the isotherms shapes are similar to type I with the pore filling starting at low pressures p/p° , indicating micropores. However, the characteristic plateau incipient from medium pressures 0.4–0.7 p/p° for samples RUN6 and RUN4, respectively, indicates mesopore contribution [39]. Furthermore, hysteresis type IV also appears, which is peculiar for porous solids containing mesopores. This

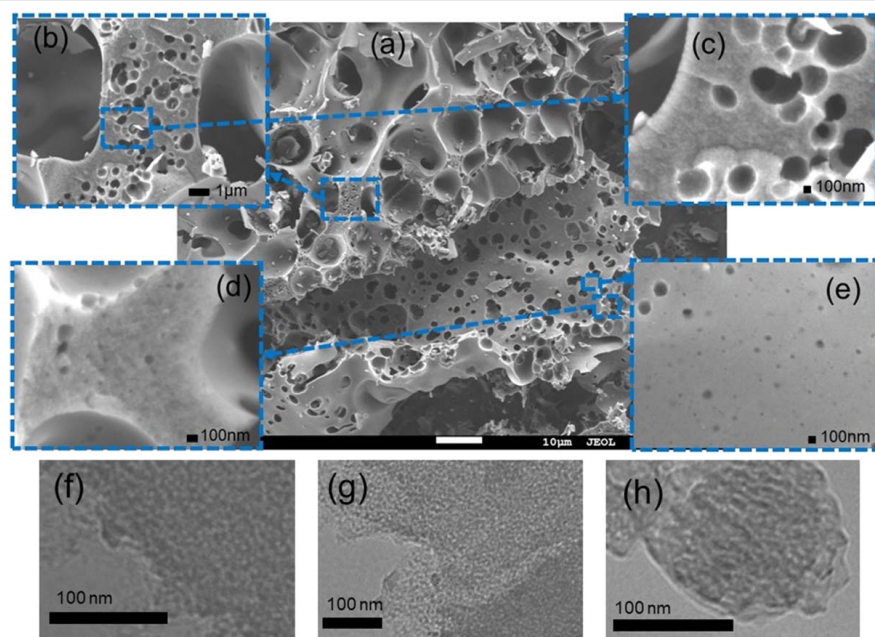


Figure 3. SEM micrographs of superactive carbon (Sample PRED1): macroporous structure (a), the cross-section reveals macropores 50–500 nm (b), interconnected macropores (c), interconnected mesopores (10–50 nm) (d), scattered mesopores <50 nm (e); TEM micrographs: meso- and micropores (f)–(h).

hysteresis is the most pronounced for the sample RUN4, which was prepared at the highest temperature and KOH amount. Pore size distribution is the most diverse for the samples prepared at 900 °C. In support of the assumed porous structure based on isotherm type and hysteresis, there is a significant number of mesopores clearly observed on NLDFT pore size distribution (figures 2(a)–(c)). Undoubtedly, the samples prepared at the highest temperature and KOH amount possess the widest pore size distribution and the highest N_2 uptake, which result in the ultra-high surface area (table 2). With increasing temperature and KOH amount, the number of mesopores in samples increases, but a more uniform microporous structure can be obtained by reducing temperature or KOH amount. Pore widening occurs due to progressive burn-off of the carbon accompanied by the fusion of micropores into mesopores [3]. Accordingly, by varying the target temperature and KOH amount, superactive carbons can be produced with the desired pore size distribution required in many applications.

The effect of time on the porous structure was studied (figure 2(d)). The N_2 isotherm and NLDFT pore size distribution of superactive carbon prepared at optimal conditions for 60 min (table 2, PRED1-60m) is presented in figure 2(d). The adsorption isotherm shows the shape of isotherm Type I, also indicating the increased curvature of N_2 uptake and a plateau starting at $p/p^\circ > 0.4$, which can be ascribed to mesopore filling similar to samples RUN4 and RUN6. The

NLDFT pore size distribution is also similar to samples prepared at 900 °C indicating the presence of mesopores alongside dominating micropores. At increased dwell time (PRED1-90m) the N_2 uptake and pore size distribution are almost identical indicating a negligible effect of increased time on porous structure. However, at a reduced time (PRED1-30m) the nitrogen uptake is significantly reduced and pores size distribution is more uniform. Therefore, the increased time has almost no influence on the porous structure while decreased time reduces the adsorption capacity and leads to uniform pore size distribution.

3.4. Mechanism of pore formation

3.4.1. Texture characteristics of superactive carbon. The texture of superactive carbon was studied using SEM and TEM (figure 3). The material demonstrates various porous structures. There are macropores of size 1–10 μm , which are intrinsic to KOH-activated carbon from KOH grains (figure 3(a)) [13, 14]. The texture consists of interconnected (figures 3(a)–(d)) and scattered pores (figure 3(e)). In a magnified SEM micrograph of the cross-section (figure 3(b)), the macropores of smaller size 50–500 nm are displayed. A detailed image of this part is shown in figure 3(c) demonstrating the rough surface. In the higher-resolution figure 3(d), the mesopores (10–50 nm) are observed. The scattered mesopores are also clear in figure 3(e) with a

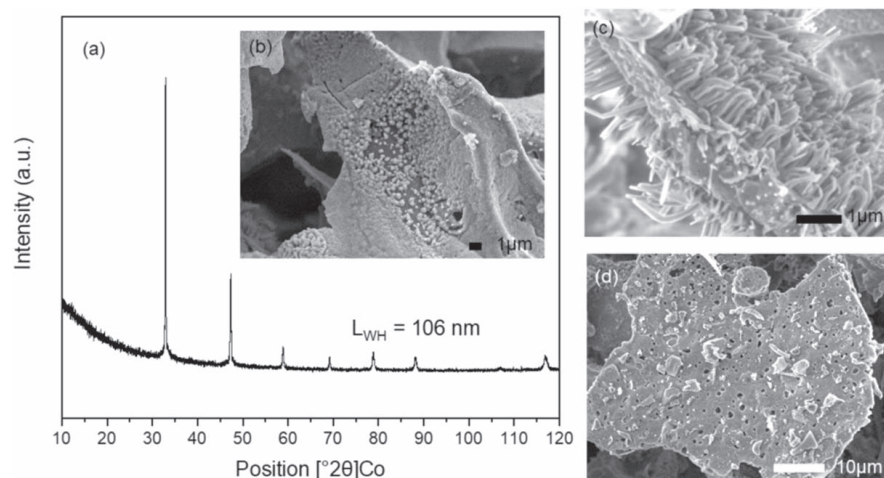


Figure 4. Superactive carbon before leaching: XRD spectra indicating KCl diffraction peaks (a); SEM micrographs: KCl crystals (b), abnormal KCl dendrites (c), KCl formations around macropores (d).

size of <50 nm on a smooth surface, unlike the rough surface observed on the cross-section surface. Meso- and microporous structures (microporous with a size close to 2 nm) are observed on TEM (figures 3(f)–(h)). The porous structure observed on SEM and TEM is in good agreement with the results derived from N_2 physisorption. The macroporous structure tallies well with literature information on porous KOH-activated carbon indicating interconnected and scattered pores [13, 14]. The diverse porous structure including macro-, meso- and micropores with wide pore size distribution was observed in SEM and TEM micrographs of the superactive carbon samples produced in this study.

Carbon samples prepared by the present method using KOH/KCl and only KOH by the literature method [22] were studied using XRD and Raman spectroscopy (figure S1, available online at stacks.iop.org/NANO/32/085605/mmedia). Both of the samples have a disordered structure since the intensities ratio of D and G bands (1340 cm^{-1} and 1590 cm^{-1}) are close to unity and XRD peaks assigned to (002) and (100) planes are broad and obscure [40].

3.4.2. The formation of macropores. Porous carbons produced by KOH activation demonstrated macropore origin through self-templating by KOH grains [13, 14]. In this case, the macropores can be also formed through the KCl template in a similar fashion to the NaCl template [20]. Figure 4 shows, the XRD spectra and SEM images of superactive carbon before leaching. X-ray diffraction peaks (figure 4(a)) are only assigned to the formed KCl crystals (ICSD 98-001-8014). The average crystal size calculated by the W–H method equals 106 nm [34]. In the SEM micrograph (figure 4(b)) crystal size of the same order is observed. Usually, KCl crystals are ordered structures with a cubic shape as shown in figure 4(b). However, here

anomalous dendrite-like structures were found (figure 4(c)). Because of the disordered nature, this structure is not observed in the XRD spectra. This kind of structure has been found in KCl or NaCl condensed systems after high-temperature treatment ($>800\text{ }^\circ\text{C}$) [41, 42]. Since the temperature of carbonisation is $900\text{ }^\circ\text{C}$, the similarity of the temperature allows assuming the same morphology of KCl. Moreover, the composition of dendrites was also confirmed by EDS spectra and mapping (supplementary material: figure S2). EDS spectra shows the strongest peak of carbon atoms related to the carbon, and the peaks of K and Cl are ascribed to the KCl. In the EDS mapping the distribution of corresponding atoms is observed. Carbon atoms are in the place of macropores frames, while dots assigned to the K and Cl are located exactly on the dendrites-like structures. The composition and distribution from the EDS spectra and the enabling of mapping assume that the dendrites are KCl morphology. Since the size of KCl cubic crystals and the base of the dendrite-like structures are of the same order as macropore size (figure 4), the template mechanism through KCl structures can be assumed. The KOH grains were not observed in figure 4 because the KOH had been decomposed and had interacted with carbon matter through the chemical reactions (discussed in the section ‘3.4.3 The formation of micropores’). In figure 4(d), the structures of KCl around macropores are observed. The KCl is not consumed in the process and remains in the same place, while the KOH grains disappear leaving macropores, which can be seen in figures 4(d) and 3 (after leaching). It can therefore be concluded that the macropore origins are KOH grains and KCl structures.

3.4.3. The formation of micropores. The SSA mainly emerges from micropores while the contribution of

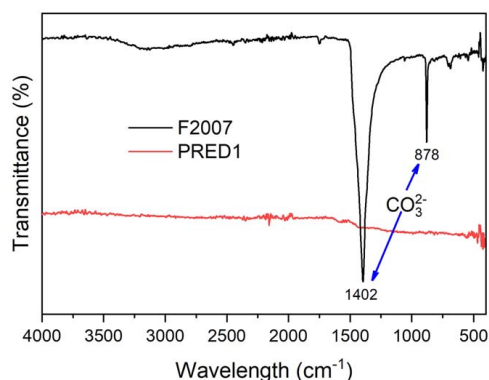
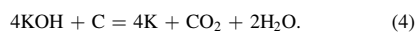
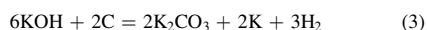


Figure 5. FTIR spectra of superactive carbons before leaching.

mesopores and macropores is negligible, so the microporous structure is essential for superactive carbon. Micropores are formed by KOH erosion and etching due to chemical reactions between carbon and KOH. According to literature, below 700 °C the KOH is converted to potassium carbonate [10, 11]. At temperatures over 700 °C, a dominating amount of metallic potassium is formed. Metallic potassium is intercalated between graphitic layers with a further drastic expansion of graphite lattice that leads to slit-like micropore formation in the carbon material [12]. Since metallic potassium is a major component for micropore origin, the temperature regime starting from 700 °C was selected [11]. The following chemical reactions were proposed for the activation mechanism by KOH [43]:



To investigate the products of chemical reactions, the superactive carbon obtained before leaching was validated by FTIR (Sample PRED1-60m). For comparison, the FTIR spectra of porous carbon prepared by only KOH activation was also measured (F2007) [22]. The spectra are presented in figure 5. In the present case (PRED1-60m), the potassium carbonate, as was proposed in reaction (3), is not observed, but strong sharp peaks assigned to carbonates at 878 and 1402 cm^{-1} [44] are observed in the sample prepared by the literature method (F2007) only using KOH. This can be explained by the different temperatures of the carbonisation. As was discussed above, the optimal temperature for producing superactive carbon in this study is 900 °C while, for the previously studied method the optimal temperature is 700 °C. For a temperature around 700 °C, chemical reaction (3) is therefore more probable while, for the process at 900 °C, the reaction (4) is more suitable. In other words, at 700 °C the potassium hydroxide is converted to K_2CO_3 , whilst at 900 °C potassium carbonate was not observed and KOH mainly consumed in the formation of metallic

potassium. These findings are confirmed by the previously reported mechanism of KOH activation [10, 11]. Furthermore, the reported earlier findings revealed that a higher temperature of activation leads to a higher degree of metallic potassium, which is in good agreement with the results presented here [45].

Since chemical reaction (4) is most probable for the activation process using KOH at temperature 900 °C, metallic potassium is expected to be observed after the process. The boiling point of metallic potassium is 759 °C, which is below the target temperature of 900 °C, so the metallic potassium is in a gas phase in the process and flows away in N_2 current from the carbon matter. This explains the voids of macropores observed in figures 3 and 4(d). In the present case, potassium was condensed in the insulation plug of the tube furnace. A considerable amount of potassium was observed. The flash of obtained metallic potassium in contact with water is presented in supplementary material (figure S3). Characteristic yellow-pink formations of potassium dioxide KO_2 due to interaction of potassium with the oxygen in the air were found on the walls of the tube furnace and insulation plug [46]. The aforementioned findings allow the assumption of the origin of metallic potassium at a temperature over 900 °C while, at 700 °C KOH was converted to potassium carbonate. These results are consistent with literature [10, 11].

To evaluate the effect of KOH etching on micropores formation carbons prepared using KOH/KCl and $\text{K}_2\text{CO}_3/\text{KCl}$ mixtures were compared (table 2, Samples RUN4 and RUN4-K₂CO₃, respectively). Potassium carbonate was selected instead of potassium hydroxide because it is also a source of metallic potassium ($\text{K}_2\text{CO}_3 + 2\text{C} = 2\text{K} + 3\text{CO}$) and has a weaker etching ability compared to KOH [47]. The mass of K_2CO_3 was the same as KOH used in the experiment. The sample prepared using a mixture containing potassium carbonate has a lower surface area and an insignificantly higher yield compared to the sample prepared with KOH. The results allow assuming that the KOH etching has a significant effect on pore formation.

Because gasification of carbon occurs through a similar mechanism as a micropore formation, KCl can be also involved in this process as a catalyst for gasification [48]. To verify that KCl does not act only as a template and evaluate its catalytic activity, the carbon sample was prepared using KOH/NaCl mixture at the optimal conditions (Sample PRED1-NaCl), because NaCl catalytic activity is lower compared to KCl [49]. The sample prepared by using NaCl instead of KCl demonstrated reduced surface area of 2435 $\text{m}^2 \text{g}^{-1}$ and negligible changes in yield (table 2). Thus, there is a catalytic effect of KCl in micropores formation and KCl is not only a template.

3.4.4. The synergy of KCl and KOH in an ultrahigh surface area genesis. To understand why the ultra-high surface area was formed at a substantially reduced consumption of KOH, the synergetic effect of KOH and KCl is discussed here. Based on the mechanism of macro- and micropore formation, a schematic representation of pore origin can be suggested in figure 6. As discussed above, KOH possesses a double role,

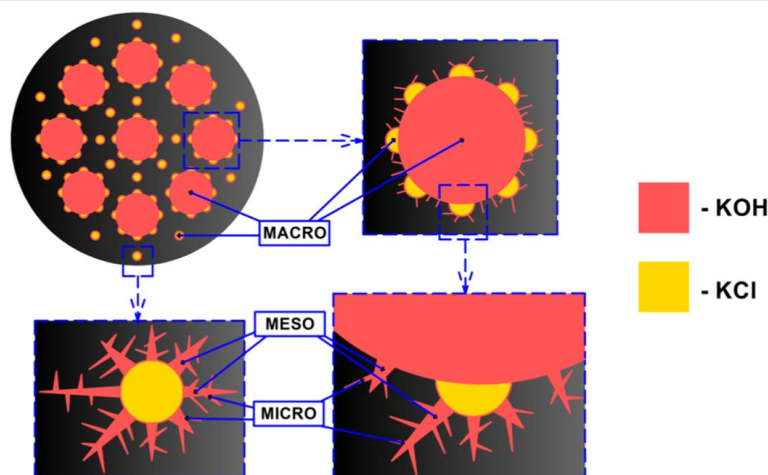


Figure 6. Schematic representation of pore origin using KOH/KCl mixture.

being the template for macropores and an etching compound for the micropores through chemical reaction (4). The micropores are schematically represented in figure 6 as slit-like pores. Most of the SSA originates from the micropores [35]. The KCl is responsible for macropore occurrence. It can be seen that micropores are formed around mesopores and macropores. Mesopores around macropores are also observed in figure 3 and discussed in the literature [13, 14], so more macropores provide more possible places for micropores. In KOH activation, the KOH grains are responsible for self-templated macropores [13, 14]. In the present case, KCl also provides additional macropores (figure 3) through a template mechanism (figures 4(b), (c)), so the amount of KOH can be reduced because the KCl can also form the macropores, which provide a place for micropores. In other words, if only KOH is used, alkali is consumed for macropores (self-template) and micropores while, in case of KOH/KCl mixture, the KCl replaces KOH as the origin of macropores.

Since there is a catalytic effect of KCl on micropores formation, the synergy between KOH and KCl that provides enhanced KCl activity can be also assumed in this case. According to previous studies, the catalytic effect depends on the melting point of the catalyst used for gasification [50]. For example, KCl catalytic effect is increased by reducing of the melting point of an eutectic mixture containing KCl and vanadium pentoxide [50]. Similar effect can be assumed for KOH/KCl mixture since its melting point is far below pure KCl [51]. Thus, this also assumes a synergistic effect between KOH and KCl and an ultra-high surface area origin at decreased KOH consumption.

4. Conclusion

Superactive carbon with ultra-high SSA was obtained from lignin by the simultaneous use of KOH and KCl. In contrast to previously studied methods, this method enables reducing a 3–4-fold reduction in KOH consumption due to the synergy between KOH activation and the KCl template. Pore size control is feasible by altering the amount of potassium hydroxide and process temperature. The present method allows the manufacturing of superactive carbon in a more cost-efficient and environmentally benign way than KOH activation, due to the reduced KOH consumption and straightforwardness of the process.

Acknowledgments

These studies were financially supported by the Finnish innovation-funding agency Business Finland (project 6886/31/2017). The authors would like to thank Professor Aleksander V Vasilyev from St. Petersburg State Forest Technical University for providing the hydrolysis lignin that was used as a raw material to produce superactive carbon. The authors appreciate the assistance of Toni Pennanen and Toni Väkiparta from LUT University for making the SEM and TEM micrographs, respectively. The authors also thank Antti Metsälä from LUT University for photographing of metallic potassium obtained during the experiments. The authors also appreciate Mirka Viitala for the help with measurements of Raman spectra and anonymous reviewers for their valuable comments which improve the quality of the manuscript.

ORCID iDs

Nikolai P Ponomarev  <https://orcid.org/0000-0003-0642-5870>

References

- [1] Marsh H and Rodríguez-Reinoso F 2006 *Activated Carbon* (Amsterdam: Elsevier)
- [2] Suhas, Carrott P J M and Ribeiro Carrott M M L 2007 Lignin—from natural adsorbent to activated carbon: a review *Bioresour. Technol.* **98** 2301–12
- [3] Sing K S W 2013 *Adsorption by Active Carbons* (Amsterdam: Elsevier)
- [4] Otowa T, Nojima Y and Miyazaki T 1997 Development of KOH activated high surface area carbon and its application to drinking water purification *Carbon* **35** 1315–9
- [5] Qiao W, Yoon S-H and Mochida I 2006 KOH activation of needle coke to develop activated carbons for high-performance EDLC *Energy Fuels* **20** 1680–4
- [6] Yu Q, Lv J, Liu Z, Xu M, Yang W, Owusu K A, Mai L, Zhao D and Zhou L 2019 Macroscopic synthesis of ultrafine N-doped carbon nanofibers for superior capacitive energy storage *Sci. Bull.* **64** 1617–24
- [7] Feng S, Liu Z, Yu Q, Zhuang Z, Chen Q, Fu S, Zhou L and Mai L 2019 Monodisperse carbon sphere-constructed pomegranate-like structures for high-volumetric-capacitance supercapacitors *ACS Appl. Mater. Interfaces* **11** 4011–6
- [8] Zhang T, Walawender W P and Fan L T 2010 Grain-based activated carbons for natural gas storage *Bioresour. Technol.* **101** 1983–91
- [9] Wennerberg A and O'Grady T 1978 Active carbon process and composition *US Patent Specification* 4,082,694
- [10] Otowa T, Tanibata R and Itoh M 1993 Production and adsorption characteristics of MAXSORB: high-surface-area active carbon *Gas Sep. Purif.* **7** 241–5
- [11] Romanos J, Beckner M, Rash T, Firlej L, Kuchta B, Yu P, Suppes G, Wexler C and Pfeifer P 2011 Nanospace engineering of KOH activated carbon *Nanotechnology* **23** 15401
- [12] McEnaney B 2002 Properties of activated carbons *Handbook of Porous Solids* (Weinheim: Wiley-VCH Verlag GmbH) 1828–63
- [13] Li M, Liu C, Cao H, Zhao H, Zhang Y and Fan Z 2014 KOH self-templating synthesis of three-dimensional hierarchical porous carbon materials for high performance supercapacitors *J. Mater. Chem. A* **2** 14844–51
- [14] Zhang W, Lin H, Lin Z, Yin J, Lu H, Liu D and Zhao M 2015 3D Hierarchical porous carbon for supercapacitors prepared from lignin through a facile template-free method *ChemSusChem* **8** 2114–22
- [15] Nishihara H and Kyotani T 2012 Zeolite-Templated Carbon—Its Unique Characteristics and Applications *Novel Carbon Adsorbents* ed Juan M D Tascón (Oxford: Elsevier) pp 295–322
- [16] Morishita T, Tsumura T, Toyoda M, Przepiórski J, Morawski A W, Konno H and Inagaki M 2010 A review of the control of pore structure in MgO-templated nanoporous carbons *Carbon* **48** 2690–707
- [17] Morishita T, Soneda Y, Tsumura T and Inagaki M 2006 Preparation of porous carbons from thermoplastic precursors and their performance for electric double layer capacitors *Carbon* **44** 2360–7
- [18] Li J, Tian L, Liang F, Wang J, Han L, Zhang J, Ge S, Dong L, Zhang H and Zhang S 2019 Molten salt synthesis of hierarchical porous N-doped carbon submicrospheres for multifunctional applications: high performance supercapacitor, dye removal and CO₂ capture *Carbon* **141** 739–47
- [19] Ma C, Wang R, Xie Z, Zhang H, Li Z and Shi J 2017 Preparation and molten salt-assisted KOH activation of porous carbon nanofibers for use as supercapacitor electrodes *J. Porous Mater.* **24** 1437–45
- [20] Ponomarev N and Sillanpää M 2019 Combined chemical-templated activation of hydrolytic lignin for producing porous carbon *Ind. Crops Prod.* **135** 30–8
- [21] Lozano-Castelló D, Lillo-Ródenas M A, Cazorla-Amorós D and Linares-Solano A 2001 Preparation of activated carbons from Spanish anthracite: I. Activation by KOH *Carbon* **39** 741–9
- [22] Fierro V, Torné-Fernández V and Celzard A 2007 Methodical study of the chemical activation of Kraft lignin with KOH and NaOH *Microporous Mesoporous Mater.* **101** 419–31
- [23] Bajwa D S, Pourhashem G, Ullah A H and Bajwa S G 2019 A concise review of current lignin production, applications, products and their environmental impact *Ind. Crops Prod.* **139** 111526
- [24] Tomani P 2010 The lignoboost process *Cellul. Chem. Technol.* **44** 53–8
- [25] Stavropoulos G G and Zabaniotou A A 2009 Minimizing activated carbons production cost *Fuel Process. Technol.* **90** 952–7
- [26] Evstigneyev E I, Yuzikhin O S, Gurinov A A, Ivanov A Y, Artamonova T O, Khodorkovskiy M A, Bessonova E A and Vasilyev A V 2016 Study of structure of industrial acid hydrolysis lignin, oxidized in the H₂O₂-H₂SO₄ system *J. Wood Chem. Technol.* **36** 259–69
- [27] Box G E P and Wilson K B 1951 On the experimental attainment of optimum conditions *J. R. Stat. Soc. B* **13** 1–45
- [28] Matranga K R, Myers A L and Glandt E D 1992 Storage of natural gas by adsorption on activated carbon *Chem. Eng. Sci.* **47** 1569–79
- [29] Gun'ko V M *et al* 2011 Activation and structural and adsorption features of activated carbons with highly developed micro-, meso- and macroporosity *Adsorption* **17** 453–60
- [30] Brunauer S, Emmett P H and Teller E 1938 Adsorption of gases in multimolecular layers *J. Am. Chem. Soc.* **60** 309–19
- [31] Rouquerol J, Llewellyn P and Rouquerol F 2007 Is the bet equation applicable to microporous adsorbents? *Studies in Surface Science and Catalysis* **160** 49–56
- [32] Dubinin M M and Radushkevich L V 1947 On the equation of the characteristic curve for active coals *Dokl. Akad. Nauk SSSR [Reports Acad. Sci. USSR]* **4** 331–4
- [33] Ravikovitch P I, Vishnyakov A, Russo R and Neimark A V 2000 Unified approach to pore size characterization of microporous carbonaceous materials from N₂, Ar, and CO₂ adsorption isotherms *Langmuir* **16** 2311–20
- [34] Williamson G K and Hall W H 1953 Discussion of the theories of line broadening *Acta Metall.* **1** 22
- [35] Thommes M, Kaneko K, Neimark A V, Olivier J P, Rodríguez-Reinoso F, Rouquerol J and Sing K S W 2015 Physisorption of gases, with special reference to the evaluation of surface area and pore size distribution (IUPAC Technical Report) *Pure Appl. Chem.* **87** 1051–69
- [36] Okada K, Yamamoto N, Kameshima Y and Yasumori A 2003 Porous properties of activated carbons from waste newspaper prepared by chemical and physical activation *J. Colloid Interface Sci.* **262** 179–93
- [37] Azarov V I, Burov A V and Obolenskaya A V 1999 *Khimiya Drevesiny i Sinteticheskikh Polimerov (Chemistry of Wood and Synthetic Polymers)* (St.Petersburg: SPbLTA) (In Russian)

- [38] Johns M M, Marshall W E and Toles C A 1999 The effect of activation method on the properties of pecan shell-activated carbons *J. Chem. Technol. Biotechnol.* **74** 1037–44
- [39] Kruk M, Jaroniec M and Sayari A 1997 Application of large pore MCM-41 molecular sieves to improve pore size analysis using nitrogen adsorption measurements *Langmuir* **13** 6267–73
- [40] Shimodaira N and Masui A 2002 Raman spectroscopic investigations of activated carbon materials *J. Appl. Phys.* **92** 902–9
- [41] Broström M, Enestam S, Backman R and Mäkelä K 2013 Condensation in the KCl–NaCl system *Fuel Process. Technol.* **105** 142–8
- [42] Wang Y and Tan H 2019 Condensation of KCl(g) under varied temperature gradient *Fuel* **237** 1141–50
- [43] Lillo-Ródenas M A, Cazorla-Amorós D and Linares-Solano A 2003 Understanding chemical reactions between carbons and NaOH and KOH: an insight into the chemical activation mechanism *Carbon* **41** 267–75
- [44] Featherstone J D B, Pearson S and LeGeros R Z 1984 An infrared method for quantification of carbonate in carbonated apatites *Caries Res.* **18** 63–6
- [45] Yuan M, Kim Y and Jia C Q 2012 Feasibility of recycling KOH in chemical activation of oil-sands petroleum coke *Can. J. Chem. Eng.* **90** 1472–8
- [46] Lidin R A, Molochko V A and Andreeva L L 2000 *Khimicheskiye svoystva neorganicheskikh veshchestv (Chemical Properties of Inorganic Substances)* (Moskow: Khimiya (Chemistry)) (In Russian)
- [47] Hayashi J, Uchibayashi M, Horikawa T, Muroyama K and Gomes V G 2002 Synthesizing activated carbons from resins by chemical activation with K_2CO_3 *Carbon* **40** 2747–52
- [48] Arnold R A and Hill J M 2019 Catalysts for gasification: a review *Sustain. Energy Fuels* **3** 656–72
- [49] Veraa M J and Bell A T 1978 Effect of alkali metal catalysts on gasification of coal char *Fuel* **57** 194–200
- [50] Hüttinger K J and Mingos R 1985 Catalytic water vapour gasification of carbon: importance of melting and wetting behaviour of the ‘catalyst’ *Fuel* **64** 491–4
- [51] Database of Facility for the Analysis of Chemical Thermodynamics (FACT) 2020 KCl-KOH phase diagram (www.crct.polymtl.ca/fact/phase_diagram.php?file=KCl-KOH.jpg&dir=FTsalt)

Publication III

Ponomarev, N.P., O'Shea, G., Nuortila-Jokinen, J., Kiljunen, S. and
Kallioinen-Mänttari, M.

**Techno-Economic assessment for
superactive carbon production from side stream lignin**

Reprinted with permission from
Biofuels, Bioproducts and Biorefining
2022

© 2022, Society of Industrial Chemistry and John Wiley & Sons Ltd.

Techno-Economic assessment for superactive carbon production from side stream lignin

Nikolai P. Ponomarev , Lappeenranta-Lahti University of Technology LUT, School of Engineering Science, Department of Separation Sciences, Mikkeli, Finland

Gregory O'Shea, Aalto University School of Business, Espoo, Finland

Jutta Nuortila-Jokinen, Samantha Kiljunen, Lappeenranta-Lahti University of Technology, School of Engineering Science, Department of Separation Science, Lappeenranta, Finland

Mari Kallioinen-Mänttari, Lappeenranta-Lahti University of Technology LUT, School of Engineering Science, Department of Separation Sciences, Lahti, Finland

Received June 14 2022; Revised September 02 2022; Accepted September 30 2022;

View online November 3, 2022 at Wiley Online Library (wileyonlinelibrary.com);

DOI: 10.1002/bbb.2445; *Biofuels, Bioprod. Bioref.* 17:226–241 (2023)



Abstract: Superactive carbon (SAC), having a high surface area of over 2500 m²/g, could be a superior choice for many applications. However, the manufacture of SAC in bulk quantities is challenging. To demonstrate the possibility of SAC manufacturing in large amounts, a techno-economic assessment was performed. For that purpose, a new method utilizing a mixture of waste lignin, KOH and KCl was employed. The chemicals were recovered after use. The technical assessment was performed based on laboratory-scale experimental findings, a simplified process diagram, and mass and heat balance calculations. The economic evaluation was assessed through the estimation of capital costs (CAPEX), operational costs (OPEX) and the minimum selling price (MSP). Moreover, to demonstrate the potential costs saving for the water treatment process, the performance of SAC for the removal of natural organic matter was compared with that of commercial active carbon. SAC was obtained at a minimized KOH amount (1 g/g) and chemicals were successfully recovered with a rate of 5–10% losses. The CAPEX, OPEX and MSP were found to be 4–21 million EUR, 1–9 million EUR/year and 4.4–2.9 kEUR/t for a 0.5–5.0 t/year production capacity, respectively, at a profitability requirement of 20% and a less than 5 year payback period. In addition, SAC demonstrated considerably higher adsorptive capacity for natural organic matter (600–900 mg total organic carbon/g) compared with commercial active carbon (40–50 mg total organic carbon/g), which could lead to substantial process savings. SAC manufacture through this method has been validated and the benefit for the potential application is sufficiently clear to promote the successful commercialization of SAC using lignin wastes. © 2022 The Authors. *Biofuels, Bioproducts and Biorefining* published by Society of Industrial Chemistry and John Wiley & Sons Ltd.

Supporting information may be found in the online version of this article.

Correspondence to: Nikolai P. Ponomarev, Lappeenranta-Lahti University of Technology LUT, School of Engineering Science, Department of Separation Sciences, LUT Mikkeli, Sammonkatu 12, FI-50130 Mikkeli, Finland.
E-mail: nikolai.ponomarev@lut.fi



Key words: activated carbon; KOH-KCl activation; economics; lignin; water

Introduction

Active carbon is a commonly used adsorbent with a diverse porous structure, having a high specific surface area (SSA) that equals 500–1500 m²/g.¹ Applications range from traditional gas or liquid purification to the non-obvious adsorption–desorption compression of gas.² Typical commercial active carbon is produced by steam or, less often, through chemical activation.³ The market for active carbon is already large: over 3.6 billion US dollars in 2021.⁴ Moreover, it is suggested that this market will grow as it offers a relatively simple alternative for the purification of different side streams, which will need to be purified in the future even more efficiently than they are today. For example, active carbon is one of the options for removing pharmaceutical residues from wastewaters.⁵ As good-quality potable water resources are becoming scarcer, the need for active carbon is also increasing as part of drinking water production.^{6,7} Superactive carbon (SAC), the surface area of which can be even higher than 2500 m²/g, has been developed to decrease the amount of the adsorbent needed in the purification processes of wastewater and drinking water.^{8,9} In addition to water treatment applications, SAC has been demonstrated to have superior properties for gas storage and electric double layer capacitors.^{10,11}

The production of SAC is technologically more demanding than the production of typical commercial active carbon (CAC). The patent for SAC was filed by the Standard Oil Company in 1976.¹² The product is now produced by Kansai Coke Chemicals under the commercial name MAXSORB[®], which is made from petroleum coke.¹³ MAXSORB[®] is the only commercial active carbon that can meet SAC specifications (surface area, pore volume, adsorptive capacity, etc.).^{9,13–15} The ultrahigh surface area is achieved by having a significant surplus amount of potassium hydroxide (KOH) used in the process: 3–4 parts of KOH are used per 1 part of raw material. There are also other methods reported in the literature that allow the production of active carbon with a surface area of up to 4000 m²/g, but their application does not go beyond lab-scale and there is no industrial manufacturing.^{16,17} Commercial SAC is not available in bulk quantities because the current product price (about 1000 EUR/kg) restricts market demand even though it would have a notably larger surface area. The high costs incurred in the manufacture of SAC are preventing its wider use in commercial applications.

A major part of the process costs is due to the use of KOH in large amounts and thus lowering KOH consumption and

increasing its reuse would decrease these costs. Recently, we published a study showing the possibility of decreasing KOH consumption in SAC production by as much as 3–4 times through the application of a novel method.^{18,19}

The manufacturing costs contain the costs of the raw material used. Generally speaking, active carbon could be made on any precursor raw material with a high carbon content. However, only some of these starting materials have been promoted as being commercially viable in the production of active carbons, such as coconut shells, coal and hardwoods.²⁰ In our approach, we propose to use hydrolysis lignin. In this particular case, lignin is a side stream of ethanol production from the carbohydrate part of wood.^{21,22} This type of lignin is affordable since no process steps are required to obtain it, unlike the precipitation of kraft lignin from black liquor or the solubilization of organosolv lignin.²³ In addition, hydrolysis lignin is more suitable for the production of activated carbon compared with lignosulphonates since the ash and sulfur contents of the latter are high.

The amount of lignin produced annually is over 100 Mt.²⁴ Lignin is a plant polymer that consists of carbon that leads to a high yield for the carbon obtained.²⁵ Moreover, there are around 20 Mt of hydrolysis lignin waste available in Russia that are causing ecological problems like fires and the leaching of residual acids to the soil, and solutions other than incineration should be found for the treatment of this waste stream.^{26–29}

In this study, a techno-economic assessment has been performed for the above-proposed process to evaluate the cost efficiency of the SAC production. As water treatment applications form a significant part of the applications that use active carbon, water purification for removing natural organic matter (NOM) has been the target for SAC. Chemical consumption can be decreased significantly if the chemicals are regenerated and reused. Since there were only a limited amount of reports available concerning this,^{30–32} regeneration experiments have been included in this study to achieve the information needed for the techno-economic assessment (TEA).

Materials and methods

Materials

Hydrolysis lignin from coniferous wood is a side stream of ethanol production from wood collected from landfills (with 6% moisture content, 10–22% carbohydrates and 1–3% ash) and was used as the raw material. All the chemicals were

corresponding calorific value (26.4 GJ/t)⁴¹ and local energy price.³⁹ The minimum selling prices of chemicals for bulk quantities were adopted from the vendors.^{42,43} Fixed costs including maintenance and repairs, operating supplies, labor, supervision, administrative costs, sales and marketing are calculated according to the literature.³⁸ The fractions used for calculations are specified in Table 1.

Since the time value of money is not included in the payback period, economic feasibility is also assessed using the net present value (NPV) and the internal rate of return (IRR). The discount rate, plant lifetime and tax rate were assumed to be 20%, 10 years and 20%, respectively (Table 1).^{44,45}

The adsorptive capacities for NOM (represented as the TOC) of SAC and CAC were evaluated to demonstrate the advantage of SAC compared with CAC for water treatment (Section 2.2.6). The amount of CAC or SAC to treat 1 m³ of water (dose, g/m³), its costs (costs, EUR/m³) and savings (%) were calculated in accordance with TOC values of the inlet and outlet water flows, adsorptive capacity and the prices of CAC and SAC. The equations used for calculations are presented in the Appendix S1.

Laboratory-scale production of superactive carbon

To achieve the data for the TEA, superactive carbon was produced at a lab scale according to the optimized procedure reported in our previous studies.¹⁸ Lignin was mixed with KOH and KCl in a mortar. The amount of KOH was 1.00 part per 1.00 part of lignin (1.00 g/g) and the amount of KCl was varied from between 0.25 and 2.00 g/g. The obtained

mixture was placed in a tube furnace, heated at 5°C/min and carbonized at 900–950°C for 60 min under 2 L/min of nitrogen flow. The material of the tube was Stainless Steel 253 (EN 1.4835). After the carbonization, a substantial amount of metallic potassium formed. Since elemental potassium reacts with water in ambient air by burning (and subsequent explosion), contact between them should be strictly avoided. For that purpose, to convert metallic potassium to KOH, the nitrogen flow was saturated with water as soon as carbonization was completed, and the temperature decreased to below 400°C. At that point, metallic potassium was not found in the opened reactor. The resultant mixture of carbon and chemicals was washed several times until a neutral pH was achieved. The produced carbon was dried at 105°C under vacuum for 16 h for further analysis. Before the NOM adsorptive capacity estimation, the obtained superactive carbon was washed at pH 2 (HCl) for 16 h at 75°C according to the procedure suggested in the literature.⁴⁶

Characterization of CAC and SAC

The SSA was calculated from the data of N₂ adsorption isotherm obtained on a Tristar II Plus using Brunauer–Emmett–Teller (BET) theory⁴⁷ and the procedure for microporous carbons⁴⁸ (identical to ISO 9277, Annex C). The total volume of pores (V_{total}) was calculated at a relative pressure $p/p^0 = 0.95$. The volume of micropores (V_{micro}) was estimated through the Dubinin–Radushkevich equation.⁴⁹ The volume of mesopores (V_{meso}) was calculated as a difference between the total volume of pores and the volume of micropores. The pore size distribution was estimated by non-local density functional theory (NLDFT) using slit-like pores kernel.⁵⁰ The yield of superactive carbon was calculated using corresponding amounts of dry lignin before carbonization and the resultant superactive carbon. The acidity or basicity of SAC and commercial sample were tested as the pH of the filtrate after stirring 200 mg of active carbon and 20 mL of deionized water for 17–19 h according to the method shown in the literature.⁵¹

Regeneration of chemicals

Potassium hydroxide (KOH) that is participating in the chemical reactions during the activation process is converted to potassium carbonate and elemental potassium.^{52,53} The process temperature (950°C) is above the boiling point of the elemental potassium (759°C). As a result, this component is vaporized and condensed on the parts whose temperature is below its boiling point. Evaporation of KOH, KCl and K₂CO₃ is also possible. Then the metallic potassium reacts with water, which leads to the formation of KOH. To determine the amount of KOH, K₂CO₃ and KCl formed, the washing

Table 1. Values used for economical assessment.

Year of assessment	2021
CEPCI 2020/2008	596/575
Discount rate	20%
Plant lifetime	10 years
Tax	20%
CAPEX ³⁵	3 × equipment costs
OPEX ³⁸	
Depreciation	10% of equipment costs
Fixed costs	
Maintenance and repairs	10% of equipment costs
Operating supplies	15% of maintenance and repairs
Labor	15% of product costs
Supervision	15% of labor
Administrative costs	20% of labor
Sales and marketing	15% of product costs
Abbreviation: CAPEX, Capital costs; OPEX, operational costs.	

water samples of the furnace tube, radiation shields, plugs and outlet gas hose were collected for further analysis.

KOH and K_2CO_3 were determined by potentiometric titration using 0.1 mol/L HCl as a titrant. The titration was conducted using automatic titrator HACH TitraLab AT1000 and the amount of consumed HCl for the determination of hydroxide and carbonate ions was estimated from the titration curves.

Potassium ions were determined by inductively coupled plasma optical emission spectrometry (Agilent Technologies 5110) at 766.5 nm wavelength. Chloride ions were analyzed by ion chromatography according to standard SFS-EN ISO 10304-2 with Thermo Fisher ICS-1100 equipment. The column used was an IonPac AG22 (4×50 mm + AS22) (4×250 mm) and the eluent was 4.5 mm Na_2CO_3 + 1.4 mm $NaHCO_3$.

The recovery percentage of chemicals was determined as a ratio between the amount determined by analytical methods (titration, inductively coupled plasma and ion chromatography) and the amount used for the preparation of superactive carbon. The residual moisture of KOH (13–15%) was accounted for in the recovery percentage calculation. The values were obtained in duplicate or triplicate.

Differential thermal analysis

The lignin used as raw material was mixed in a mortar with KOH and KCl with a ratio of 1:1:2. Similarly, the lignin was ground in a mortar without any chemicals. Then the samples of lignin and lignin–KOH–KCl were analyzed using DTA with the Netzsch STA449F3. The device was calibrated in a temperature range of 25–1600°C using sapphire at the same heating rate, argon flow and using the same crucible. The sensitivity coefficient was varied in the temperature range 25–1600°C. The temperature was calibrated using different metals with corresponding melting points. The reference

material in the measurements was an empty alumina crucible. The sample size was 15 ± 0.5 mg. The reference and the sample crucibles were heated at 5°C/min to 900°C and the temperature was kept constant for 60 min.

To calculate the total enthalpy of the process, ΔH (J/g), the total heat flow was calculated as an area under the curve of heat flow Q (mW = mJ/s) vs. process time τ (s) for the entire range of the process ($\tau_s - \tau_f$) and divided by the sample mass m (mg):

$$-\Delta H = \frac{\int_{\tau_s}^{\tau_f} Q d\tau}{m} \quad (1)$$

The curve of heat flow vs. time for the lignin–KOH–KCl sample is presented in Fig. 2. The area under the curve gives the total heat flow (mJ) per mass of a sample. To obtain the value of the heat of the reaction (J/g) the heat flow is divided by the mass of the sample (mg). The values were obtained in duplicate. The calculated total enthalpy of the process was used for the heat balance calculation of the techno assessment.

The estimation the adsorptive capacity of CAC and SAC for NOM

Equilibrium isotherm. The adsorptive capacity of the SAC and CAC samples was evaluated according to the static method presented in the literature.⁴⁶ Powdered vacuum-dried samples of CAC or SAC were weighed and placed in a 100 mL bottle with a cap. A 50 mL water sample from the local water treatment plant that was collected before the activated carbon unit stage was added to each bottle. The bottles were shaken at 275 rpm at 23°C. The shaken time was 17–19 h. The pH was measured before and after adsorption. Each point was performed in triplicate. The reference sample was also treated similarly without

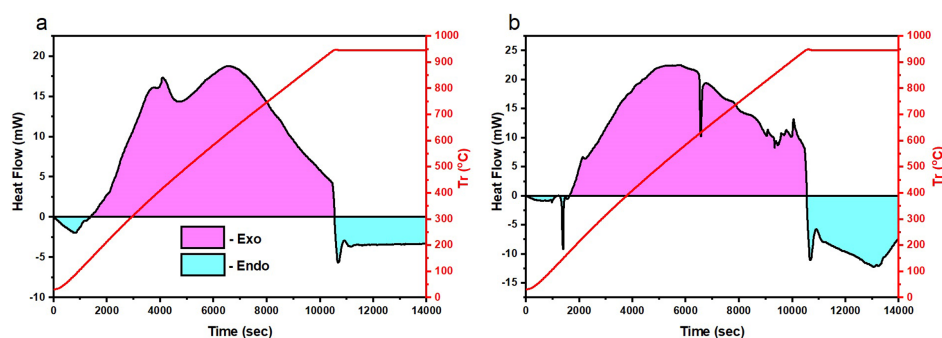


Figure 2. Heat flow vs. time of (a) lignin and (b) lignin–KOH–KCl.

carbon and the value was used as an initial concentration C_0 . The Isotherm was plotted using equilibrium concentration C_e vs. equilibrium adsorptive capacity q_e using a logarithmic scale. Adsorption of NOM on active carbons is a complicated mechanism which could involve physisorption and chemisorption simultaneously.⁵⁴ The well-known adsorption models (Langmuir, BET, Dubinin, etc.) cannot adequately describe such complex adsorption.⁵⁵ The Freundlich isotherm is an empirical equation which does not have a theory behind it and can be used to fit the experimental data.⁵⁶ Moreover, based on the literature it is widely accepted to use it for the estimation of adsorptive capacity for NOM.^{46,57} Thus, the adsorptive capacity q was calculated by obtaining a linear equation of a Freundlich isotherm at the corresponding C_0 ⁵⁷:

$$\log q = \log K + n \log C_0 \quad (2)$$

where K and n are intercept and slope of the Freundlich isotherm, respectively. The results of calculations are presented in Table 7.

Non-purgeable organic carbon (NPOC) determination. To quantify the amount of NOM in drinking water the determination of TOC was used (EN1484). The NPOC was determined instead of the traditional TOC, because the amount of carbonates was substantial and the general requirement of the method was not met ($\text{TOC} > \text{total inorganic carbon}$, EN1484). The NPOC was determined using the Analytical Jena equipment. For acidification [to convert (hydro)carbonates to CO_2], 2 mol/L HCl was used. The obtained values of NPOC were used as the equilibrium concentration C_e . The results are presented as

concentration of total carbon per liter. In this method it is assumed that all CO_2 has been purged out and the total carbon equals TOC.

Results and discussion

Characteristics of laboratory-scale-produced superactive carbon

The characteristics of the SAC produced with this process, in which KOH was used as an activation agent with a combination of KCl, are presented in Table 2.^{18,19} The samples have high specific surface areas of 2459 and 2490 m^2/g , achieved with significantly reduced KOH consumption (1.00 g/g) compared with samples produced with the previously reported methods.^{13,58} The yield of SAC was also higher (27%) compared with that typically achieved in the traditional steam-activated carbon manufacturing process (18%). In the traditional process the achieved specific surface areas are typically lower, 700–800 m^2/g .⁵⁹ The total pore volume measured for the SAC produced here was about 1.5 cm^3/g with a dominating micropore volume of 1.0 cm^3/g . This indicates that the produced SAC has a microporous structure. In addition, the analysis revealed that there was a significant difference between the total and micropore volume of 0.5 cm^3/g . This demonstrates the presence of mesopores, which being the pathway to micropores are therefore necessary for the adsorbent.⁶⁰

The amount of the KCl used in the manufacturing process has an influence on the costs of the process: the smaller the amount of chemicals the higher the amount of raw material in the feed mixture that has led to the higher

Table 2. Characteristics of obtained carbons using KOH activation agent and KCl template.

KOH/KCl-to-lignin (g/g)	1.00/2.00	1.00/1.00	1.00/0.50	1.00/0.25
Target temperature (°C)	950			
Dwell time (min)	60			
SSA (m^2/g)	2459	2490	2218	2125
V_{total} (cm^3/g)	1.47	1.49	1.24	1.15
V_{micro} (cm^3/g)	1.01	1.01	0.86	0.83
V_{meso} (cm^3/g)	0.46	0.48	0.38	0.32
Yield (%)	27.6	26.6	24.7	27.3
Recovery degree (%) ^a				
$\text{KOH} + \text{K}_2\text{CO}_3$	88.3 ± 1.4	90.5 ± 6.2	90.1 ± 0.0	89.1 ± 0.0
K^+	94.3 ± 3.2	—	—	—
Cl^-	94.1 ± 1.5	—	—	—
K_2CO_3 of ($\text{KOH} + \text{K}_2\text{CO}_3$)	21.1 ± 3.0	23.9 ± 0.7	31.3 ± 3.0	34.2 ± 0.0

^aEach experiment was performed at least twice.

Abbreviation: SSA, Specific surface area. V_{total} , total volume of pores; V_{micro} , volume of micropores; V_{meso} , volume of mesopores.

amount of the final product. Moreover, the working space of the furnace is used in a more efficient way since there is more raw material. Thus, samples with a lower KCl content were prepared: 0.50 and 0.25 g/g (Table 2). The result show that the decrease in the KCl amount from 2.00 to 1.00 g/g did not significantly influence the properties of the SAC produced. The specific surface area and pore volume were the same and the difference was negligible. However, if the KCl amount was lower and equaled 0.50 and 0.25 g/g, the obtained carbons exhibited lower degrees of porosity that is, lower surface areas (2218 and 2125 m²/g) and pore volumes (1.24 and 1.15 cm³/g). The influence of the KCl amount on yield was negligible and varied between 25 and 28% (Table 2). Consequently, the optimal amount of KCl is 1.00 g/g. The data from the experiments, in which the KCl amount is 1.00 g/g, was utilized in the TEA.

Regeneration of chemicals

As already mentioned, one of the key essential aspects of the process's feasibility is the possibility of regenerating and re-using the needed chemicals. The superactive carbon is prepared by the simultaneous use of an activation agent (KOH) and template (KCl). The recovery degrees of KOH, K⁺ and Cl⁻ as well as the potassium carbonate content in KOH, are discussed in this section and presented in Table 2. The recovery percentages are then accounted for further in the techno-economic assessment.

The potassium hydroxide interacts with carbon through the redox reactions (i.e. gasification) at over 700°C and is converted to metallic potassium and potassium carbonate.^{52,53} The elemental potassium is then converted to KOH by interaction with water. Based on our experimental findings, the regenerated amount of KOH + K₂CO₃ containing 21–34% of K₂CO₃ was approximately 90% of the initially used KOH amount (Table 2). These experimentally obtained values are similar to the results reported in the literature.^{30–32} The potassium chloride was also almost fully recovered, indicating an approximately 94% recovery percentage. This is most probably due to KCl acting as a template for pore formation and its contribution to the chemical reactions is negligible.¹⁸

Estimation of the total enthalpy of the carbonization process using DTA

The heat balance of the carbonization was derived from the results of DTA. Figure 2 shows the heat flow vs. process time for the entire process. The area above the baseline is related to the heat release (exothermic effect) while the area below the baseline is the heat consumption (endothermic effect). The estimated values of $-\Delta H$ (J/g) are summarized in Table 3 and discussed below. The units of the enthalpies are Joules per gram of the sample that was used for analysis (J/g).

The results presented in Fig. 2 show that the carbonization of lignin is exothermic (Fig. 2(a)). From 30 to 150°C there is a small endothermic peak, which arises from the vaporization of water. The enthalpy for this process is -87 ± 6 J/g. Then the heat is released owing to the carbonization of lignin. The estimated value is 7355 ± 255 J/g, which is slightly higher than what is published in the literature (1.9–5.9 MJ/kg, estimated by Hess's law).⁴¹ In the isothermal range (starting at 950°C) the heat is consumed. A major part of lignin has been carbonized at this range and there is no heat release anymore. The energy is consumed for the sensible heat to maintain the temperature of the residual sample mass (char).

For the lignin–KOH–KCl mixture (Fig. 2(b)) the heat is consumed for the water vaporization (-83 ± 53 J/g–mixture) and melting of the phenoxide (150°C) that is formed by the interaction between KOH and lignin hydroxyls.²⁵ The latter requires -34 ± 11 J/g of heat. Starting from 160°C the process became exothermic since the heat was released owing to the carbonization of lignin and interaction between KOH and CO₂ with the formation of potassium carbonate.^{41,52} On the other hand, the melting of the eutectic KOH–KCl mixture (peak at 630°C), the redox reaction at 800–950°C and the melting of formed K₂CO₃ (900°C) requires heat because of its endothermic nature.^{52,61,62} However, their contribution to the total heat balance is lower compared with lignin carbonization and K₂CO₃ formation and therefore the process occurs with heat release until the isothermal range. The heat release at 160–950°C is 10076 ± 1732 J/g. Starting at 950°C (isothermal range) the lignin has been carbonized and endothermic reactions, as well as sensible

Table 3. Enthalpy of the processes $-\Delta H$ (J/g) calculated from differential thermal analysis curves (Fig. 2).

Process	Range (°C)	Lignin	Lignin–KOH–KCl	Lignin–KOH–KCl (GJ/t-product)
Water evaporation	30–150	-87 ± 6	-83 ± 53	-0.94 ± 0.60
Melting of phenoxide	150	—	-34 ± 11	-0.39 ± 0.12
Lignin carbonization and K ₂ CO ₃ formation	160–950	7723 ± 507	10076 ± 1732	114.35 ± 19.66
Isothermal range	950–	-280 ± 260	-1428 ± 1112	-16.12 ± 12.61
Total		7355 ± 255	8532 ± 2801	96.8 ± 31.8

heat, mainly contribute to the heat consumption. The consumed heat at 950°C for 60 min is from -642 to -2215 J/g. The total enthalpy of the process using lignin-KOH-KCl is 8532 ± 2801 J/g.

Techno assessment

The assessment was established on the experimental findings discussed in Sections 3.1–3.3. The flowsheet of the process is shown in Fig. 1. Only the major process units are demonstrated in the diagram. Dark lines show the material flows while red lines demonstrate the heat flows. The estimated amounts of consumables and utilities are given for 1 t of produced carbon (Table 4). The electricity consumption (3.19 MWh/t) is assumed to be equal to similar processes of activated carbon production and the value was adopted from the literature.³⁶

Lignin with a moisture content of 6% is supplied to a silo (1). The moisture of raw material is in a suitable range and no additional drying is required. KOH and KCl are mixed with the lignin in a ball mill (2) and ground to a homogenized powder form. The amount of lignin is calculated according to a product yield that equals 3.70 t/t. The consumption of chemicals is calculated in accordance with a corresponding amount of lignin and degree of recovery. The KOH consumption is 0.32 t/t when the loss is evaluated on the basis of the experimental findings (Table 2). It is assumed that 21–24% content of K_2CO_3 in the regenerated KOH- K_2CO_3 mixture would not appreciably influence the final properties of SAC since the K_2CO_3 -KCl mixture results in a similar surface area (>2600 m²/g) to KOH-KCl in line with our previous studies.¹⁸ Based on the experimental data, 5% of KCl is lost in the processing. This is in good agreement with the data presented in the literature.⁶³ Determined from the

calculated consumption per 1 t of lignin and its losses the amount of KCl needed is 0.18 t/t.

The mixture is transferred to the carbonization furnace (3) where lignin is carbonized and the porous structure of the resulting carbon is formed. The process occurs continuously at 900–950°C under the flow of nitrogen in the carbonization furnace (3) (D 1.2 m x L 12 m) for the total residence time of 60 min. The design of the carbonization furnace is acquired from the amount of the feed material, total residence time and simplified heat calculations (Appendix S1).^{64–66} The amount of nitrogen flow to create an inert atmosphere is 36 kg per 1 t of carbon adopted from the literature.⁶⁷ The nitrogen is supplied from the gas tank (13). In the carbonization furnace (3) the following processes occur: (1) carbonization of lignin with a formation of char, gaseous products, condensed liquid and tar;⁴¹ (2) gasification of the obtained char with porous structure formation; (3) vaporization of water contained in the lignin and chemicals; and (4) fusion of KOH, KCl and the formed K_2CO_3 . These processes are accounted for in the mass and heat balance calculations (Appendix S1).

The heat balance calculation for the carbonization furnace (3) was developed from the DTA results (Section 3.3). The results show that the total process is exothermic, and heat is released since the exothermic lignin carbonization and potassium carbonate formation are substantial and their contribution to the overall heat balance is more significant compared with endothermic processes (Table 3). If the values of the process's enthalpy of DTA is recalculated to the values of the heat released/consumed per ton of the product, then the total heat release is 96.8 ± 31.8 GJ/t-product. However, the heat is consumed for the evaporation of water (-0.94 ± 0.60 GJ/t-product), phenoxide melting (-0.39 ± 0.12 GJ/t) and isothermal range (-16.12 ± 12.61 GJ/t). To be on the safe side of the techno assessment, the heat of the exothermic reaction is omitted, and only endothermic heat is accounted for in the heat consumption. Moreover, the heat losses are also added, which are assumed to be 10% of the total required heat. Overall, the total required heat for the carbonization furnace (3) would be 19.28 GJ/t-product.

As soon as the carbonization has been completed, the flow of N_2 is saturated with water to convert metallic potassium to KOH. Cooling of the obtained mixture and conversion of elemental K to KOH are carried out in a separate process step to eliminate the possible safety issues concerning the formed metallic potassium. For that purpose, the cooler (4) is used and that is then taken into account for the present TEA. The mixture of chemicals and the obtained carbon are then transferred to the washing tank (5) to leach out the chemicals from the produced carbon. The required amount of water is 4.96 t/t, adopted from the literature for a similar process.⁶⁷

Table 4. Raw materials and energy consumptions per 1 t of product.

Consumable	Quantity/t-product	Cost per unit (EUR)
Hydrolysis lignin (t)	3.70	161.11 ⁴⁰
KOH (t)	0.32	331.83 ⁴²
KCl (t)	0.18	330.50 ⁴³
N ₂ (t)	0.036	2500.00 ³⁶
Water (t)	1.01	5.00 ⁴⁴
Heat (MWh)	6.51	23.06 ³⁹
Electricity (MWh)	3.19	23.06 ³⁹

^aThe price of lignin is defined as a price of energy⁴⁰ applying corresponding calorific value (26.4 GJ/t)⁴¹ and local energy price.³⁹

The washing water from the washing tank (5) through the dewatering (6), containing chemicals used for activation, is pumped to the dryer (12) for regeneration. The losses of chemicals after regeneration are assumed to be the same as the values obtained in experimental findings: 10% of KOH and 5% of KCl (Table 2). The required heat for the drying according to the heat balance calculation is 11.78 GJ/t-product. After drying, the chemicals are used again in step (2) and fresh chemicals are fed according to the regeneration loss. The carbon is separated from the solution using dewatering (6), pelletized (7) and dried in a drier (8). The heat consumption of the drier is 1.15 GJ/t to reduce the moisture content of carbon from 30 to 3%. Most of the water is regenerated in the process and assuming 10% losses the total water consumption is 1.01 t/t. After screening (9) the ready product is stored in a silo (10) and distributed after the packaging stage (11).

There are substantial amounts (2.044 t/t-product) of side products (gas, liquid and tar) produced in the carbonization furnace which have a significant calorific value. These components could be incinerated to produce energy.⁶⁸ For this purpose, the side products are burnt in the thermal combustor (14) and the produced energy is taken into account for the total required heat. The amount of produced heat was calculated by applying the corresponding calorific values of gas (6.59 MJ/kg), condensed liquid (0.61 MJ/kg) and tar (0.01 MJ/kg) adopted from the literature and equals 8.78 GJ/t-product.⁴¹ The suspended solids after incineration are removed in a cyclone (15) from the flue gas.

In addition, the total required heat for the entire process is 23.43 GJ/t-product which equals 6.51 MWh/t-product (Table 4), including the consumed heat for the carbonization furnace (3) (19.28 GJ/t-product) and driers (8, 12) (11.78 and 1.15 GJ/t-product) and released heat obtained by the incineration of the side products (8.78 GJ/t-product).

Economic assessment

The CAPEX ranges between 4.17 and 20.91 million EUR for a corresponding product capacity of 0.5–5.0 kt/year, as presented in Table 5. The values are in agreement with previous studies related to the techno-economic assessment

Capacity (kt/year)	CAPEX (million EUR)	OPEX (million EUR/year)	MSP (kEUR/t)
0.5	4.17	1.11	4.36
1.0	6.78	2.08	3.82
2.0	11.01	3.95	3.39
5.0	20.91	9.30	2.93

of active carbon production at similar capacities.^{35,36,67–70} The equipment costs used here are one-third of the CAPEX. They are based on a vendor's quotation (2021) and the literature.³⁵ The biggest part of the equipment costs (66%) is the cost of the indirect fired rotary kiln (carbonization furnace). The price is 1.3 million US dollars for the kiln, which has a diameter of 1.2 m and length of 12 m with a total inlet feed of 1000 kg/h. The kiln is made from Alloy 253 that is chemically resistant to alkali and potassium chloride at the process temperature. The additional material costs are accounted for in the price of the furnace made from special Alloy 253. Owing to the corrosion resistance of Alloy 253, there would be no significant influence on the furnace lifetime or maintenance and repairs costs. However, the equipment costs are higher, which in turn increases the CAPEX. Using the six-tenth rule the price was recalculated to the appropriate capacities of 0.5–5.0 kt/year. The price of the kiln is in agreement with a price found in the literature for a similar process.³⁵ The rest of the equipment costs (44%) are adopted from the same literature source and updated using the CEPCI index.³⁵ The equipment costs are presented in Appendix S1.

The annual operating expenditures for varied production capacities of 0.5–5.0 kt/year vary between 1.11 and 9.30 million EUR (Table 5). The OPEX consists of variable costs and fixed costs of production, and are demonstrated in Fig. 3 for a plant with a production capacity of 1.0 kt/year.

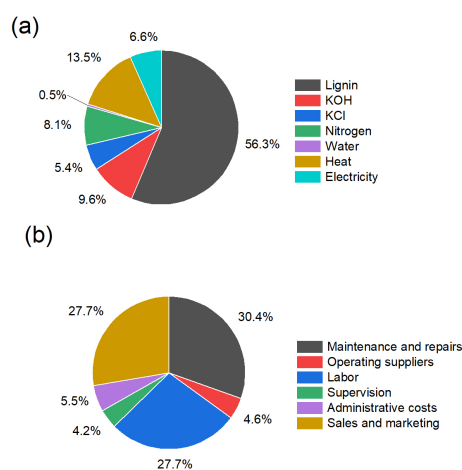


Figure 3. Contribution of variable costs (a) and fixed costs (b) to the operational costs (OPEX) for a plant with a production capacity of 1.0 kt/year.

Variable costs include the costs of lignin, chemicals and utilities used in the process to produce superactive carbon. The amounts of each consumable per 1 t of product and the price for 1 t or a corresponding quantity are summarized in Table 4. The variable costs (Fig. 3(a)) are the costs of raw material (lignin) (56.3%) followed by the required heat (13.5%), KOH (9.6%), nitrogen (8.1%), electricity (6.6%) and KCl (5.4%). Chemicals and utility prices are adopted from vendors. The lignin price is calculated using its calorific value, which results in 161 EUR/t (Table 4). This value matches well a previously reported value of 150 EUR/t solid fuel lignin.²² However, the price of hydrolysis lignin is substantially lower compared with the kraft lignin price of 400 EUR/t because additional process stages are needed to obtain the latter from black liquor.⁴⁴ On the other hand, the price for hydrolysis lignin is comparable with or even lower than the prices of typical precursors for activated carbon.⁴⁰ Since the consumption (and purchase prices) of the raw material, heat and chemicals are the highest among the consumables, the developing methods should be aimed at the reduction of chemical consumption (mostly KOH) and increasing product yield, which directly influences the needed amount of raw material and the required heat. The water costs (0.5%) are negligible because most of the water volume is recovered, and water losses are assumed at 10%.

The major contributors to fixed costs (Fig. 3(b)) are maintenance and repairs (30.4%), sales and marketing costs (27.7%) and labor (27.7%). The minor contributors are administrative costs (5.5%), operating suppliers (4.6%) and supervision (4.2%). The variable and fixed costs are 53 and 36% of the OPEX, respectively. Depreciation is also accounted for in the OPEX. Since depreciation mainly comes from the wearing of the equipment, the value is calculated to be 10% of the equipment costs. This sum is equal to 11% of the OPEX.

The NPV and IRR are also used for the economic assessment as the time value of money has not been accounted for. These values are also used for MSP estimation. The revenue from SAC production is generated from selling the main product (SAC). In Fig. 4 the NPV is calculated for different production capacities, and different selling prices of 1.5–6.5 kEUR/t. The minimum selling price for the corresponding product capacity is calculated at the point when the NPV is zero and the IRR equals the discount rate (20%).⁷¹ Production is profitable and it is worth investing if the IRR is higher than or equal to the discount rate. Thus, the product should be sold at the MSP defined in this way. The values for the MSP are demonstrated in Table 5 for each production capacity. In Fig. 4, the MSP can be identified as a line intersection of a certain production capacity with the line representing zero.

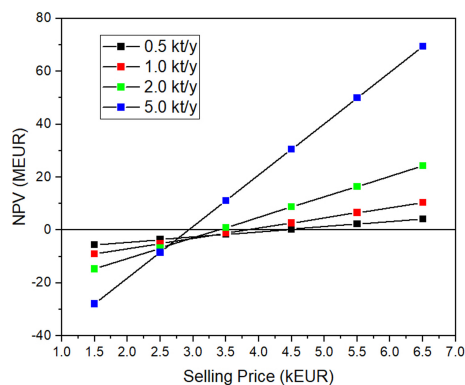


Figure 4. The net present value (NPV) for a varied production capacity calculated for different selling prices.

The minimum selling price decreases with increasing production capacity. For the smallest production volume (0.5 kt/year) SAC should be sold at 4.36 kEUR/t. However, for 1.0, 2.0 and 5.0 kt/year production volumes, the minimum selling price should be 3.82, 3.39 and 2.93 kEUR/t, respectively (Table 5). According to the literature and vendor information, the price for conventional active carbon with a surface area of 500–1500 m²/g is 1.0–2.5 kEUR/t, depending on the quality.⁷² These prices, however, cannot be directly applied to SACs even though they are true for typical active carbons. The comparison is more challenging since there are very few producers and the material is not available in bulk quantities. Therefore, to determine the market price for SAC, the price-per-area method was adopted.^{40,70} If we assume a price of 2.0 kEUR/t for 1000 m²/g of porous carbon, the market price for SAC with a surface area of 2500 m²/g would be assumed to be 5.0 kEUR/t. Since the MSP of superactive carbon produced by this method is lower compared with the price-per-area (5.0 kEUR/t), we can further assume that the SAC can be sold at a competitive price and the production is feasible and profitable. Moreover, the payback period is only 4.87 years. However, it should be noted that the time value of money is not accounted for in the payback period calculation and the NPV with IRR is a more appropriate method for economic evaluation.

Sensitivity analysis

To evaluate the effect of variations in the OPEX, CAPEX, discount rate, lignin price, tax rate, heat price and KOH price on the minimum selling price, sensitivity analysis was performed based on a capacity of 1.0 kt/year. The base values

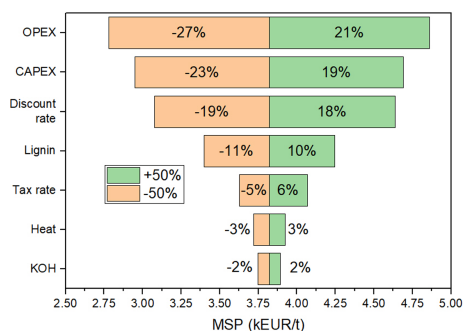


Figure 5. Sensitivity analysis of varied economic factors on minimum selling price (MSP) for a plant with a production capacity of 1.0 kt/year.

are the corresponding values of OPEX and CAPEX which are 2.08 and 6.78 million EUR, respectively, and a discount rate of 20% and a tax rate of 20% are used (Tables 5 and 1). Lignin, heat and KOH base prices are 161.11, 331.83 and 23.06 EUR/unit, respectively (Table 4), which are altered in a range of $\pm 50\%$ (Table 5). The results of the sensitivity analysis are also presented in Fig. 5. The largest influence on the minimum selling price is OPEX. More specifically, a 50% decrease in OPEX leads to a 27% decrease in MSP while a 50% increase in OPEX leads to a 21% increase in MSP. The next big effect on MSP is contributed by CAPEX, which causes a variation between -23 and 19% in the total amount, mainly dependent on purchase equipment costs. Therefore, any changes in equipment prices have a strong influence on the minimum selling price. A further influence is exerted by variations in the discount rate ($-19/18\%$). Since the lignin cost is one of the largest contributors to the OPEX, a reduction in the amount used is essential for the profitability of the process. In particular, a 50% decrease or increase in the cost of lignin leads to an approximately 10 – 11% decrease or increase in the MSP. The effects of 50% changes to the tax rate, heat and KOH price are less noticeable, and equate to $-5/6\%$, $-3/3\%$ and $-2/2\%$ of the MSP, respectively. In general, 50% changes to the OPEX, CAPEX, discount rate, lignin price, tax rate and heat or KOH prices did not lead to substantial changes in the MSP, so that the MSP does not exceed 5.0 kEUR/t (Fig. 5).

Benefit for the water treatment plant

Characteristics of the CAC and SAC used in the treatment of the water from the drinking water production plant are presented in Table 6. The SAC sample used for the NOM adsorptive capacity estimation was prepared in different

Table 6. Characteristics of the commercial active carbon (CAC) and superactive carbon (SAC) samples used in the experiments to compare the materials in water treatment.

	CAC	SAC
SSA, m^2/g	523	2473
V_{total} , cm^3/g	0.43	1.46
V_{micro} , cm^3/g	0.22	0.96
V_{meso} , cm^3/g	0.21	0.50
pH of active carbon	11.16 ± 0.04	5.10 ± 0.57

batches, thus its characteristics are presented here separately (Table 6). As can be seen, the SAC has much higher SSA (about $2500 \text{ m}^2/\text{g}$) and total ($1.46 \text{ cm}^3/\text{g}$), meso- ($0.50 \text{ cm}^3/\text{g}$) and micropore volumes ($0.96 \text{ cm}^3/\text{g}$) compared with CAC. The pH of CAC is alkaline, indicating a basic nature. SAC shows an acidic nature with a pH below 7. The difference in textural properties and pH of SAC and CAC are essential for the application.⁵⁴

Figure 6 shows the N_2 physisorption isotherms (Fig. 6(a)) and NLDFT pores size distribution (Fig. 6(b)) of the used CAC and SAC samples. The adsorption isotherm of SAC for N_2 (Fig. 6(a)) shows a much higher nitrogen uptake compared with CAC, leading to a much higher surface area and total pore volume (Table 6). Both isotherms of CAC and SAC are Type I of microporous materials and a desorption hysteresis type H4 could be ascribed for micro- and mesopores of carbons that are in agreement with the values of pore volumes and NLDFT pore size distribution (Fig. 6(b)).⁷³ In Fig. 6(b) the NLDFT pore size distribution of CAC shows a significant presence of micropores and mesopores with sizes of 0.96 – 1.35 and 5.85 – 10.57 nm, respectively. SAC has the most probable peaks of micropores and mesopores in ranges of 1.31 – 1.95 and 2.36 – 9.88 nm, respectively.

Drinking water samples were collected before the active carbon unit stage at two different local water treatment plants (samples water#1 and water#2). The results are presented in Table 7 and in Fig. 6(c) and (d) for water#1 and water#2, respectively. Both water samples have similar initial TOC values (3.4 – 4.6 mg/L). The adsorptive capacity of SAC (619 – 906 mg/g) seems to be from 16 to 19 times higher compared with that of Norit CAC (39 – 48 mg/g). The adsorptive capacity of the CAC is in agreement with that of typical conventional activated carbon at between 10 and 70 mgTOC/g .⁷⁴ The performance of SAC obtained by this method is also comparable with the high surface area carbon MAXSORB®. In particular, it demonstrates an adsorptive capacity for TOC over 3–6 times higher compared with CAC for the treatment of primary sewage effluents.⁸

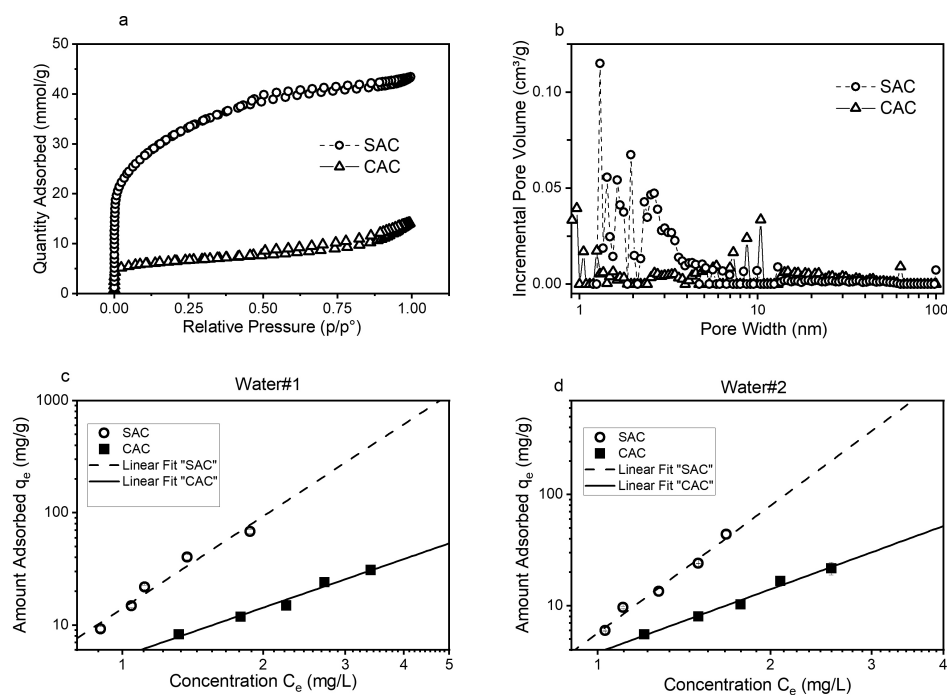


Figure 6. Nitrogen adsorption isotherms (a), non-local density functional theory (NLDFT) pore size distribution (b), natural organic matter (NOM) adsorption isotherms (c) and (d) of the commercial active carbon (CAC) and superactive carbon (SAC).

The equilibrium isotherms of SAC have a higher slope and the equilibrium concentrations are in a lower range compared with CAC (Fig. 6(c), (d)). The R^2 is close to unity, indicating a good linear fit. The pH after adsorption of SAC is almost the same while for CAC the solutions are slightly alkaline (Table 7).

According to the experimental results the adsorptive capacity of SAC for NOM is significantly higher compared with CAC. This can lead to substantial process savings when a cubic meter of water is treated at a typical water treatment plant with the active carbon. The inlet concentration of water samples was around 4.6 and 3.4 mgTOC/L for water#1 and water#2, respectively (Table 7). The TOC limit of treated water is taken from the EU directive (98/93/EC) and equals around 2.0 mgTOC/L (recalculated using the oxidizability value). The dose of conventional activated carbon to treat the water samples according to the TOC limit is 184 and 101 g per cubic meter while the SAC dose would be a few times less and equal to only 28 and 18 g per cubic meter for water#1

and water#2, respectively (Table 7). The price of conventional activated carbon is approximately 1.0 kEUR/t (or EUR/kg) based on the price-per-area approach and the SAC minimum selling price was evaluated as be between 2.93 and 4.36 kEUR/t (or EUR/kg) depending on the production capacity. Taking into account the price for the CAC, the costs for the treatment of 1 m³ of water#1 and water#2 would be 18 and 10 euro cents (EUR-cent), respectively. If SAC was used, and using its price variations, the treatment costs of water#1 and water#2 would be 8–12 and 5–8 EUR-cent/m³, respectively. Thus, despite the lower selling price of commercial activated carbon, the use of SAC in a water treatment process could lead to substantial process savings (34–55 and 23–48% less for water#1 and water#2 compared with CAC owing to the significantly lower SAC consumption). Therefore, the use of SAC is clearly economically beneficial for water treatment.

In addition, SAC meets the technical specification for water treatment plants. Since the granular form is used in adsorption

Table 7. Characteristics of water samples, Freundlich isotherm parameters, CAC and SAC adsorptive capacities and parameters for the benefit evaluation of SAC for the water treatment.

Water sample	Water#1		Water#2	
	CAC	SAC	CAC	SAC
Carbon				
Initial concentration, C_0 (mg total organic carbon/L)	4.64 ± 0.06	4.61 ± 0.13	3.42 ± 0.00	3.43 ± 0.12
pH-initial	7.84	7.75	7.76	7.83
pH-final	8.0–8.55	7.8	8.1–9.0	7.8
Slope, n	1.438	2.733	1.891	3.811
Intercept, $\log_{10}K$	0.723	1.147	0.579	0.754
R^2	0.978	0.964	0.985	0.982
Adsorptive capacity, q_e (mg total organic carbon/g-carbon)	47.96 ± 0.95	905.96 ± 78.02	38.82	619.32 ± 82.83
Price (EUR/kg)	1.00	2.93–4.36	1.00	2.93–4.36
Dose (kg/m ³)	1.84 · 10 ⁻¹	2.80 · 10 ⁻²	1.01 · 10 ⁻¹	1.79 · 10 ⁻²
Costs (EUR-cent/m ³)	18	8–12	10	5–8
Costs savings (%)	—	34–55%	—	23–48%

columns of water treatment plants and increases the specific weight, the powdered SAC is pelletized using a pelletizer (7).^{46,57} According to the literature and our previous studies, alkali-activated carbons or alkali-salt activated carbon can be produced in granular form.^{8,13,75} The ash content of chemically activated carbon is low as well as being a soluble fraction since an additional washing stage is used.^{35,76,77} The aforementioned properties further make SAC suitable for water treatment.

Eco-design aspects

The suggested process follows eco-design guidelines and promotes the transition to the circular economy.⁷⁸ The lignin originates from renewable industrial side streams. The process chemicals are affordable and could be recovered from tailings or other industrial side streams. Moreover, the non-toxic process chemicals are regenerated in the process and no overall waste or harmful chemicals are created. The manufacturing process is intensified to contain pyrolysis and activation in a single process step, thus lowering the overall energy consumption and total investment. In addition, the novel method increases the performance of the final product significantly compared with the product from the traditional process. However, the analysis is based on laboratory-scale experiments. More studies are needed to better elucidate and characterize effluent streams and their environmental impact.

Conclusion

The techno-economic evaluation was performed for a novel process, in which superactive carbon (SSA approximately 2500 m²/g) can be produced with

significantly reduced KOH consumption. In agreement with the experiments, the chemicals needed in the process can be recovered in the process and the KOH and KCl losses are only 10 and 5%, respectively. The TEA showed that the minimum selling price varied from 2.93 to 4.36 kEUR/t depending on the process capacity (5.0–0.5 kt/year). Thus, it was lower than the assumed market price of 5.0 kEUR/t based on a price-per-area approach. The CAPEX and OPEX were identified for different production capacities, and it was seen that the equipment costs make the most substantial contribution to CAPEX. The largest influence on the minimum selling price arises from the OPEX, mainly consisting of the costs of raw materials and energy costs. It has been shown that the SAC produced in the evaluated process demonstrates a superior adsorptive capacity for NOM compared with commercial activated carbon in a water treatment application. The use of SAC could lead to substantial cost savings (between 23 and 55%) in the treatment of the tested waters owing to the amount of the SAC needed for the task being substantially lower compared with the reference CAC. The TEA and the experimental results, which show the potential of the SAC in water treatment, reveal that the novel process is a promising option for the production of an efficient adsorbent product from an industrial side stream.

Acknowledgements

This work was financially supported by the Finnish innovation funding agency Business Finland (project 1662/31/2020).

References

- McEnaney B, Properties of activated carbons. *Handb Porous Solids*, 3:1828–1863 (2002).
- Sdanghi G, Nicolas V, Mozet K, Schaefer S, Maranzana G, Celzard A et al., A 70 MPa hydrogen thermally driven compressor based on cyclic adsorption-desorption on activated carbon. *Carbon N Y* 161:466–478 (2020).
- Marsh H and Rodríguez-Reinoso F, Activated carbon. *Activated Carbon (Origins)* 1:13–86 (2006).
- Mordor Intelligence, Activated carbon market - growth, trends, COVID-19 impact, and forecasts 2022–2027 (2022), <https://www.mordorintelligence.com/industry-reports/activated-carbon-market>, (accessed 4 April 2022).
- Ek M, Baresel C, Magnér J, Bergström R and Harding M, Activated carbon for the removal of pharmaceutical residues from treated wastewater. *Water Sci Technol* 69:2372–2380 (2014).
- Grand View Research, Activated Carbon Market Size, <https://www.grandviewresearch.com/industry-analysis/activated-carbon-market>, (accessed 4 February 2022).
- FEEO International, Activated Carbon: A Growing Market of Opportunity, <https://feeco.com/activated-carbon-a-growing-market-of-opportunity/>, (accessed 4 February 2022).
- O'Grady TM and Wennerberg AN, *Petroleum-derived carbons*, Vol. 303. American Chemical Society, Washington, D.C., pp. 302–309 (1986).
- Otowa T, Nojima Y and Miyazaki T, Development of KOH activated high surface area carbon and its application to drinking water purification. *Carbon* 35:1315–1319 (1997).
- Zhang T, Walawender WP and Fan LT, Grain-based activated carbons for natural gas storage. *Bioresour Technol* 101:1983–1991 (2010).
- Qiao W, Yoon S-H and Mochida I, KOH activation of needle coke to develop activated carbons for high-performance EDLC. *Energy Fuel* 20:1680–1684 (2006).
- Arnold N, Wennerberg and Thomas M. O'Grady, Active carbon process and composition. US patent 4082694, 1978.
- Otowa T, Tanibata R and Itoh M, Production and adsorption characteristics of MAXSORB: high-surface-area active carbon. *Gas Sep Purif* 7:241–245 (1993).
- Harrison BH, Barton SS, Dacey JR and Sellors JR, Characterization of superactivated carbons. *J Colloid Interface Sci* 71:367–374 (1979).
- Sing KSW, *Adsorption by Active Carbons*, 2nd edn. Elsevier Ltd, Amsterdam, (2013).
- Jansta J, Dousek FP and Patzelová V, Low temperature electrochemical preparation of carbon with a high surface area from polytetrafluoroethylene. *Carbon* 13:377–380 (1975).
- Nishihara H and Kyotani T, *Zeolite-Templated Carbon – Its Unique Characteristics and Applications*. Elsevier, Oxford, pp. 295–322 (2012).
- Ponomarev N and Kallioinen M, Synergy between alkali activation and a salt template in superactive carbon production from lignin. *Nanotechnology*. 32:085605 (2021) <https://doi.org/10.1088/1361-6528/abc9eb>.
- N. Ponomarev and M. Sillanpää, Method for producing activated carbon. FI patent 128625B, 2020.
- Marsh H and Rodríguez-Reinoso F, in *Activated Carbon*, ed. by Marsh H and Rodríguez-Reinoso FBT-AC. Elsevier Science Ltd, Oxford, pp. 13–86 (2006).
- Chudakov MI, *Promushlennoe Ispolzovanie Lignina (Industrial Applications of Lignin)*. Lesnaya Promyshlennost, Moscow (1983).
- Xu CC, Dessbesell L, Zhang Y and Yuan Z, Lignin valorization beyond energy use: has lignin's time finally come? *Biofuels, Bioprod Biorefining* 15:32–36 (2021).
- Vishtal A and Kraslawski A, Challenges in industrial applications of technical lignins. *BioResources* 6:3547–3568 (2011).
- Bajwa DS, Pourhashem G, Ullah AH and Bajwa SG, A concise review of current lignin production, applications, products and their environmental impact. *Ind Crops Prod* 139:111526 (2019).
- Azarov VI, Burov AV and Obolenskaya AV, *Khimiya drevesiny i sinteticheskikh polimerov (chemistry of wood and synthetic polymers)*. SPbLTA, StPetersburg (1999).
- Zarubin MJ, Alekseev SR and Krutov SM, *Hydrolysed lignin. Structure and perspectives of transformation into low molecular products*, in: Recent Adv. Environ. Compat. Polym., Woodhead publishing, pp. 155–160 (2001).
- Hatakeyama H, Tsujimoto Y, Zarubin MJ, Krutov SM and Hatakeyama T, Thermal decomposition and glass transition of industrial hydrolysis lignin. *J Therm Anal Calorim* 101:289–295 (2010).
- Berlin A and Balakshin M, in *Industrial Lignins*, ed. by Gupta VK, Tuohy MG, Kubicek CP, Saddler J and Xu A. Elsevier, Amsterdam, pp. 315–336 (2014).
- Rabinovich ML, Lignin by-products of soviet hydrolysis industry: resources, characteristics, and utilization as a fuel. *Cellul Chem Technol* 48:613–631 (2014).
- Yuan M, Kim Y and Jia CQ, Feasibility of recycling KOH in chemical activation of oil-sands petroleum coke. *Can J Chem Eng* 90:1472–1478 (2012).
- Hilton R, Bick P, Tekeei A, Leimkuehler E, Pfeifer P and Suppes GJ, Mass balance and performance analysis of potassium hydroxide activated carbon. *Ind Eng Chem Res* 51:9129–9135 (2012).
- Montes V and Hill JM, Activated carbon production: recycling KOH to minimize waste. *Mater Lett* 220:238–240 (2018).
- Khan E and Subramania-Pillai S, Interferences contributed by leaching from filters on measurements of collective organic constituents. *Water Res* 41:1841–1850 (2007).
- Wendlandt WW, *Thermal Methods of Analysis*. Wiley, New York (1974).
- Lima IM, McAloon A and Boateng AA, Activated carbon from broiler litter: process description and cost of production. *Biomass Bioenergy* 32:568–572 (2008).
- Vanreppelen K, Kuppens T, Thewys T, Carleer R, Yperman J and Schreurs S, Activated carbon from co-pyrolysis of particle board and melamine (urea) formaldehyde resin: a techno-economic evaluation. *Chem Eng J* 172:835–846 (2011).
- Chemical Engineering Magazine, 2020 annual CEPCCI average value, <https://www.chemengonline.com/2020-annual-cepci-average-value/>, (accessed 4 February 2022).
- Peters MS, Timmerhaus KD and West RE, *Plant Design and Economics for Chemical Engineers*, 5th edn. McGraw-Hill, New York (2003).
- Statistics Finland, Energy prices, https://www.stat.fi/til/ehi/2021/03/ehi_2021_03_2021-12-09_tau_002_en.html, (accessed 28 January 2022).
- Stavropoulos GG and Zabanitout AA, Minimizing activated carbons production cost. *Fuel Process Technol* 90:952–957 (2009).
- Sadakata M, Takahashi K, Saito M and Sakai T, Production of fuel gas and char from wood, lignin and holocellulose by carbonization. *Fuel* 66:1667–1671 (1987).
- Alibaba, Potassium Hydroxide Price, www.alibaba.com, (accessed 28 January 2022).
- Alibaba, Potassium Chloride Price, [Alibaba.com](http://www.alibaba.com), (accessed 28 January 2022).
- Bangalore Ashok RP, Oinas P, Lintinen K, Sarwar G, Kostianen MA and Österberg M, Techno-economic

- assessment for the large-scale production of colloidal lignin particles. *Green Chem* **20**:4911–4919 (2018).
45. Gómez Millán G, Bangalore Ashok RP, Oinas P, Llorca J and Sixta H, Furfural production from xylose and birch hydrolysate liquor in a biphasic system and techno-economic analysis. *Biomass Convers Biorefinery* **11**:2095–2106 (2021). <https://doi.org/10.1007/s13399-020-00702-4>.
 46. Randtke SJ and Snoeyink VL, Evaluating GAC adsorptive capacity. *J AWWA* **75**:406–413 (1983).
 47. Brunauer S, Emmett PH and Teller E, Adsorption of gases in multimolecular layers. *J Am Chem Soc* **60**:309–319 (1938).
 48. Rouquerol J, Llewellyn P and Rouquerol F, Is the bet equation applicable to microporous adsorbents? *Studies in Surface Science and Catalysis* **106**:49–56 (2007).
 49. Dubinin MM and Radushkevich LV, Equation of the characteristic curve of activated charcoal proceedings of the academy of sciences. *Akad. Nauk SSSR [Reports Acad. Sci. USSR]* **4**:331–334 (1947).
 50. Ravikovitch PI, Vishnyakov A, Russo R and Neimark AV, Unified approach to pore size characterization of microporous carbonaceous materials from N₂, Ar, and CO₂ Adsorption isotherms. *Langmuir* **16**:2311–2320 (2000).
 51. El-Sayed Y and Bandoz TJ, Adsorption of valeric acid from aqueous solution onto activated carbons: role of surface basic sites. *J Colloid Interface Sci* **273**:64–72 (2004).
 52. Hüttinger KJ and Minges R, Influence of the catalyst precursor anion in catalysis of water vapour gasification of carbon by potassium. *Fuel* **65**:1112–1121 (1986).
 53. Hayashi J, Kazehaya A, Muroyama K and Watkinson AP, Preparation of activated carbon from lignin by chemical activation. *Carbon* **38**:1873–1878 (2000).
 54. Newcombe G, in *Interface Science in Drinking Water Treatment*, Vol. 10, ed. by Newcombe G and Dixon T. Elsevier, pp. 133–153 (2006).
 55. Knappe DRU, in *Interface Science in Drinking Water Treatment*, Vol. 10, ed. by Newcombe G and Dixon T. Elsevier, pp. 155–177 (2006).
 56. Rouquerol F, Rouquerol J, Sing KSW, Maurin G and Llewellyn P, Principles, Methodology and Applications, in *Adsorption by Powders and Porous Solids*, ed. by Rouquerol F, Rouquerol J, Sing KSW, Llewellyn P and Maurin SE. Academic Press, Oxford, pp. 1–24 (2014).
 57. Perrich JR, *Activated Carbon Adsorption for Wastewater Treatment*, 1st edn. CRC Press, Boca Raton (1981).
 58. Fierro V, Torné-Fernández V and Celzard A, Methodical study of the chemical activation of Kraft lignin with KOH and NaOH. *Microporous Mesoporous Mater* **101**:419–431 (2007).
 59. Johns MM, Marshall WE and Toles CA, The effect of activation method on the properties of pecan shell-activated carbons. *J Chem Technol Biotechnol* **74**:1037–1044 (1999).
 60. Morishita T, Tsumura T, Toyoda M, Przepiórski J, Morawski AW, Konno H et al., A review of the control of pore structure in MgO-templated nanoporous carbons. *Carbon* **48**:2690–2707 (2010).
 61. FACT Database, KCl-KOH phase diagram, http://www.crct.polymtl.ca/fact/phase_diagram.php?file=KCl-KOH.jpg&dir=FTsalt, (accessed 4 February 2022).
 62. Knudsen JN, Jensen PA and Dam-Johansen K, Transformation and release to the gas phase of Cl, K, and S during combustion of annual biomass. *Energy Fuel* **18**:1385–1399 (2004).
 63. Arnold RA and Hill JM, Catalysts for gasification: a review. *Sustain. Energy Fuels* **3**:656–672 (2019).
 64. Kunii D and Chisaki T, in *Heat Transfer in Rotary Reactors, Indirect Heating*, ed. by Kunii D and Chisaki T. Elsevier, Amsterdam, pp. 11–25 (2008).
 65. Kunii D and Chisaki T, in *Heat Transfer in Rotary Reactors, Indirect Heating*, ed. by Kunii D and Chisaki T. Elsevier, Amsterdam, pp. 127–142 (2008).
 66. Kunii D and Chisaki T, in *Heat Transfer in Rotary Reactors, Indirect Heating*, ed. by Kunii D and Chisaki T. Elsevier, Amsterdam, pp. 143–162 (2008).
 67. Choy KKH, Barford JP and McKay G, Production of activated carbon from bamboo scaffolding waste—process design, evaluation and sensitivity analysis. *Chem Eng J* **109**:147–165 (2005).
 68. Ko DCK, Mui ELK, Lau KST and McKay G, Production of activated carbons from waste tire – process design and economical analysis. *Waste Manag* **24**:875–888 (2004).
 69. Ng C, Marshall WE, Rao RM, Bansode RR and Losso JN, Activated carbon from pecan shell: process description and economic analysis. *Ind. Crops Prod.* **17**:209–217 (2003).
 70. Fingolo AC, Klein BC, Rezende MCAF, Silva e Souza CA, Yuan J, Yin G et al., Techno-economic assessment and critical properties tuning of activated carbons from Pyrolyzed sugarcane bagasse. *Waste and Biomass Valorization* **11**:1–13 (2020).
 71. Ou L, Dou C, Yu J-H, Kim H, Park Y-C, Park S et al., Techno-economic analysis of sugar production from lignocellulosic biomass with utilization of hemicellulose and lignin for high-value co-products. *Biofuels Bioprod. Biorefining* **15**:404–415 (2021).
 72. Girods P, Dufour A, Fierro V, Rogauze Y, Rogauze C, Zoulalian A et al., Activated carbons prepared from wood particleboard wastes: characterisation and phenol adsorption capacities. *J Hazard Mater* **166**:491–501 (2009).
 73. Thommes M, Kaneko K, Neimark AV, Olivier JP, Rodriguez-Reinoso F, Rouquerol J et al., Physisorption of gases, with special reference to the evaluation of surface area and pore size distribution (IUPAC technical report). *Pure Appl Chem* **87**:1051–1069 (2015).
 74. Roberts PV and Summers RS, Performance of granular activated carbon for total organic carbon removal. *J Am Water Works Assoc* **74**:113–118 (1982).
 75. Ponomarev N and Sillanpää M, Combined chemical-templated activation of hydrolytic lignin for producing porous carbon. *Ind. Crops Prod.* **135**:30–38 (2019).
 76. Macià-Agulló JA, Moore BC, Cazorla-Amorós D and Linares-Solano A, Activation of coal tar pitch carbon fibres: physical activation vs. chemical activation. *Carbon* **42**:1367–1370 (2004).
 77. Yahya MA, Al-Qodah Z and Ngah CWZ, Agricultural bio-waste materials as potential sustainable precursors used for activated carbon production: a review. *Renew Sustain Energy Rev* **46**:218–235 (2015).
 78. International Organization for Standardization, ISO 14006:2011 Environmental management systems—Guidelines for incorporating ecodesign, <https://www.iso.org/standard/43241.html>, (accessed 4 February 2022).



Nikolai Pavlovich Ponomarev

Nikolai Pavlovich Ponomarev, MSc (Chemical Engineering). He is a researcher in the field of active carbon production from lignin and charcoal. He has been working on the development of novel methods for active carbon with a high surface area and its applications. The results of his work are several scientific publications and two patents.



Gregory Richard O'Shea

Dr Gregory Richard O'Shea has a professional background in corporate strategy and was former Head of Business Development in the UK's largest retailer then Director of

Corporate Finance Director for a UK retailer and then managing director of two consulting companies in Finland, as well as a partner in a Cambridge based consultancy specializing in transformation and innovation, where his main clients were global, IT brands. He is now mainly an academic specializing in developing regional, novel, technology-based, innovative and entrepreneurial ecosystems.



Jutta Nuortila-Jokinen

Jutta Nuortila-Jokinen, DSci (Tech), currently works as Industry Professor of separation technology for circular economy at LUT University. She got her doctorate degree in 1997 from LUT University and has since then worked both in industry and academia

developing sustainable technological solutions for industrial challenges for more than 30 years.



Samantha Kiljunen

Dr Samantha Kiljunen. PhD in Chemical Engineering. Has a background in R&D and business, especially in chemicals and wastewater treatment. Her role is

focused on providing application knowledge in water and wastewater treatment where she has 12 years of experience and wide network. In addition, Samantha has more than 18 years of expertise in IPR patent strategy and has 11 patents.



Mari Kallioinen-Mänttari

(Dr Tech since 2008) is with her team focused to develop understanding and knowledge, which supports and facilitates the development of sustainable and resource efficient separation technology applications for biorefineries.

To achieve this aim, research is implemented at three focus areas: (1) Understanding of separation, fouling and cleaning phenomena in biorefinery applications, (2) Development of novel processes and (3) Development of novel separation matrices. The research vision of the team is that the improved understanding on separation, fouling and cleaning phenomena can take the utilization of separation technology processes and resource efficiency to the next level in biorefining industry and have a strong influence on the transformation from linear economy to circulation economy. Thus, it is crucial to understand the possible interactions between the biomass compounds and separation matrices as well as between the biomass compounds with each other in different conditions.

ACTA UNIVERSITATIS LAPPEENRANTAENSIS

1045. RYYNÄNEN, MARKO. A forecasting model of packaging costs: case plain packaging. 2022. Diss.
1046. MAILAGAHA KUMBURE, MAHINDA. Novel fuzzy k-nearest neighbor methods for effective classification and regression. 2022. Diss.
1047. RUMKY, JANNATUL. Valorization of sludge materials after chemical and electrochemical treatment. 2022. Diss.
1048. KARJUNEN, HANNU. Analysis and design of carbon dioxide utilization systems and infrastructures. 2022. Diss.
1049. VEHEMAANPERÄ, PAULA. Dissolution of magnetite and hematite in acid mixtures. 2022. Diss.
1050. GOLOVLEVA, MARIA. Numerical simulations of defect modeling in semiconductor radiation detectors. 2022. Diss.
1051. TREVES, LUKE. A connected future: The influence of the Internet of Things on business models and their innovation. 2022. Diss.
1052. TSEHING, TENZIN. Research advancements and future needs of microplastic analytics: microplastics in the shore sediment of the freshwater sources of the Indian Himalaya. 2022. Diss.
1053. HOSEINPUR, FARHOOD. Towards security and resource efficiency in fog computing networks. 2022. Diss.
1054. MAKSIMOV, PAVEL. Methanol synthesis via CO₂ hydrogenation in a periodically operated multifunctional reactor. 2022. Diss.
1055. LIPIÄINEN, KALLE. Fatigue performance and the effect of manufacturing quality on uncoated and hot-dip galvanized ultra-high-strength steel laser cut edges. 2022. Diss.
1056. MONTONEN, JAN-HENRI. Modeling and system analysis of electrically driven mechatronic systems. 2022. Diss.
1057. HAVUKAINEN, MINNA. Global climate as a commons — from decision making to climate actions in least developed countries. 2022. Diss.
1058. KHAN, MUSHAROF. Environmental impacts of the utilisation of challenging plastic-containing waste. 2022. Diss.
1059. RINTALA, VILLE. Coupling Monte Carlo neutronics with thermal hydraulics and fuel thermo-mechanics. 2022. Diss.
1060. LÄHDEAHO, OSKARI. Competitiveness through sustainability: Drivers for logistics industry transformation. 2022. Diss.
1061. ESKOLA, ROOPE. Value creation in manufacturing industry based on the simulation. 2022. Diss.
1062. MAKARAVA, IRYNA. Electrochemical recovery of rare-earth elements from NdFeB magnets. 2022. Diss.
1063. LUHAS, JUKKA. The interconnections of lock-in mechanisms in the forest-based bioeconomy transition towards sustainability. 2022. Diss.

1064. QIN, GUODONG. Research on key technologies of snake arm maintainers in extreme environments. 2022. Diss.
1065. TAMMINEN, JUSSI. Fast contact copper extraction. 2022. Diss.
1066. JANTUNEN, NIKLAS. Development of liquid–liquid extraction processes for concentrated hydrometallurgical solutions. 2023. Diss.
1067. GULAGI, ASHISH. South Asia's Energy [R]evolution – Transition towards defossilised power systems by 2050 with special focus on India. 2023. Diss.
1068. OBREZKOV LEONID. Development of continuum beam elements for the Achilles tendon modeling. 2023. Diss.
1069. KASEVA, JANNE. Assessing the climate resilience of plant-soil systems through response diversity. 2023. Diss.
1070. HYNNINEN, TIMO. Development directions in software testing and quality assurance. 2023. Diss.
1071. AGHAHOSSEINI, ARMAN. Analyses and comparison of energy systems and scenarios for carbon neutrality - Focus on the Americas, the MENA region, and the role of geo-technologies. 2023. Diss.
1072. LAKANEN, LAURA. Developing handprints to enhance the environmental performance of other actors. 2023. Diss.
1073. ABRAMENKO, VALERII. Synchronous reluctance motor with an axially laminated anisotropic rotor in high-speed applications. 2023. Diss.
1074. GUTIERREZ ROJAS, DANIEL. Anomaly detection in cyber-physical applications. 2023. Diss.
1075. ESANOV, BAKHTIYOR. Adaptive user-controlled personalization for virtual journey applications. 2023. Diss.
1076. SILTANEN, JUKKA. Laser and hybrid welding of high-strength structural steels. 2023. Diss.
1077. NOUSIAINEN, JALO. Model-based reinforcement learning and inverse problems in extreme adaptive optics control. 2023. Diss.
1078. USTINOV, STANISLAV. Fast and accurate simulation of fluid power circuits in the presence of small volumes using advanced methods and models for numerical stiffness elimination. 2023. Diss.
1079. HUSSAIN, HAFIZ MAJID. Heuristic-based packetized energy management for residential electricity demand. 2023. Diss.
1080. HÄMÄLÄINEN, MINNA. Principals managing entrepreneurship education in schools. 2023. Diss.
1081. WANG, ZHAO. Photocatalytic degradation of pharmaceutical and person care products (PPCPs) by commercial and synthesized catalysts under UV irradiation. 2023. Diss.
1082. LOHRMANN, ALENA. The water footprint of the global power sector: Status quo, challenges, and opportunities for tackling the global water crisis. 2023. Diss.



ISBN 978-952-335-955-0
ISBN 978-952-335-956-7 (PDF)
ISSN 1456-4491 (Print)
ISSN 2814-5518 (Online)
Lappeenranta 2023